7-27-2023

Design of an Accelerated Lifetime Tester for Industrial Gas Compressor Poppet Valves

Michael W. Anderson
mwa2912@rit.edu

Recommended Citation

Anderson, Michael W., "Design of an Accelerated Lifetime Tester for Industrial Gas Compressor Poppet Valves" (2023). Thesis. Rochester Institute of Technology. Accessed from

Design of an Accelerated Lifetime Tester for Industrial Gas Compressor Poppet Valves

Michael W. Anderson

A Thesis Submitted in Partial Fulfillment of the Requirements for the Degree of Master of Science in Mechanical Engineering

Supervised by

Dr. Jason Kolodziej
Department of Mechanical Engineering
Kate Gleason College of Engineering
Rochester Institute of Technology
Rochester, New York
July 27th, 2023

Thesis Approved By:

Dr. Jason Kolodziej

Professor, Primary Advisor, Department of Mechanical Engineering

---

Dr. Agamemnon Crassidis

Professor, Committee Member, Department of Mechanical Engineering

---

Dr. Patricia Iglesias-Victoria

Professor, Committee Member, Department of Mechanical Engineering

---

Dr. Sarilyn Ivancic, Department Representative, Department of Mechanical Engineering

DEDICATION

Deze thesis is opdragen aan mijn opa, Wim Lam. Hartelijk bedankt voor uw voortdurende ondersteuning en inzicht, niet alleen tijdens dit project, maar ook gedurende mijn hele leven. U bent mijn inspiratie.

ABSTRACT

There is increasing interest within the petrochemical industry in the development of predictive maintenance algorithms for gas compressors and pipelines. To this end, this thesis outlines an analysis of the feasibility and design of a lifetime accelerator for poppet valves used in industrial gas compressors. First, we investigate the most common compressor and valve types. We then compare existing valve accelerators to determine the gap in current research on poppet valve lifetime accelerators. We demonstrate our design for a lifetime accelerator with the ability to actuate poppet valves at 100[Hz], which is more than 15 times higher than the normal operating rate of 6.4[Hz]. Based on preliminary calculations, the system will not operate near the resonant frequency, and the system will be able to safely hold 100[psig]. Further, an orifice-flow system model indicates the design will be able to transfer air through the system quickly enough to support desired valve actuation rate. Finally, our constructed system demonstrates that the system will be able to achieve and maintain pressures of up to 100[psig] safely and with the possibility to function beyond the initially designed parameters.

Contents

LIST OF FIGURES

NOMENCLATURE

Variables:

$\%Open$	Percentage of Disc Surface Hole Takes Up [-]
A	Area of Orifice [in^2]
A_{Plate}	Area of Plate [in^2]
A_{sect}	Area of Sector [in^2]
A_{seg}	Area of Circle Segment [in^2]
a	Distance a [in]
a_{loc}	Radius of Circle in Polar Coordinates [in]
α	Coefficient of Thermal Expansion [μin/in°F]
A_p	Surface Area of Poppets [in^2]
b	Distance b [in]
b_{tri}	Base of Triangle [in]
c	Distance c [in]
C	Inegration Constant [-]
C_d	Discharge Coefficient [-]
d	Diameter [in]
E	Young's Modulus [psi]
ϵ	Normal Strain [-]
F	Force [lb$_f$], [N]
f_{act}	Acting Frequency of Poppet Valves [Hz]
g	Gravity [ft/sec^2]
h	Height of Triangle [in]
I	Cross-Sectional Area Moment of Inertia [in^4]
k	Compressible Flow Constant [-]
$k_{a,b,c,d,e,f,g}$	Marin's Factors [-]
k_{shaft}	Spring Constant of Rotating Shaft [lb$_f$/in]
L	Length [in]

M	Moment [ft*lb_f], [N*m]
m	Mass [slug], [kg]
$\dot{m}$	Mass Flow Rate [slug/sec], [kg/sec]
n	Factor of Safety [-]
n_c	Critical Speed [RPM]
P	Pressure [psi]
r	Radius [in]
R	Ideal Gas Constant (Air) [(in*lb_f)/(slug*°R)], [J/(kg*K)]
R_L	Left Reaction Force [lb_f]
R_R	Right Reaction Force [lb_f]
ρ	Density [kg/m^3]
T	Temperature [°F]
t	Thickness [in]
$\boldsymbol{t}$	Time [sec]
θ	Angular Displacement [°], [rad]
U	Load (Distributed) [lb_f/in]
V	Shear Force [lb_f]
W	Load, Used Interchangeably w/ Force [lb_f]
x	Displacement [m]
δ	Deflection [in]
σ_a	Alternating Stress [psi]
σ_e	Endurance Limit [psi]
$\sigma_e{}'$	Rotational Endurance Limit [psi]
σ_h	Hoop Stress [psi]
σ_m	Mean Stress [psi]
$\sigma_{pressure}$	Stress Due to Internal Pressure [psi]
σ_t	Tangential Stress [psi]
σ_{ut}	Ultimate Stress [psi]

Common Subscripts:

cr	Critical
d	Downstream
i	Inner
M	Manifold
max	Maximum Condition
o	Outer
T	Tank
u	Upstream

Other:

CAD	Computer-Aided Design
COMP	Reference to Input Compressor
FBD	Free Body Diagram
HI	Reference to High-Pressure Vessel
ID	Inner Diameter
KGCOE	Kate Gleason College of Engineering
LO	Reference to Low-Pressure Vessel
MAN	Reference to Manifold Volume
MAWP	Maximum Allowable Working Pressure
MECE	Mechanical Engineering
OD	Outer Diameter
PTFE	Polytetrafluoroethylene
RIT	Rochester Institute of Technology
STP	Standard Temperature and Pressure
TANK	Reference to Mid-Pressure Vessel

1.0 PROBLEM INTRODUCTION

In the petrochemical industry, reciprocating gas compressors are commonly used to drive gas products from one location to another. Any downtime, whether for planned or unplanned maintenance, can cost companies hundreds to thousands of dollars per hour in lost revenue, labor costs, and part costs. As such, an area of interest for the industry lies in predictive maintenance techniques to determine compressor performance and whether specific components need replacement. Predictive maintenance processes rely on collecting performance data on a system, specifically in those components most prone to failure. In reciprocating gas compressors, valve degradation is an important health condition directly affecting the efficiency of the system. However, these valves have a normal operational lifetime of 40,000 hours or four and a half years of continuous operation. As such, we currently have no way to reliably recreate compressor performance during various stages of valve failure without either being able to access valves that have undergone use in various stages of their rated lifetime or by creating seeded faults within the valves themselves. Since we cannot source used valves across a broad spectrum of their rated lifetime, compressor performance is currently being collected through seeded faults such as drilling holes into specific valves or grinding away material from contacting surfaces. It is unclear whether these seeded faults accurately represent the actual performance characteristics of the compressor under lifetime wear, and which stages of valve failure are represented by specific seeded faults. As such, there is a current need for a method to accelerate the lifetime wear of compressor valves rapidly and accurately to provide valve samples across a range of lifetime conditions. No such device exists to our knowledge, so the primary objective of this thesis is to explore the development of an accelerated lifetime tester for poppet valves to actuate the valves at 100[Hz]. This will be achieved through analysis of the pressure differential across the valve assembly as well as the displacement and vibration characteristics of the valves.

2.0 THE RESEARCH QUESTION

The main objective of this thesis is to determine if it is possible to design a lifetime accelerator for poppet valves commonly used in reciprocating compressors. The accelerator is intended to be able to increase the actuation rate of the poppet valves from their normal 6.4[Hz] to at least 100[Hz]. This is a commonly accepted method of accelerating component wear and represents an acceleration factor in the frequency of valve actuation events by more than 15x.

3.0 LITERATURE REVIEW

3.1 COMMON INDUSTRIAL GAS COMPRESSORS

Within the petrochemical industry, there are three common types of compressors used for the transport of gases. Screw compressors are positive displacement systems that operate via a twin-shaft rotary piston, which drives two sets of meshing screws with diminishing space between them. Gas is pushed into the system through an inlet, where the helical screws capture the gas and force it upwards through the threads. As the space diminishes between the screws, the captured gas undergoes compression at a fixed rate until it is released through a discharge port or nozzle. They generally come in two variations, with the screws either lubricated with oil or unlubricated. By lubricating the screws, these compressors can obtain higher pressures at the expense of slower gas flow rates upon discharge. Lubricating these screws can cause contamination of the gas being compressed with aerosolized oil particulates, however, necessitating filters on the discharge port[1].

The main advantages of screw compressors lie in their ability to achieve compression ratios up to 23:1, as well as their higher energy efficiency and lower amount of heat generated by the compression process. However, these systems are greatly limited by the amount of pressure they can generate upon discharge, with lubricated systems providing a maximum of 865psi, and oil-free systems providing a maximum of 400psi[2].

Centrifugal compressors operate via dynamic compression rather than positive displacement. In these systems, an impeller is driven by a motor, which imparts kinetic energy gas medium. The gas enters the impeller’s eye, which causes it to be forced radially across the impeller. Some of this gas then encounters the impeller blades, which drive it in a circular motion. The resultant centrifugal force causes compression due to the velocity of the gas being converted into static pressure. Further compression is then achieved by driving the gas exiting the impeller through a diffuser. Here, the gas is pushed through a chamber with a radial passage starting at the same width as the impeller blade before expanding in radial area, which further compresses the gas by converting gas velocity to static pressure[1].

The main advantages of using centrifugal compressors are their ability to handle much higher flow rates than the other two compressor types, with a maximum flow of over 100,000acfm. However, centrifugal compressors have a very low compression ratio, with single-stage compressors only being rated for roughly 2:1 compression. This necessitates multi-stage compressors, with multiple driven impellers, diffusers, and other compressor stages to achieve higher compression ratios[2].

Reciprocating compressors are positive displacement systems that operate using a motor-driven piston. The motor drives a crankshaft at a specific speed, which translates the rotational movement into reciprocating linear movement of a cylindrical steel piston. As the piston moves forward, it compresses the gas ahead of it within a shrinking volume. This causes the gas to undergo compression until a specified pressure is reached. Once this occurs a set of valves are pushed open, allowing for the pressurized gas to escape the shrinking volume and discharge to the desired location. As the piston bottoms out and begins to travel backward through the system, the increasing volume creates a low-pressure region in the compressor. This shuts the discharge valves and opens a separate set of intake valves, allowing more gas to enter the compressor. This is the type of compressor in our laboratory, as well as the main compressor of interest in the creation of the poppet valve life accelerator. The Dresser-Rand ESH-1 compressor in the laboratory is single-state double-acting, which means it undergoes this process at opposite sections of the compression cycle both ahead and behind the piston at the same time.

Figure 1: Dresser-Rand ESH-1 Reciprocating Compressor in Laboratory

The main advantages of reciprocating compressors are their ability to generate the highest pressures out of the three common compressors with the lowest flow rates. However, this means in applications where high volumes of gas need to be continuously compressed at lower pressures, the reciprocating compressor is unable to keep up with demand. Further, due to their relative complexity and tendency to be used in continuous operation, reciprocating compressors have the most wearable parts of the three common compressor types. This means failures are more likely to occur and happen more rapidly in reciprocating compressors than in screw or centrifugal compressor systems[1,2]. Within reciprocating compressors, components such as the intake/discharge valves, the crankshaft, and the connecting rod are known to be the most common points of failure in the system[3]. As such, an emerging area of interest in the petrochemical industry is the development of health monitoring and predictive maintenance routines to diagnose component failures. More specifically Novity, the company sponsoring our research, is interested in retroactively installed health monitoring systems for these types of compressor systems.

3.2 COMMONLY USED TYPES OF VALVES

Among the components within a reciprocating compressor, the intake and discharge valves have a 36% chance to be the cause of a compressor shutdown and consist of 50% of the cost of maintenance per repairable item[4]. As such, understanding the different types of valve assemblies used in these systems is critical in the development of future health monitoring techniques.

At a fundamental level, each of these valve types operates identically. A valve component, often made of metal or rigid plastics is placed into a metal body acting as the valve seat. A spring element is placed behind the valve to provide the restorative force required to close the valve during operation. The valve-spring assembly is then sandwiched between a valve guard and the valve seat, which is secured using a screw. Gas transfer is facilitated by the pressure differential across the valve applying a force that exceeds the force of the spring, pushing the valve open.

The differences between the ported plate, ring, and poppet valves lie in their geometry and the gas transfer paths they allow. In ported plate valves, the valve is a single body with holes throughout the body to facilitate gas transfer. Complimentary mating extrusions are machined into the valve seat, covering the holes in the valve. Since the valve is a single body, this allows for gas transfer uniformly, with all gas transfer pathways being opened at the same time. Ported plate valves are most advantageous for use in high-speed applications (>500[RPM], or >8.3[Hz]), where a mass damping plate can be placed into the assembly between the plate valve and the restorative springs. This mass damping plate reduces valve impact velocity against the valve seat at higher valve displacements[5].

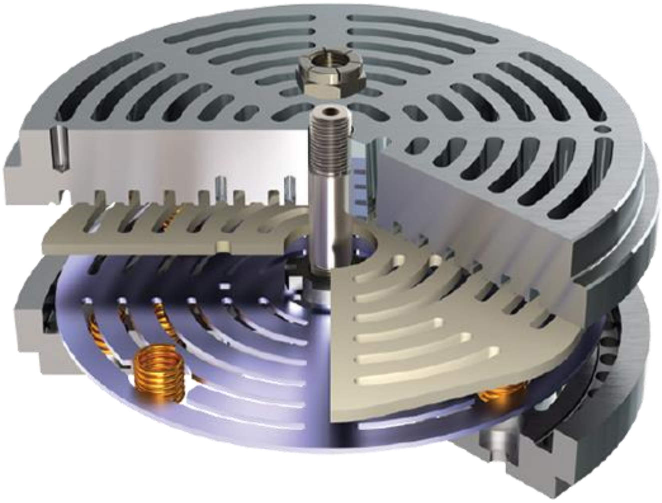

Figure 2: Ported Plate Valve Assembly[6]

In ring valve configurations, gas transfer is facilitated by sets of concentric valves with increasing diameters. These valves require several sets of springs spread along the circumference of each concentric valve to ensure the restorative spring force is evenly distributed. These are designed to work with higher lift ranges than ported plate valves, which allow for a higher flow area for the compressed gas to pass through. However, the increased lift range also makes the impact velocity of the ring valves higher, increasing the likelihood of valve flutter and wear to the assembly.[7]

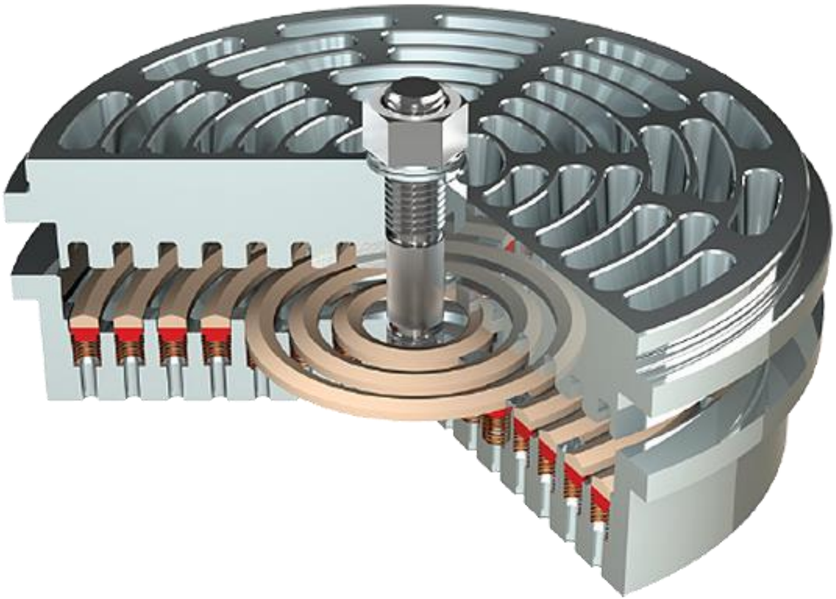

Figure 3: Ring Valve Assembly[6]

Poppet valves operate as an array of individual valves generally placed into a grid configuration. Each valve is an individual cylinder made of plastic or metal, which is forced into the closed position by individual springs. Due to their geometry and ability to obtain higher lift ranges than even ring valves, poppets are most favored for use in high gas flow operations. However, their high lift range makes poppet valves more susceptible to valve flutter and wear from high-impact velocities than either ring or ported plate valves[7]. Poppet valves also have larger spring diameters, vent holes, and spring pockets, which help reduce damage to the valves due to gas impurities[5]. Due to their tendency to be used in high-flow applications where contaminants are likely to be present, within the umbrella of health monitoring for reciprocating compressors, the performance and failure mechanics of poppet valves are an area of considerable interest to the petrochemical industry.

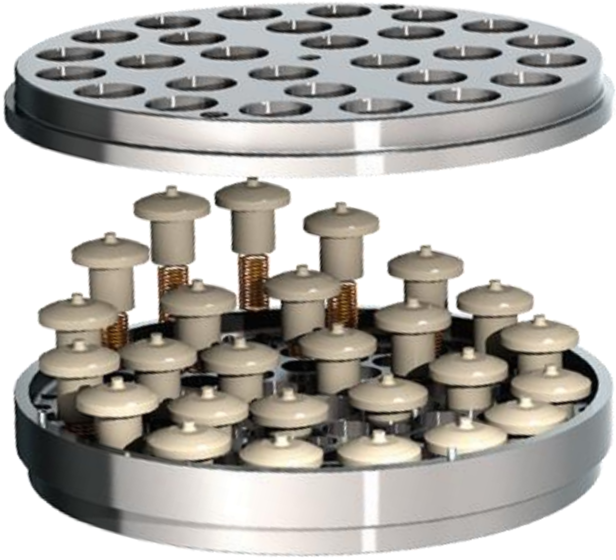

Figure 4: Poppet Valve Assembly[6]

3.3 FAILURE MECHANICS OF POPPET VALVES

Failures in reciprocating compressor poppet valves can be attributed to numerous sources. In his study on field failures of poppet valves, Motriuk attributes the failures to a variety of sources. He noticed a combination of widely varied operating conditions, excessive pressure pulsations in the pipe, and the existence of resonances through the cylinder passage all resulted in valve failures. He also identifies improper installation as a potential source of failure but eliminates this option by inspecting the valve. They also eliminate varied operating conditions as a source of failure since the compressor system was run at a constant speed [8].

Metcalf and Chaykosky identify the most common failure mechanisms as valve seat wear, spring fatigue, and wear of the seat and stop plates of the assembly. As stated earlier, increased valve lift on the poppet valves allows for more valve travel[5,7]. This allows the valves to attain higher velocities, allowing for more energetic impacts. Over time, this causes wear on both impacting surfaces as well as cracks in the poppet valve itself, creating leakage paths and eventually leading to compressor failure. Spring fatigue mainly occurs due to the cyclical forces imparted on the valves over extended periods. When the spring eventually fails, the restorative force keeping the valve shut during the initial stages of compression is lost, creating a leakage path affecting the efficiency of the system, and leading to an eventual loss in gas compression.

Chaykosky also identified impurities in the gas moving through the compressor as a frequent cause of valve failure. With valves made of harder materials such as metal, particulate intrusions such as dirt, sand, or metal shavings can cause the valves to clog up, sticking them into a single position despite the changing pressure differential across the valve assembly. With valves made of softer materials such as PEEK resin, these particulates become embedded within the valve rather than becoming wedged between the valve and its housing. This allows for the valve to continue operating at reduced efficiency but also accelerates valve and housing wear[7].

While knowledge of the different types of failures poppet valves see is helpful, the issue with these prior studies is twofold. First, while they describe the type of material failure or wear in the poppet valves causing failure, these studies fail to quantify the amount of material wear, and crack characteristics. In the case of Metcalf, even specific operating conditions such as the cycling rate of the valves or the compression pressure and ratio of the gas at the outlet are omitted. The lack of quantitative data on reciprocating compressor poppet valve failures presents an opportunity for future exploration of failure mechanics via the development of a device that can reliably create samples of valves at various stages of failure.

3.4 ACCELERATED LIFETIME TESTING BACKGROUND

Accelerated Lifetime Testing (ALT) is the process of taking a component and increasing one or two of the operating parameters beyond normal limits. By exaggerating these parameters, the number of cycles the component can operate under before failure can be decreased significantly[9]. In electrical systems, this can be achieved by modifying such as increasing ambient temperature, boosting the DC Voltage bias across the components, or switching the transient input through the system[10]. In mechanical systems, the modified parameters may entail increased applied loads to components, increased actuation rates of cycling systems, or changing the operational humidity or temperature of a system toward failure[11].

Chernoff developed some of the earliest generalized procedures for accelerated lifetime testing. In his paper, he outlines the process of optimizing experimental setups to determine the predicted lifetime of a product over a shortened testing period[12]. Unfortunately, this approach is limited in its applicability to our system. Chernoff's models fundamentally require knowledge of the statistical failure characteristics of the component and are looking for statistical results such as the reliability of the component tested. Further, since we have neither access to valves that have been subjected to true lifetime wear nor detailed performance and failure information on the poppet valves being tested, we are unable to provide the necessary information to create a true accelerated lifetime test model. This means the best approach to developing a lifetime acceleration model is to simply create and test the system using a specified set of stress factors[9]. Additionally, since the end goal of this experiment is to obtain the performance data of our reciprocating compressor with valves at various stages of failure, we care more about creating said valve samples than we do about the development of the lifetime model. The development of the accelerated lifetime model will come after collecting said performance data and most likely be done by the client for their proprietary predictive maintenance algorithm.

3.5 EXISTING LIFETIME ACCELERATORS FOR VALVES

While there are several examples of lifetime accelerators for ported plate, poppet, and flapper valves in various use case scenarios, there are currently no such test apparatuses for poppet valves in reciprocating compressor environments.

One example of a previously designed lifetime accelerator was for testing reed valves used in reciprocating compressors. In this system, the modified test parameters were valve actuation rate and humidity. To achieve a higher actuation rate, the authors utilized a motor-driven disc with a hole cut out along its radius. This allowed for the actuation rate of the valve to be controlled by the speed of the motor, while the humidity of the system was controlled using a filter dryer along the gas inlet line[13].

While this device does provide good inspiration for how to easily achieve high valve actuation rates, there are some issues with the system. Firstly, the system as designed can only actuate one valve at a time. This is fine if only one or two valve components are creating a barrier for gas backflow, but our system has sixteen individual poppet valves. This would mean we would need to run the accelerator sixteen times to obtain a single set of fatigued valves. Second, this system is designed for a completely different set of valves. While fundamentally they operate similarly, differences in gas flow, wear mechanics, and applications for these two valves mean the performance results from this system are not equitable to our design, even though this tester is also designed to simulate a reciprocating compressor.

Another example of a valve lifetime accelerator was for use in an engine exhaust valve. In this system, the parameters increased to induce early failure were the temperature of the system, the actuation rate, and the magnitude of the load acting on the valve. The increased operational temperature was achieved using a set of variable furnaces and coolers, while increased actuation was achieved using a motor with a crankshaft. This system also simulated the movement of the valves rotationally using a separate motor and a valve lifter/cam roller combination[14].

Although this system valve does use a type of poppet valve, this variety of poppet in this system fundamentally operates differently. First, the valves in engine exhaust applications are actuated mechanically using a spinning cam rather than a pressure differential as in a reciprocating compressor. Secondly, the poppets used in this application, while being functionally similar to the poppets in reciprocating compressors, have different failure mechanics. In exhaust valves, failure commonly occurs in the stem of the valve, which is tapered down so the restorative spring can slide in around it. This differs from reciprocating compressor poppets, where the restorative spring is socketed inside the poppet to protect it from gas intrusions and particulates. As was seen in the previous accelerator, this system is also only able to test valves individually, which would be impractical to create worn valves for our sixteen-valve assembly. Perhaps most importantly, however, this accelerator was not built to simulate the environment of a reciprocating compressor. This test rig was developed with engine exhaust ports entirely in mind. This is reflected in the importance the design places on temperature controls, the vastly different geometry of the poppet valves, and the drastic necking failure seen in their valves at the end of testing. This apparatus, while visually similar, does not create an environment that would be comparable enough to a reciprocating compressor system to be usable. This study also fails to address the acceleration factor achieved by their test rig, and was instead, more focused on creating accelerated valve samples more accurately than a previous valve accelerator they built[14].

The final example of a valve lifetime accelerator was designed by Ingersoll-Rand in the ‘80s. This system, which served as the inspiration for our design, chose to increase the actuation rate and pressure differential across a ported plate valve to induce lifetime acceleration. The system used a single rotating disc with two holes cut into it to simulate inlet and outlet channels to a high- and low-pressure vessel respectively. Behind the valve assembly, a vessel would be held at a median pressure to provide additional restorative force to the assembly. The disc would be driven by a 40hp motor to induce the desired actuation rate, with a high-pressure tank at ~35[psig], a mid-pressure tank at ~20[psig], and a low-pressure tank at roughly 0[psig] or atmospheric pressure. The authors also identified the most important pieces of the system to accelerate were the actuation rate and the valve impact velocity (which is raised by increasing differential pressure). This, on top of the system decreasing the lifetime of a ported plate valve from six to twelve months down to twenty hours of continual operation, served as the initial inspiration for this design.[15]

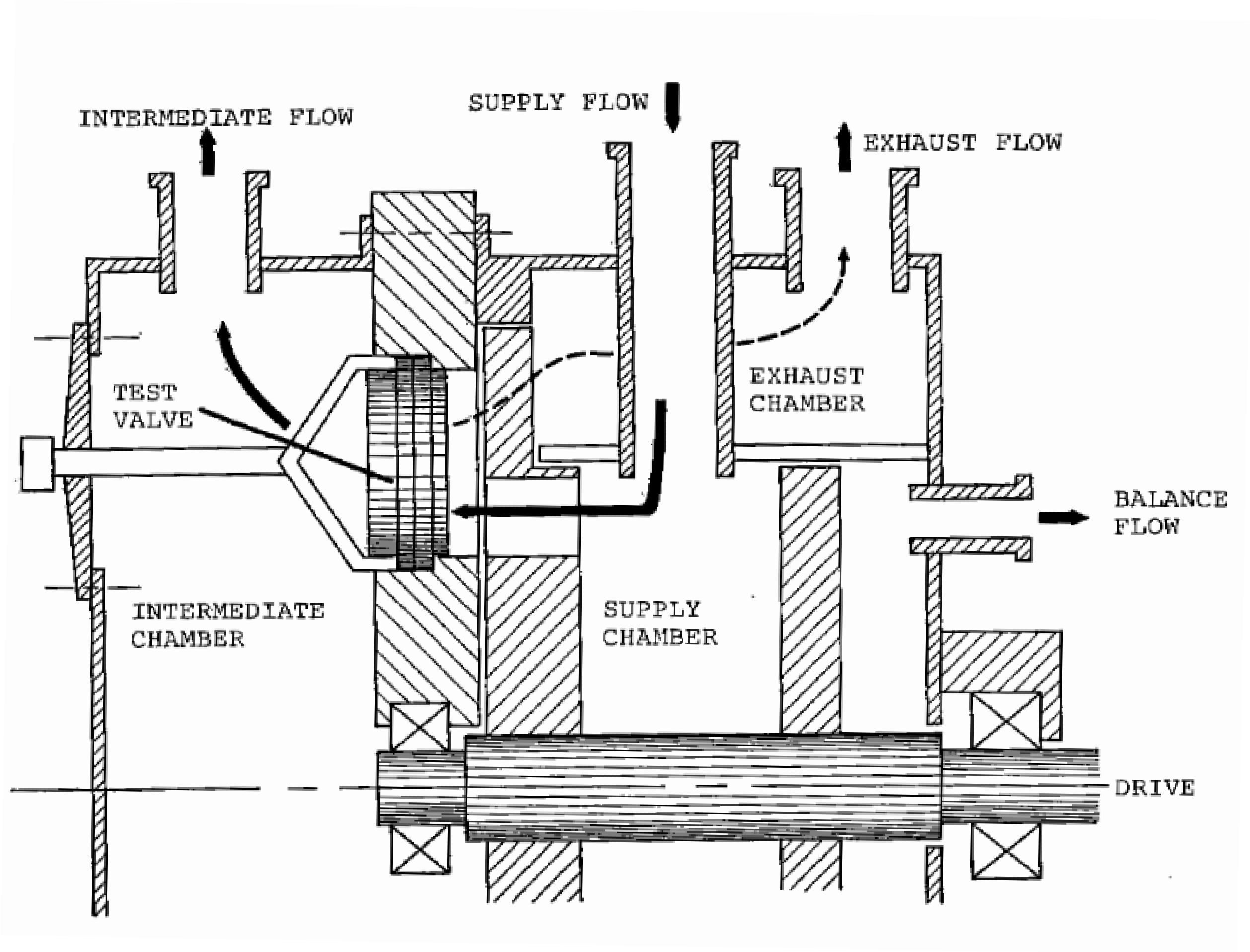

Figure 5: Diagram of Ingersoll-Rand Tester[15]

While this Ingersoll-Rand solution seemed the most promising out of the other accelerators we found, there were still some fundamental issues with the system. First, due to the single disc design used, the system had to utilize a system of nested pressure vessels to provide the necessary differential to actuate the valves. This creates problems with sealing and leakage mitigation between the low- and high-pressure tanks when the spinning disc sits as the only barrier between the two. This system also appears to be the size of a room according to the schematics and images provided, which would be wildly impractical given the space available to us in our lab. Further, this system was designed for ported plate valves whose native actuation rate was 20[Hz] and rated for a maximum high-pressure vessel pressure of 100[psig]. For our system, we are targeting 100[psig] as a starting point, with room to increase the operating pressure in the future. Further, the failure mechanics of ported plate valves are different than poppet valves. Ported plate valves experience failures due to pieces of the valve snapping off rather than the gradual warping of geometry from wear seen with poppet valves. As such, while the system provides a great proof-of-concept for our intended design, differences in the failure mechanics and gas flow through the ported plate valve versus poppet valves mean this system is not directly equivalent[15].

All three of these systems represent good examples of how to develop lifetime accelerators for valves, but all fail to demonstrate the failure mechanics and operational conditions of poppet valves in reciprocating compressors. The first and third designs, while using a similar actuation method to our design, are unable to simulate the wear mechanics of poppet valves due to using different valve types[13,15]. The second design, while using a variation of the poppet valve, fails to simulate the environment of a reciprocating compressor. It also fails to use a type of poppet with the appropriate failure mechanics for what would be expected in reciprocating compressor poppet valves. This lack of poppet valve lifetime accelerators, paired with existing accelerators' utility for use in high-flow compressor applications, presents a gap in the current research that this accelerator intends to fill.

4.0 LIFETIME ACCELERATOR DESIGN

4.1 INITIAL DESIGN CONCEPT

When first developing the lifetime accelerator, two concepts were generated in tandem. The first concept, based on Hartshorn's ported plate valve accelerator design, included a single motor-driven shaft with nested pressure vessels[15].

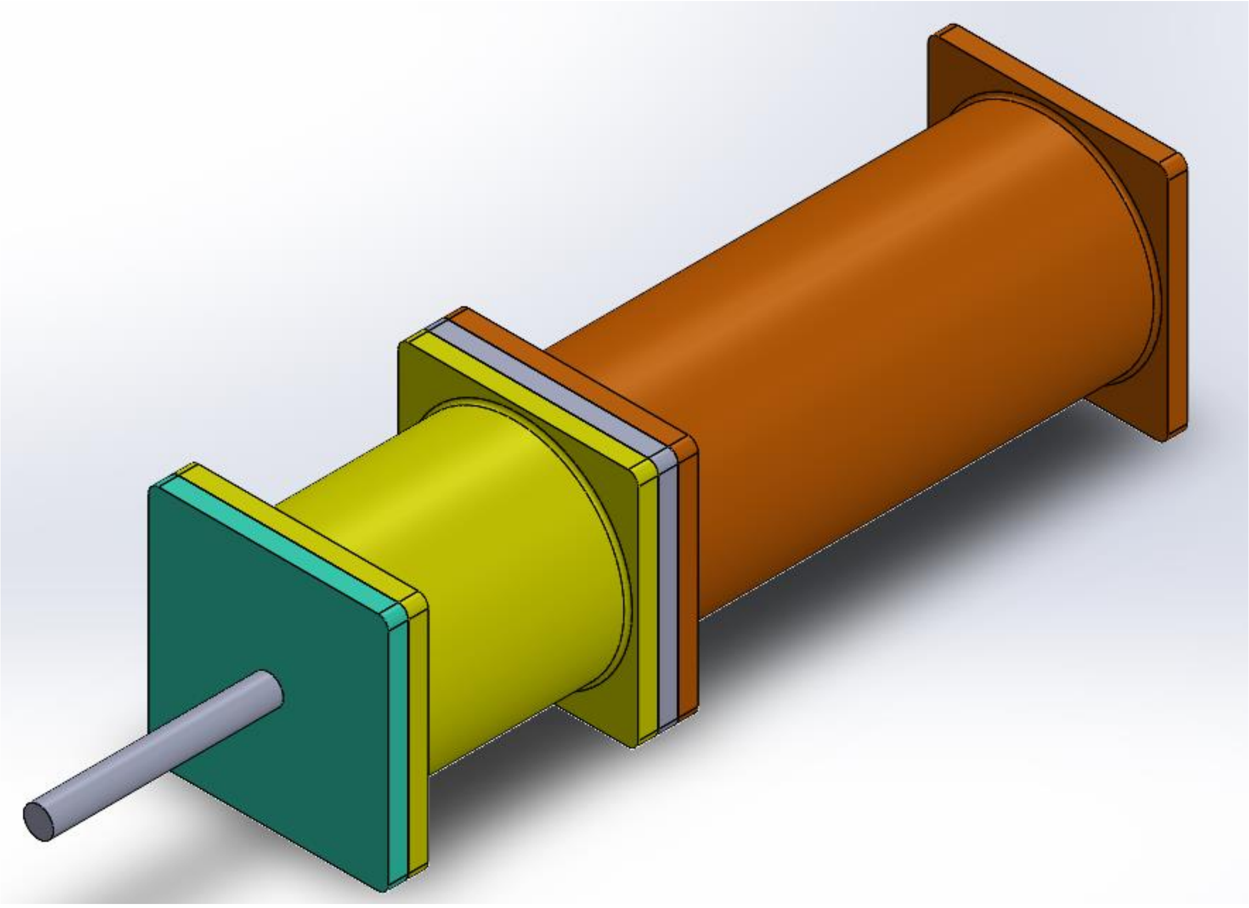

Figure 6: Single Shaft Design Assembly

In this design, pressure is maintained using a high-pressure internal vessel (in red), a low-pressure external vessel (in yellow), and a mid-pressure vessel (in orange) at the end of the stack-up. These vessels create the pressure differentials between the opening and closing events for the poppets.

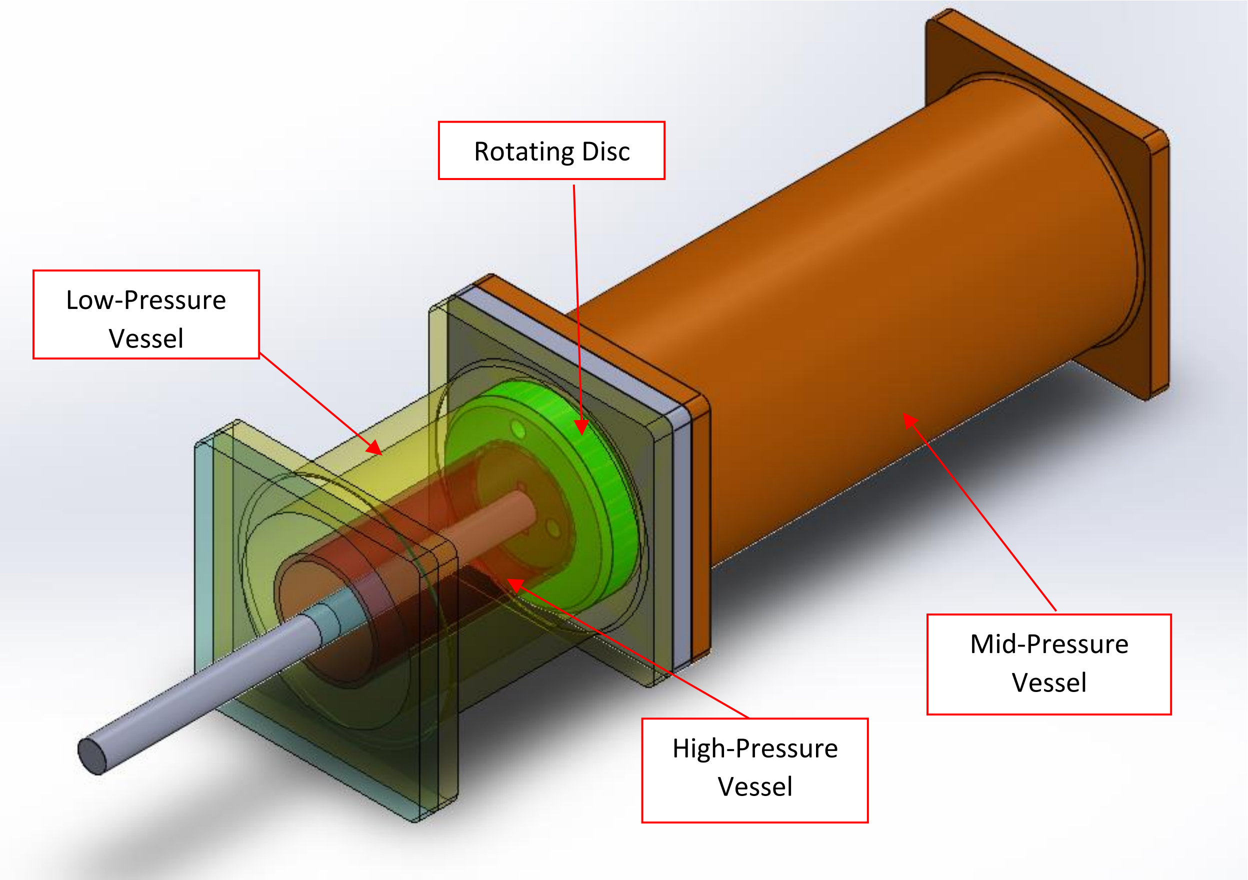

Figure 7: Single Shaft Pressure Vessel Internals

The shaft is driven by a motor to spin the green disc, which has two holes drilled through it. These holes are drilled at specified angles from each other, which determines the timing between the opening and closing events. As the disc is spun, the inner hole on the disc lines up with a pass-through hole in the grey plate. This allows high-pressure gas to pass into the mid-pressure vessel, forcing the poppet valves to open. As the disc continues rotating, this passthrough hole closes, stopping gas transfer to the mid-pressure vessel until the outer hole aligns with another passthrough hole in the grey plate. This facilitates gas transfer from the mid-pressure vessel to the low-pressure vessel, slamming the poppet valves closed. This process can be seen in Figure 8.

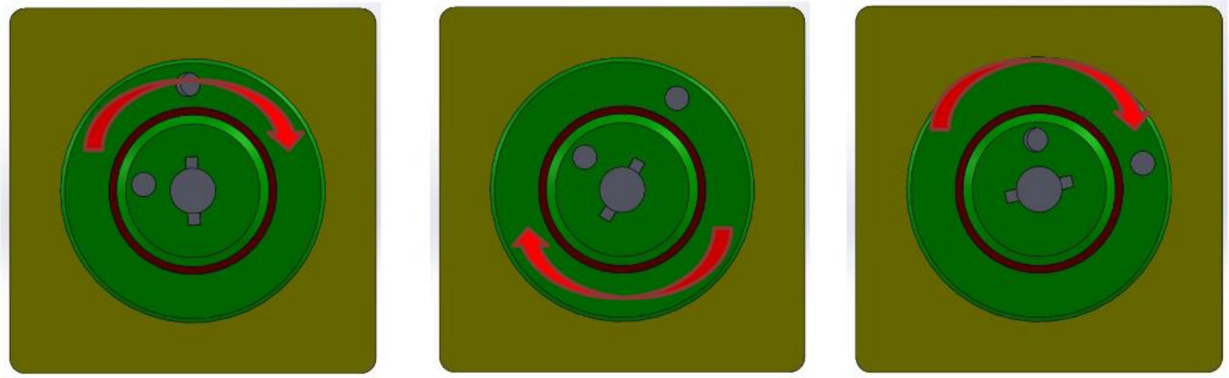

Figure 8: Single Shaft Design Rotating Disc

There are a few issues with this design that make it infeasible from the outset. First, this design relies on a contacting surface between the rotating disc and the nested pressure vessels to create a seal between the two. In practice, it would be incredibly difficult to maintain a seal between the high-pressure and low-pressure chambers with the disc spinning at a minimum of 3000[RPM] to obtain a valve actuation rate of 100[Hz]. Further, due to the high speed of rotation, commonly available shaft seals would wear too quickly, necessitating constant replacements to maintain the desired pressure in each vessel. Further, due to there being only a single rotating disc, the user is unable to easily adjust the timing of actuation events in the system. If the user wants to adjust relative opening or closing times, they need to replace the entire disc with a newly machined one upon each adjustment. This also requires the user to disassemble and reassemble the system, wasting testing time on maintenance instead.

4.2 FINAL DESIGN CONCEPT

Due to the issues seen in the single shaft design, an alternative design using similar principles was created. In this alternative design, there are two rotating shafts kept in time with each other using a timing belt. These shafts each lead into two separate and distinct pressure vessels, with one kept at high pressure, and the other kept at low pressure.

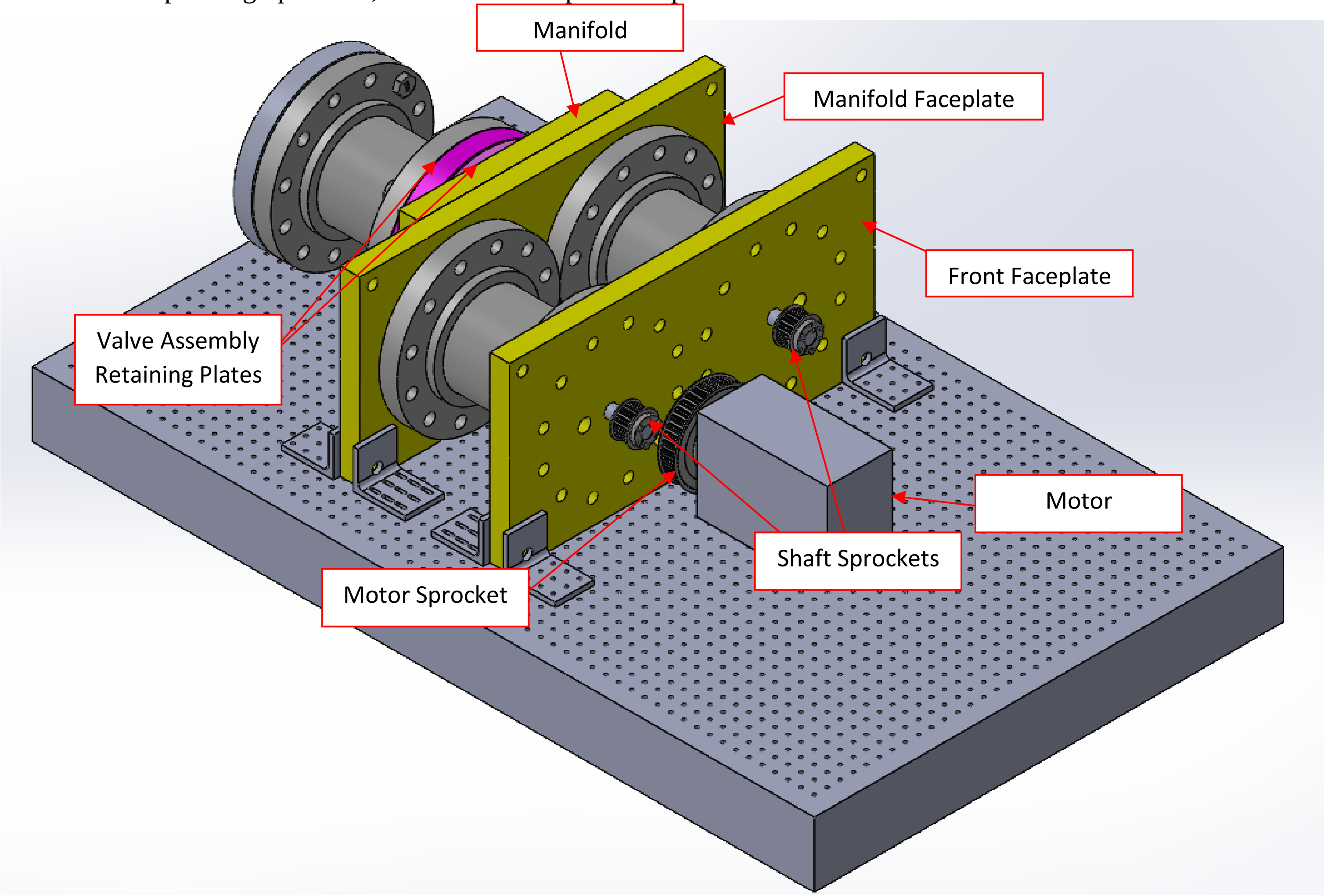

Figure 9: Dual Shaft Design Assembly

Behind the two rotating discs is a small ‘manifold’ volume which exists as a buffer region to the valve assembly. Behind the valve assembly, there is a mid-pressure vessel acting as the ‘closing’ pressure for the valves. The low- and mid-pressure vessels are maintained at their designated pressures using controllable back pressure regulators, while a control system will regulate the high-pressure vessel's pressure. The current test plan calls for using air as a gas medium, which is maintained at 100[psig] and 50[psig] at the high- and mid-pressure vessels respectively. The low-pressure tank will be maintained at 0[psig] (atmospheric pressure). These pressures were selected for two reasons. First, they were designated as design requirements by our sponsor. Secondly, these pressures create an environment where the poppet valves experience twice the differential pressure they do in normal operating conditions, assisting in accelerating their lifetime.

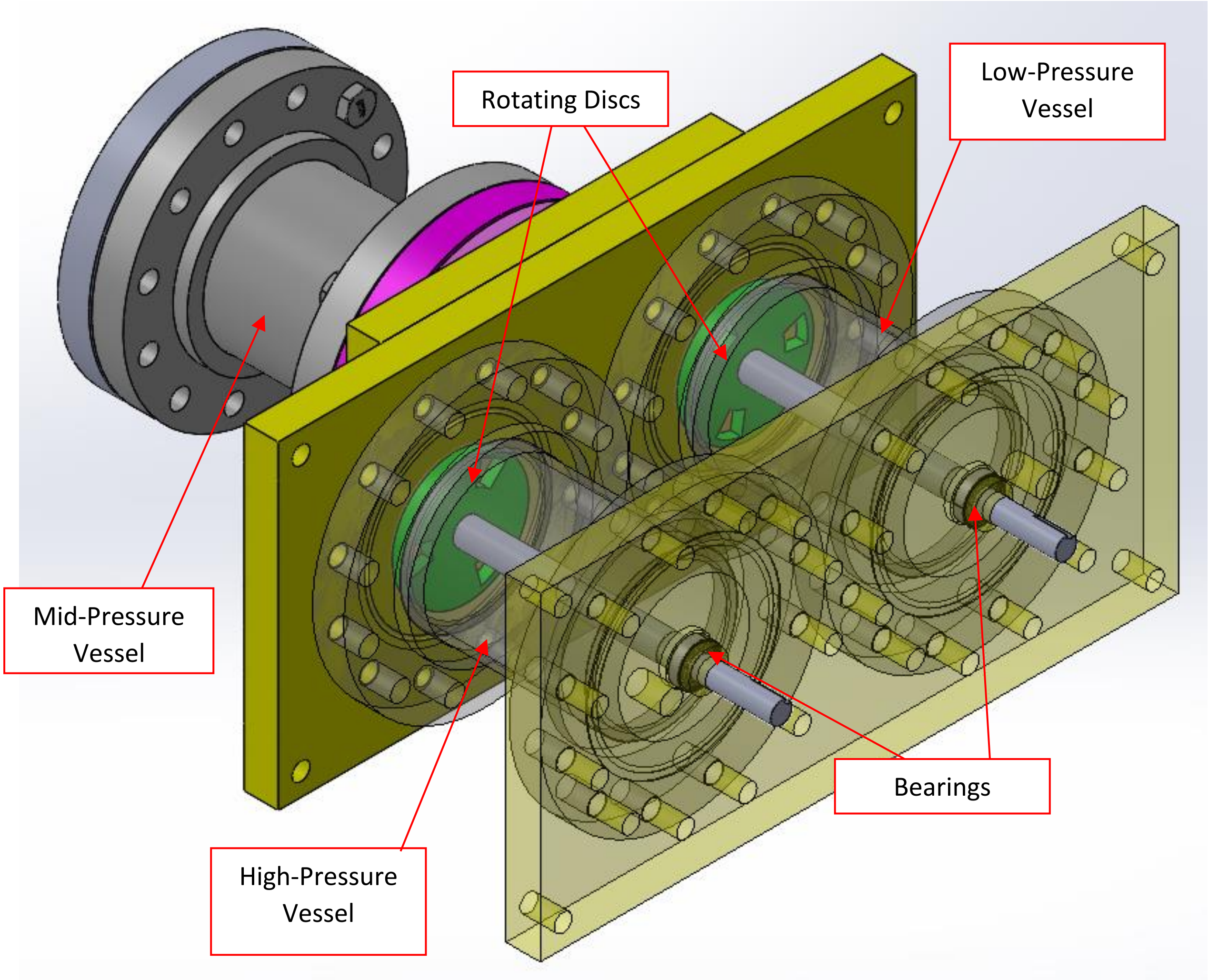

Figure 10: Dual Shaft Pressure Vessel Internals

The main advantage of the dual shaft system is the relative ease of sealing it. The single shaft design requires sealing at the rotating green disc as well as sealing the rotating shaft. The dual shaft design only requires sealing at one location: at the high-pressure vessel rotating shaft. Further, according to shop staff, a skilled machinist would be able to reduce the gap between the rotating discs and the manifold to <10 [thou]. As such, the amount of leakage would be negligible and therefore not require extra sealing.

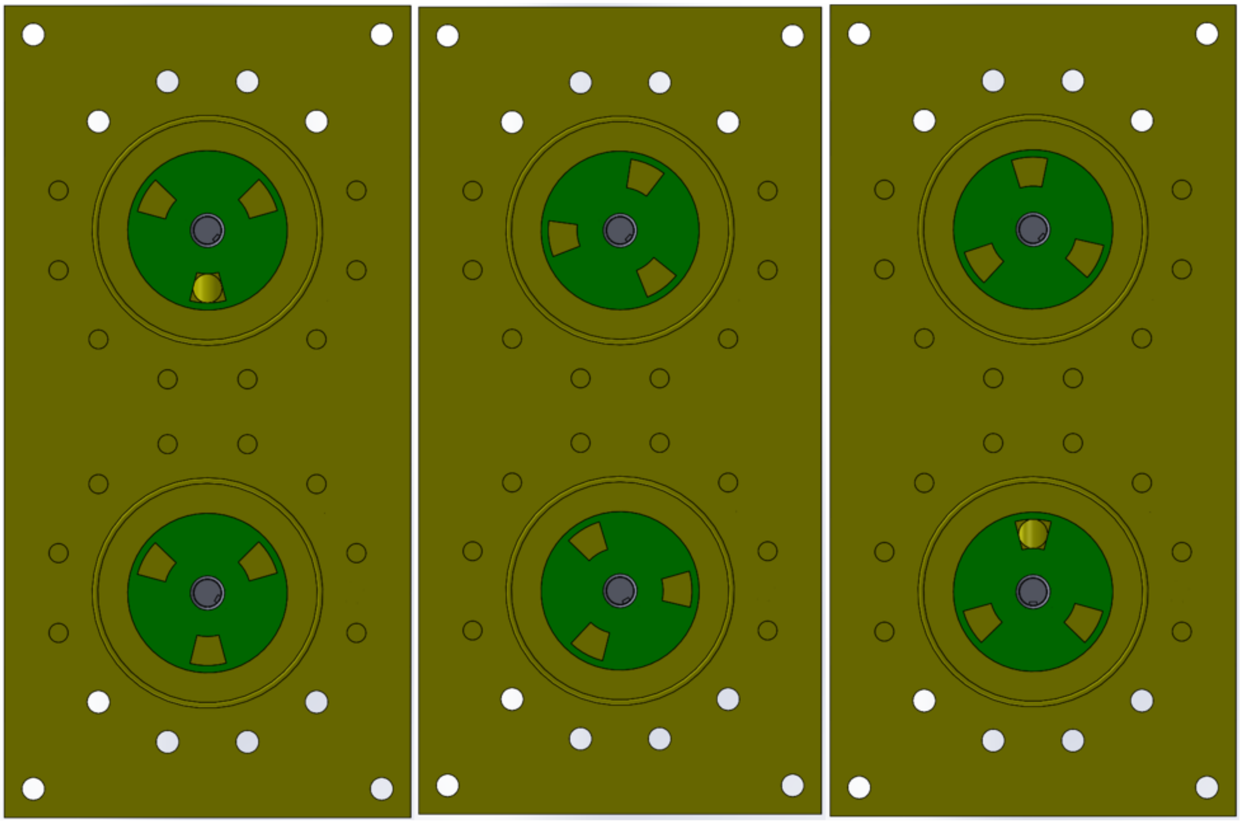

Figure 11: Dual Shaft Design Rotating Disc

Another advantage of this design lies in allowing the user some degree of control over the timing of valve actuation events. In the single shaft design, opening and closing events are determined by the angular offset between the hole cut in the disc for the high-pressure side and the hole for the low-pressure side. In the dual shaft design, this timing can be adjusted using the timing belt.

By simply rotating one of the shafts by the desired amount, the relative angular offset between the holes in the discs can be adjusted.

4.3 PRESSURE VESSEL STRESS CALCULATIONS

While the pressure vessels were being designed, the strength of the pressure vessels presented a point of concern for failures. Since the vessels are being created using a standard pipe size 6 (6.625” OD, 6.125” ID), a set of calculations was performed to determine the stress throughout the thickness of the vessels. From Shigley’s book on mechanical design, hoop, and longitudinal stresses can be calculated using[16]:

$$\sigma_h = \frac{P_i r_i^2 - P_o r_o^2 - \frac{r_i^2 r_o^2 (P_o - P_i)}{r^2}}{r_o^2 - r_i^2} \tag{1}$$

$$\sigma_r = \frac{P_i r_i^2 - P_o r_o^2 + \frac{r_i^2 r_o^2 (P_o - P_i)}{r^2}}{r_o^2 - r_i^2} \tag{2}$$

Using these equations, the stress profile along the thickness of the vessel was calculated and plotted in Fig. 12.

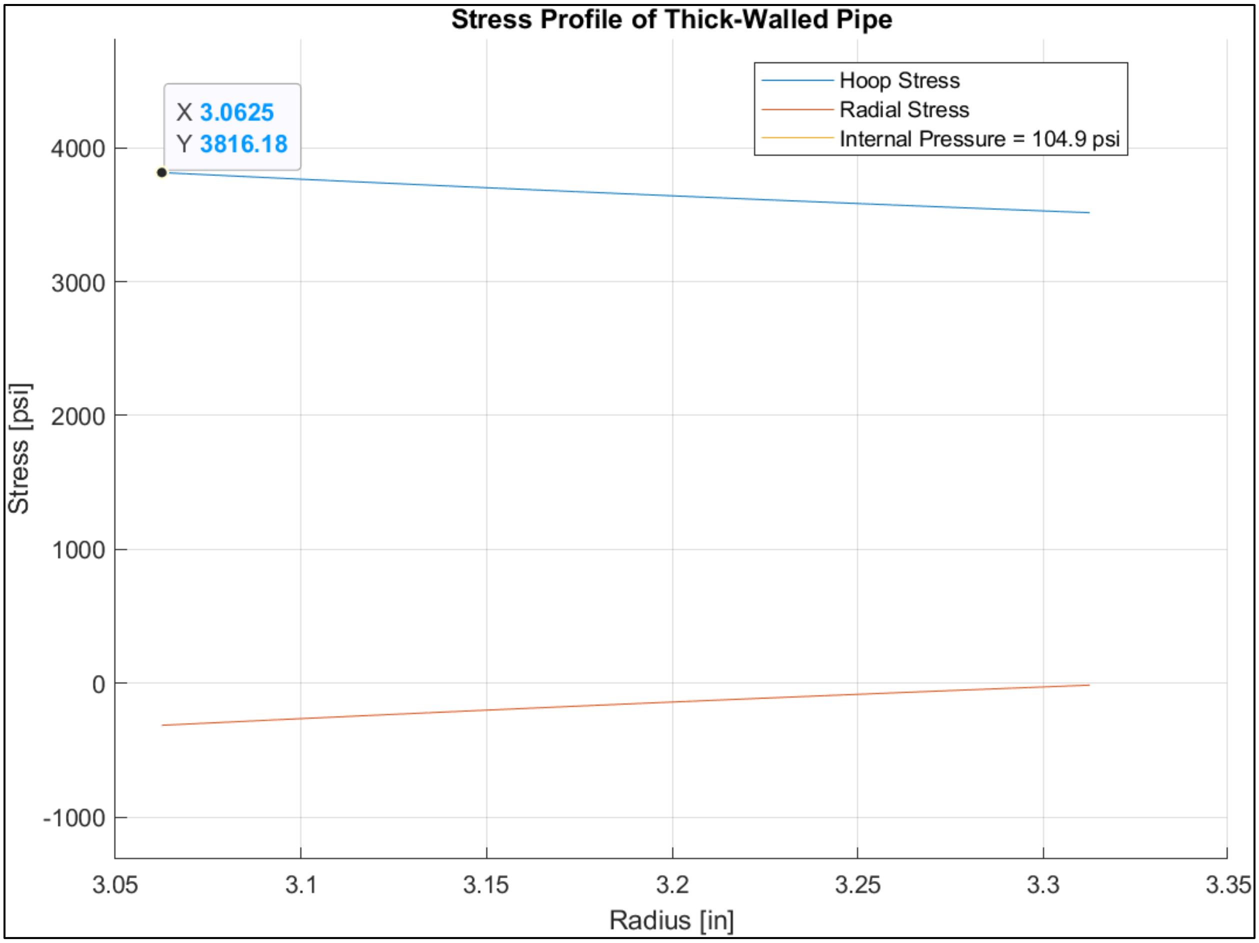

Figure 12: Hoop and Radial Stresses Through Pipe Wall (100[psig])

With an inbuilt conservative factor of safety of 3, the maximum stress the piping sees is 3816.18[psi], which is well below the yield tensile strength of 31200[psi][17]**.** Further, when investigating the theoretical maximum pressure for future testing, we determined the testbed can potentially hold a pressure of up to 814[psig].

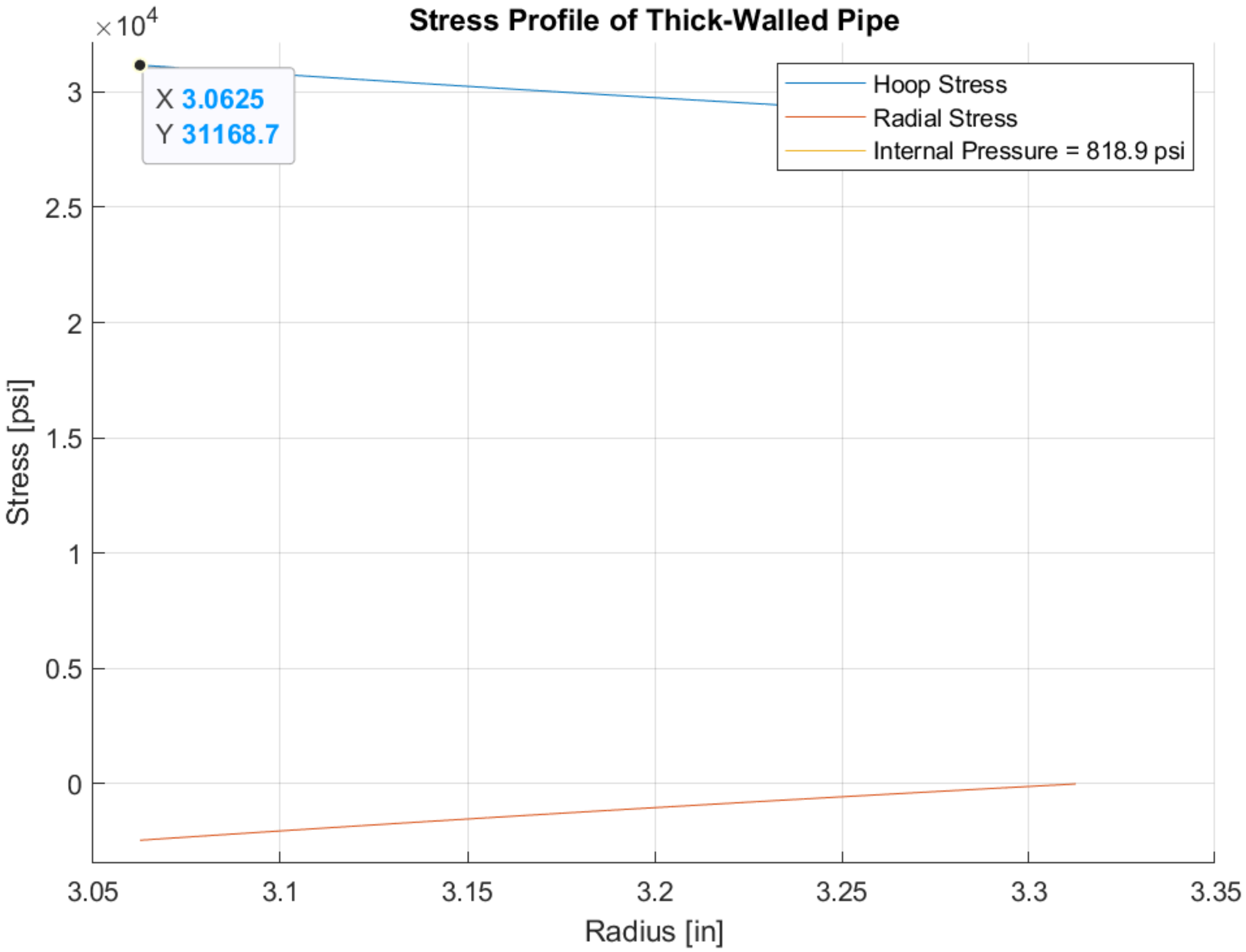

Figure 13: Hoop and Radial Stresses Through Pipe Wall (814[psig])

However, according to the manufacturer, the flanges we sourced for use in our pressure vessels have already been rated by the manufacturer for a maximum of 600[psig] at 72[°F], or 300[psig] at 360[°F]. As such, to be safe the highest pressure that should be used before any further investigation is 300[psig].

4.4 VIBRATION CALCULATIONS

Another major concern with this design was the potential for the rotating disc-shaft assembly to operate at its natural frequency. To check for this, shear and bending diagrams were first generated. These were based on this model of the shaft:

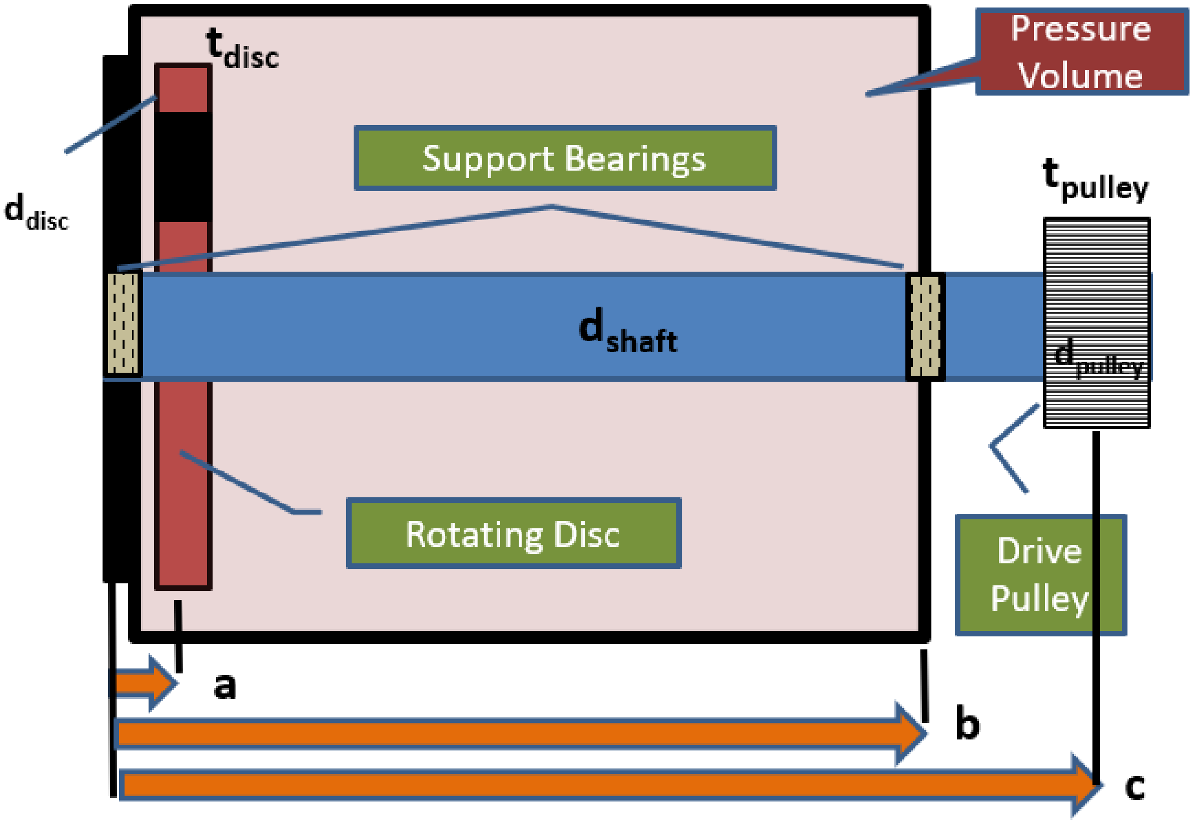

Figure 14: Model of Shaft

In this system, there are two effective point loads at the location of the drive pulley and the disc. These point loads represent the weight of the disc, and the force due to belt tension acting on the pulley. However, according to Juvinall[18], since the belts being used are timed and not tension belts, the force acting on the shaft is assumed to be negligible. There are also two reaction forces located at the bearings, which do not restrict the shaft from bending. As such, the free-body diagram of a shaft with its mass accounted for as a distributed load presents itself as:

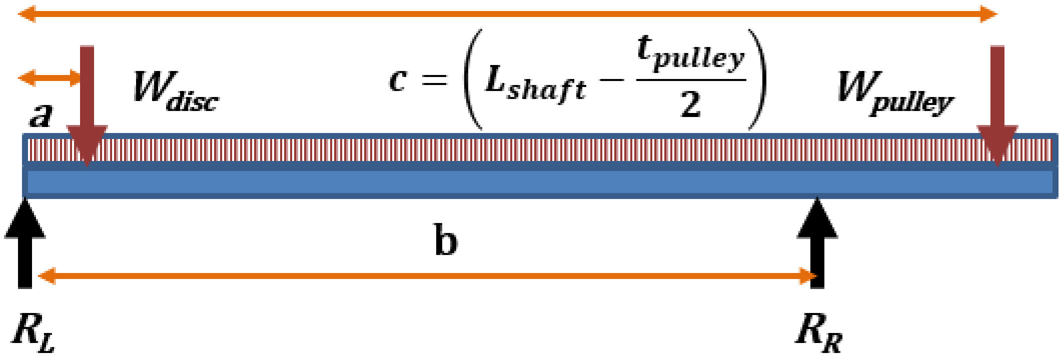

Figure 15: FBD of Shaft

Assuming the shaft is homogenous, the weight of the steel disc can be calculated using the equation:

$$W_{disc} = g\rho_{steel}\pi r_{disc}^2 t_{disc} \tag{3}$$

And the distributed load can be calculated using the equation:

$$U = g\rho_{steel}\pi r_{shaft}^2 \tag{4}$$

The weight of the pulley is calculated using its mass, which is a known quantity taken from the part information for the bushing-sprocket system. Using this information, the shear singularity function creating a singularity function for the system can be written as:

$$V(x) = R_L < x >^0 - W_{disc} < x - a >^0 + R_R < x - b >^0 - W_{pulley} < x - c >^0 - U < x >^1 \tag{5}$$

Integrating this function once yields the moment singularity function. This is written as:

$$M(x) = R_L < x >^1 - W_{disc} < x - a >^1 + R_R < x - b >^1 - W_{pulley} < x - c >^1 - \frac{U}{2} < x >^2 + C_1 \tag{6}$$

Where C_1 is the integration constant. To resolve this constant, we need to first determine the position at which there is no moment in the system. Since we assume that the bearings are only simply supported and are free to pivot slightly in place, we can assume that there is no bending moment at these locations. As such, by setting equation (6) to 0 at x=0, we find:

$$M(0) = 0 = R_L < 0 >^1 - W_{disc} < 0 - a >^1 + R_R < 0 - b >^1 - W_{pulley} < 0 - c >^1 - \frac{U}{2} < 0 >^2 + C_1 \quad (7)$$

This results in all terms except for the integration constant canceling out, which sets $C_1=0$, allowing it to be ignored.

Next, integrating the moment singularity function yields the function:

$$E_{steel} I_{shaft} \Theta(x) = \int M(x)dx \tag{8}$$

Which can be rewritten to solve for the angular displacement $\Theta(x)$ to determine the angular displacement singularity function:

$$\Theta(x) = \frac{1}{E_{steel} I_{shaft}} \begin{pmatrix} \frac{R_L}{2} < x >^2 - \frac{W_{disc}}{2} < x - a >^2 + \frac{R_R}{2} < x - b >^2 \\ - \frac{W_{pulley}}{2} < x - c >^2 - \frac{U}{6} < x >^3 + C_2 \end{pmatrix} \tag{9}$$

Where C_2 is the integration constant due to the angular position integral. Integrating once more and negating the equation finally yields us the beam deflection singularity function:

$$\delta(x) = -\frac{1}{E_{steel} I_{shaft}} \begin{pmatrix} \frac{R_L}{6} < x >^3 - \frac{W_{disc}}{6} < x - a >^3 + \frac{R_R}{6} < x - b >^3 \\ - \frac{W_{pulley}}{6} < x - c >^3 - \frac{U}{24} < x >^4 + C_2 x + C_3 \end{pmatrix} \tag{10}$$

Where C_3 is the integration constant due to the deflection integral. To determine the values for the integration constants we need to first assume that there is no deflection in the shaft at the bearing sites. First, setting eqn. 10 to 0 at x=0 yields:

$$\delta(0) = 0 = -\frac{1}{E_{steel}I_{shaft}}\begin{pmatrix}\frac{R_L}{6} < 0 >^3 - \frac{W_{disc}}{6} < 0 - a >^3 + \frac{R_R}{6} < 0 - b >^3 \\ -\frac{W_{pulley}}{6} < 0 - c >^3 - \frac{U}{24} < 0 >^4 + C_2 0 + C_3\end{pmatrix} \quad (11)$$

This resolves to $C_3 = 0$, allowing us to eliminate the term from the beam deflection singularity function. Next, we set the set eqn. 10 to 0 at x=b to yield:

$$\delta(b) = 0 = -\frac{1}{E_{steel}I_{shaft}}\begin{pmatrix}\frac{R_L}{6} < b >^3 - \frac{W_{disc}}{6} < b - a >^3 + \frac{R_R}{6} < b - b >^3 - \frac{W_{pulley}}{6} < b - c >^3 - \\ \frac{U}{24} < b >^4 + C_2 b\end{pmatrix} \quad (12)$$

This simplifies the equation into:

$$\delta(b) = 0 = -\frac{1}{E_{steel}I_{shaft}}\left(\frac{R_L}{6} < b >^3 - \frac{W_{disc}}{6} < b - a >^3 - \frac{U}{24} < b >^4 + C_2 b\right) \quad (13)$$

Solving for the integration constant C_2 yields the equation:

$$C_2 = \frac{-R_L}{6} < b >^2 + \frac{W_{disc}}{6b} < b - a >^3 + \frac{U}{24} < b >^3 \quad (14)$$

As such, the generalized beam deflection singularity function is written in the form:

$$\delta(x) = -\frac{1}{E_{steel}I_{shaft}}\begin{pmatrix}\frac{R_L}{6} < x >^3 - \frac{W_{disc}}{6} < x - a >^3 + \frac{R_R}{6} < x - b >^3 - \frac{W_{pulley}}{6} < x - c >^3 \\ -\frac{U}{24} < x >^4 + (\frac{-R_L}{6} < b >^2 + \frac{W_{disc}}{6b} < b - a >^3 + \frac{U}{24} < b >^3)x\end{pmatrix} \quad (15)$$

Before we can generate the beam deflection curve using eqn. 15 above, we first need to determine the reaction forces R_L and R_R. We do this by first taking the Free-Body Diagram in Fig. 15 and creating an equivalent force for the distributed load representing the weight of the rotating shaft. This equivalent force, which is applied at the middle of the beam $(0.5 * L_{shaft})$, is determined via the equation:

$$W_{shaft} = \; g\rho_{steel}\pi r_{shaft}^2 L_{shaft} \tag{16}$$

Next, we can take the moment equilibrium equation about the point x=0, which eliminates R_L and yields the equation:

$$M_0 = 0 = -W_{disk}a - W_{shaft}(0.5L_{shaft}) + R_R b - W_{pulley}c \tag{17}$$

Since all values in this equation except for R_R are known, this can be rewritten as:

$$R_R = \frac{W_{disk}a + W_{shaft}(0.5L_{shaft}) + W_{pulley}c}{b} \tag{18}$$

To determine the reaction force R_L, we simply need to create a force equilibrium equation in the y-direction, which yields the following:

$$\Sigma F_y = 0 = R_L - W_{shaft} - W_{disk} + R_R - W_{pulley} \tag{19}$$

Which is simply rewritten into the equation:

$$R_L = W_{shaft} + W_{disk} - R_R + W_{pulley} \tag{20}$$

The reaction forces are substituted back into eqn. 15 to create the full beam deflection diagram. The values in Table 1 were used to generate the deflection curve for the system.

Table 1: Values for Deflection Curve Generation

Variable [unit]	Value
$\rho_{steel}\ \left[\frac{kg}{m^3}\right]$	8000
$r_{shaft}\ [m]$	0.025
$L_{shaft}\ [m]$	0.3810
$E_{steel}\ [GPa]$	193
$I_{shaft}\ [m^4]$	1.9175e-08
$r_{disc}\ [m]$	0.0125
$t_{disc}\ [m]$	0.0127
$a\ [m]$	0.0235
$b\ [m]$	0.2745
$c\ [m]$	0.3588

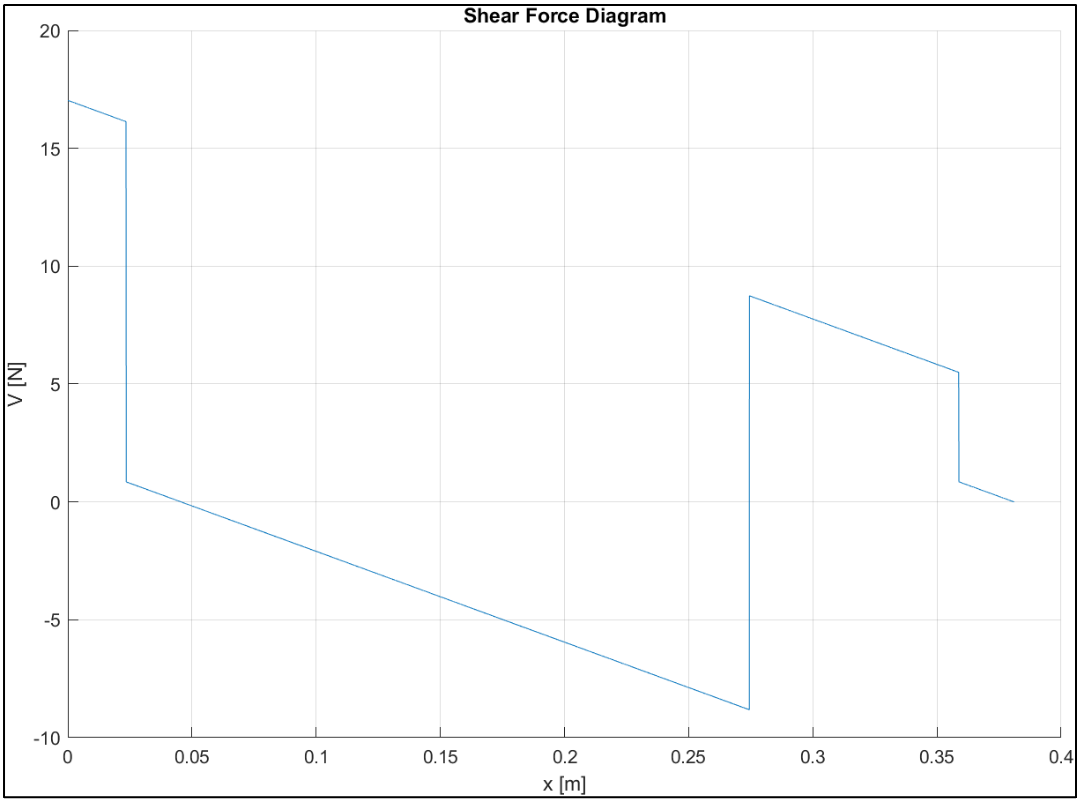

Figure 16: Shear Force Diagram for Rotating Shafts

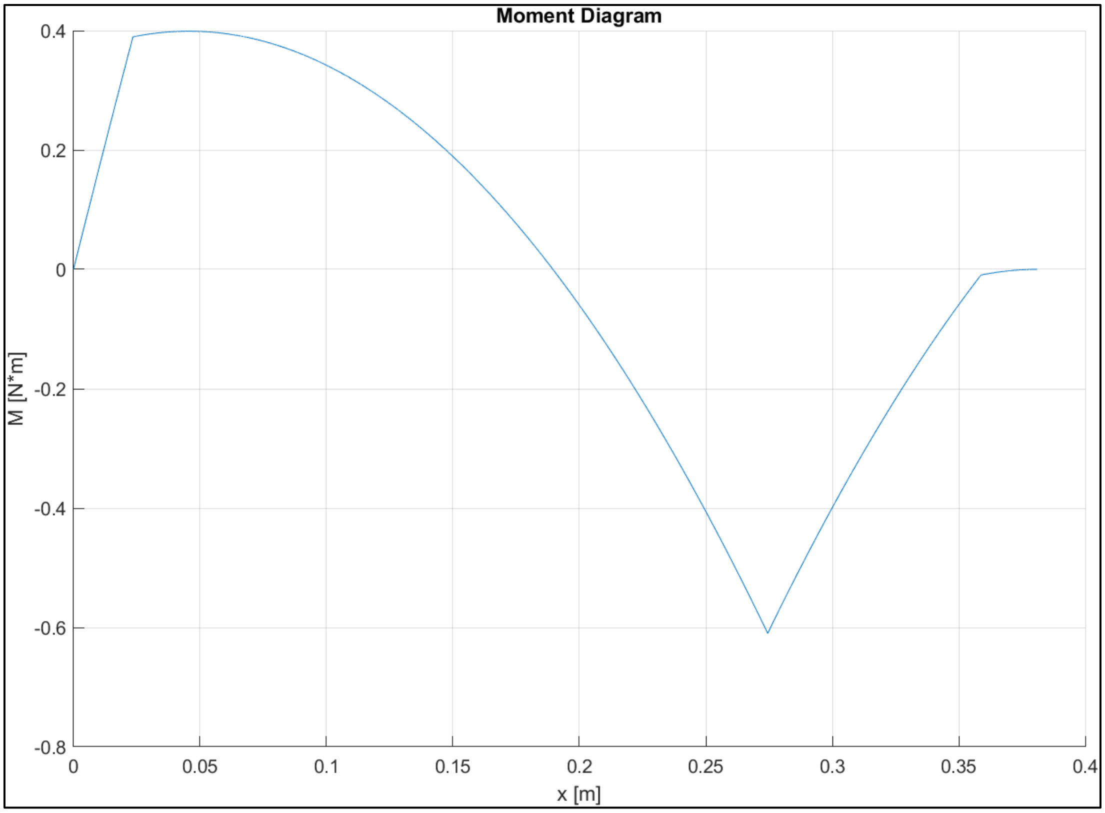

Figure 17: Moment Diagram for Rotating Shafts

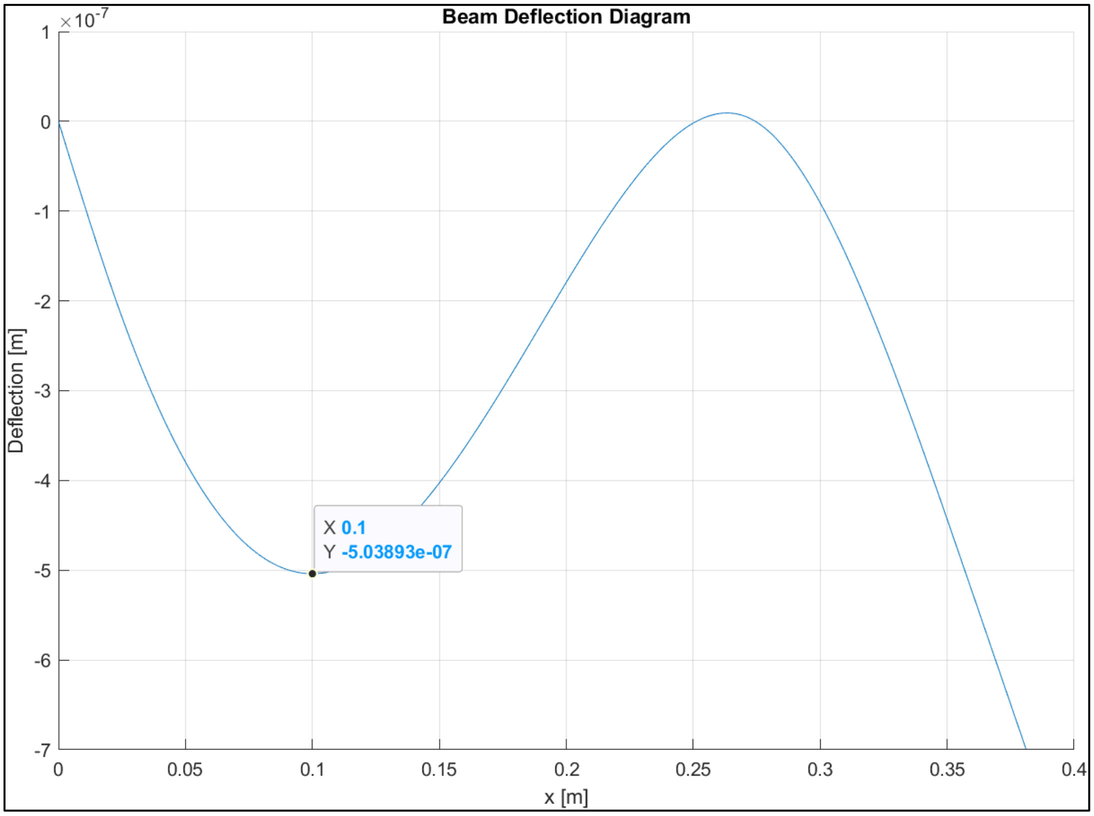

Figure 18: Beam Deflection Diagram for Rotating Shafts

By iterating the beam deflection singularity function along the length of the beam, we were able to generate the beam deflection diagram in Fig. 18. From this diagram, at the point x = 0.1 [m] the maximum deflection between the rotating bearings is $5.03893*10^{-7}$ [m]. These results generally match those found while using SkyCiv's beam deflection calculator. The shear, moment, and deflection diagrams in Fig. 16, Fig. 17, and Fig. 18 from the singularity functions are generally similar to those found by SkyCiv in Fig, 19, Fig. 20, and Fig. 21 respectively.

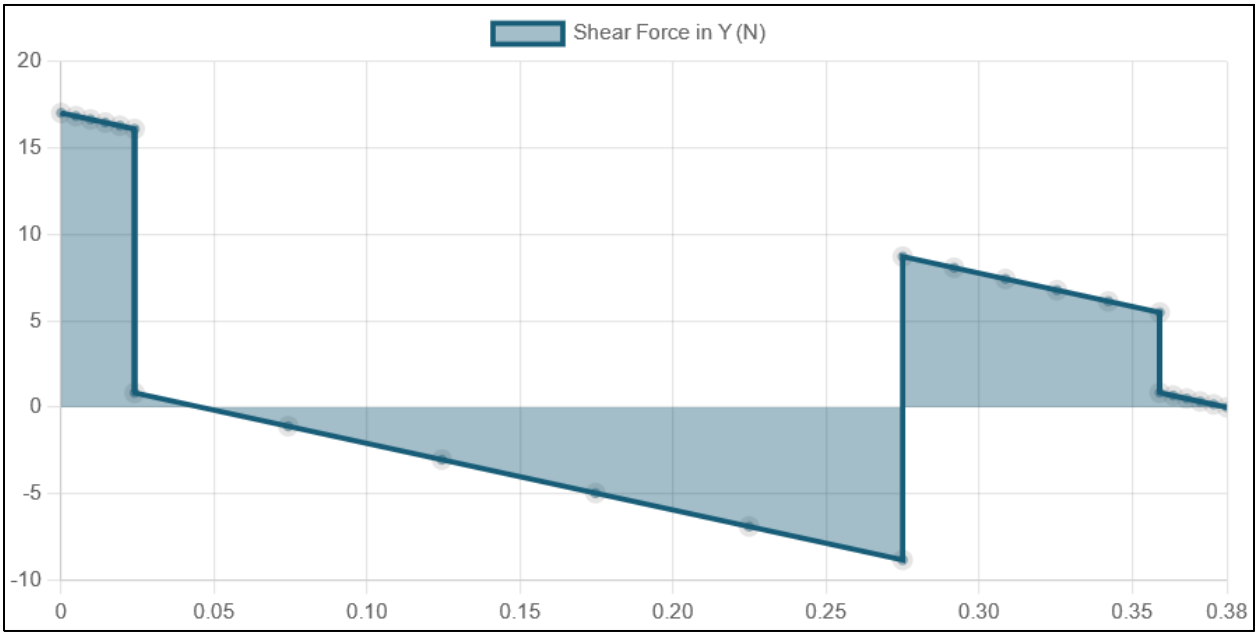

Figure 19: SkyCiv Shear Diagram of Shaft[19]

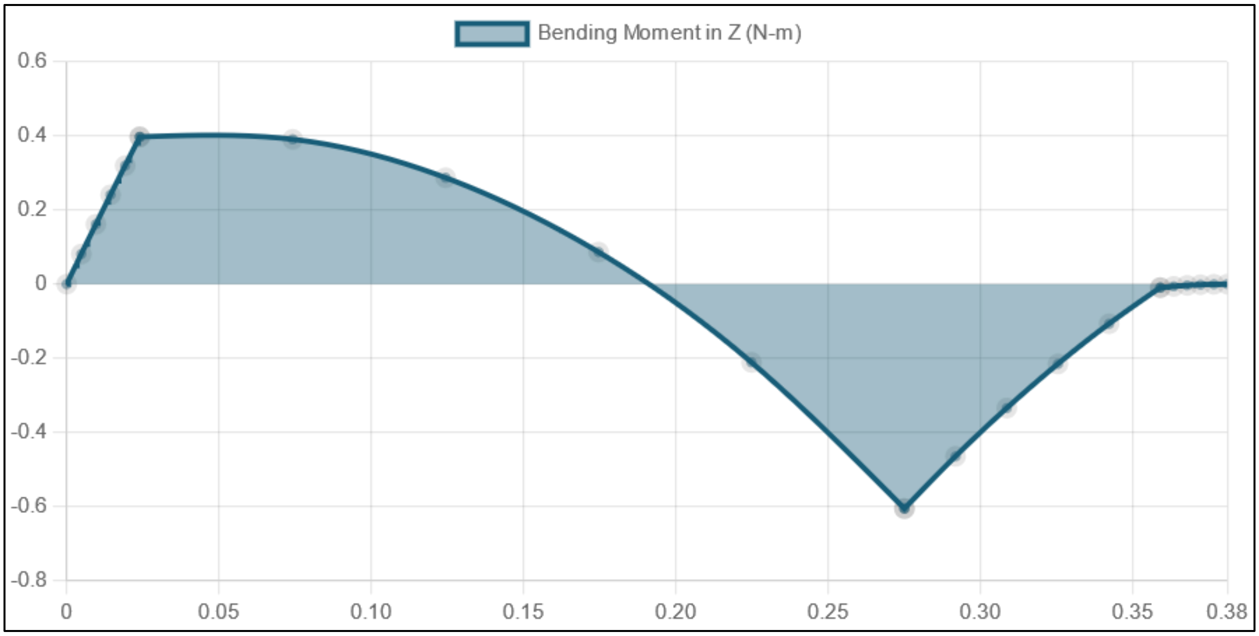

Figure 20: SkyCiv Moment Diagram of Shaft[19]

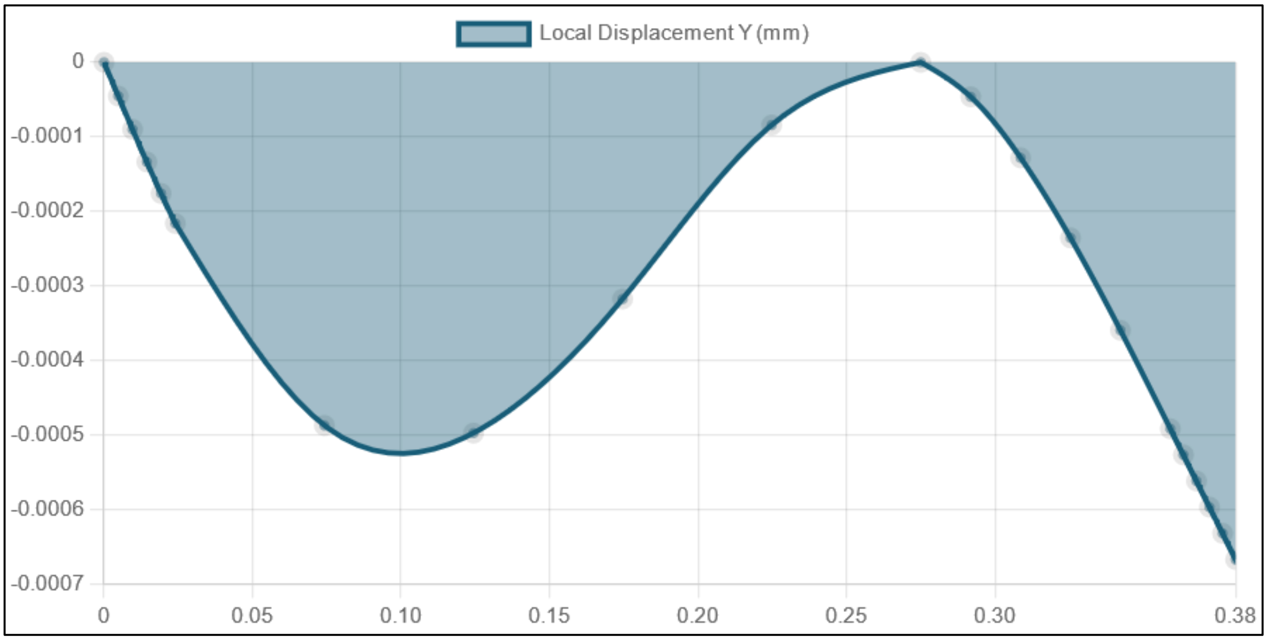

Figure 21: SkyCiv Beam Deflection Diagram of Shaft[19]

The critical speed of a rotating body is the rotational velocity at which the body is rotating at its natural frequency. According to Juvinall, the critical speed of a rotating shaft with only rod mass can be approximated as[18]:

$$n_c = \frac{30}{\pi}\omega_n = \frac{30}{\pi}\sqrt{\frac{k_{shaft}}{m_{disc}}} \tag{21}$$

Where the spring constant of the shaft k_{shaft}, is calculated from:

$$k_{shaft} = \frac{W_{disc}}{\delta_{max}} \tag{22}$$

And the mass of the disc can be rewritten as

$$m_{disc} = \frac{W_{disc}}{g} \tag{23}$$

Plugging these into eqn. 7 yields the equation:

$$n_c = \frac{30}{\pi}\sqrt{\frac{W_{disc}g}{W_{disc}\delta_{max}}} = \frac{30}{\pi}\sqrt{\frac{W_{disc}}{W_{disc}}}\sqrt{\frac{g}{\delta_{max}}} = \frac{30}{\pi}\sqrt{\frac{g}{\delta_{max}}} \tag{24}$$

Which calculates out to a critical speed of 42134[RPM].

At 100[Hz] actuation, with three holes in our rotating discs, we only need to drive the shaft at 33.333[Hz]. Converting this to RPM gives us a shaft speed of 2000[RPM], which is well below the critical speed of both the shaft alone and the shaft-disc system. When running tests during normal operation, it will still be important to monitor the vibratory characteristics of the system. This calculation assumes the location of the extra mass is negligible so long as it is between the two pinned locations on the beam.

4.5 BOLT FATIGUE CALCULATIONS

Due to the cyclical nature of the pressures within each of the vessels over long periods, one concern in this design is the potential for fatigue failure in the bolts holding pressure vessels and plates together. To determine whether the bolts would fatigue throughout their lifetime, we used the Modified-Goodman approach [16]. This is governed by the equation:

$$\frac{\sigma_a}{\sigma_e} + \frac{\sigma_m}{\sigma_{ut}} = \frac{1}{n} \tag{25}$$

Where the alternating stress is calculated using:

$$\sigma_a = \frac{\sigma_{high} - \sigma_{low}}{2} \tag{26}$$

And the mean stress is calculated using:

$$\sigma_m = \frac{\sigma_{high} + \sigma_{low}}{2} \tag{27}$$

For the high-pressure vessel, we assume that the pressure within the vessel will not deviate more than 20[psig] below the targeted pressure of 100[psig]. Since the alternating stresses need to be calculated for the stress seen by the bolt and not just the cycling pressure inside the vessel, we first need to determine the load on the bolt. This is calculated by the equation:

$$F_{Bolt} = \frac{\sigma_{pressure} * A_{Plate}}{\# \, Bolts} \tag{28}$$

Where A_{Plate} is defined by the area of the section of the faceplate that is being subjected to increased pressure relative to ambient. This is calculated using:

$$A_{Plate} = \pi r_{Tube}^2 = \pi * (3in)^2 = 9\pi \ [in^2] \tag{29}$$

With this, the forces seen by the bolts for internal vessel pressures of 100[psig] and 80[psig], are 235.6194 [lbf] and 188.4956[lbf] respectively. These bolts are 3/4”-10 UNC with a known cross-sectional area of 0.302 [in^2]. Using these values and the equation:

$$\sigma_{Bolt} = \frac{F_{Bolt}}{A_{Bolt}} \tag{30}$$

The values of the high- and low-end bolt stresses calculate out to 780.2 [psi] and 624.2 [psi] respectively. Plugging these stresses into eqns. 26 and 27 allows us to determine the alternating and mean stresses to be 18.1 [psi] and 702.2 [psi] respectively. Rewriting eqn. 25 to solve for the minimum allowable endurance limit σ_e yields the equation:

$$\sigma_e = \frac{\sigma_a}{\frac{1}{n} - \frac{\sigma_m}{\sigma_{ut}}} \tag{31}$$

With a factor of safety at n = 3 and 304 stainless steel bolts with an ultimate stress of 73.2[kpsi][17], this provides an allowable endurance limit of 3.1685 [kpsi].

However, while this is a minimum allowable endurance limit according to design parameters, this does not represent the true endurance limit of the bolt. The rotational endurance limit of the bolts can be considered a derivation of the endurance limit of steels. It is known to be:

$$\sigma_e{}' = \begin{cases} 0.504\sigma_{ut} & \sigma_{ut} \leq 200[kpsi] \\ 100[kpsi] & \sigma_{ut} > 200[kpsi] \end{cases} \tag{32}$$

The bolts we selected for use in the testbed are medium-strength steel meant for structural applications, with a rated ultimate stress of 120 [kpsi]. As this is below 200[kpsi], the rotating endurance limit calculates out to 60.48 [kpsi]. From this, the true machine element endurance limit can be determined by multiplying the Marin Factors by the rotating element endurance limit[16].

$$\sigma_{e_{true}} = k_a k_b k_c k_d k_e k_f \sigma_e' \tag{33}$$

k_a is the surface factor, which is calculated using:

$$k_a = a\sigma_{ut}^{b} \tag{34}$$

a and b are coefficients which are determined from the table below.

Table 2: Parameters for Marin Surface Factor (k_a)

	Factor a		
Surface Finish	S_{ut} [kpsi]	S_{ut} [MPa]	Factor b
Ground	1.34	1.58	-0.085
Machined/Cold-Drawn	2.7	4.51	-0.265
Hot-Rolled	14.4	57.7	-0.718
As-Forged	39.9	272	-0.995

Since the bolts are machined when they are tapped to create the thread, we select the values in the second row, allowing us to calculate a surface factor of 0.7592 [-].

k_b is the size factor. Since the bolts will not be rotating in the system, this is set to 1 [-].

k_c is the loading factor. Depending on whether the loading on the bolt is bending, axial, or torsional, this value can be set to either 1, 0.85, or 0.59 respectively. Since the bolts are assumed to only be affected by cyclical loading in the axial direction, k_c is set to 0.85.

k_d is the temperature factor. Normally, this is calculated by the 4th Order equation:

$$k_d = 0.975 + 0.432(10^{-3})T_F - 0.115(10^{-5})T_F^2 + 0.104(10^{-8})T_F^3 - 0.595(10^{-12})T_F^4 \quad (35)$$

However, since the operating temperature is assumed to be at room temperature, k_d is set to 1 [-].

k_e is the reliability factor and is dependent on the desired reliability of the system.

Table 3: Parameters for Marin Reliability Factor (k_e)

Reliability %	Transformation Variate z_a	Reliability Factor k_e
50	0.000	1.000
90	1.288	0.897
95	1.645	0.868
99	2.326	0.814
99.9	3.091	0.753
99.99	3.719	0.702
99.999	4.265	0.659
99.9999	4.753	0.620

Since this system is intended to run for weeks or possibly months at a time, higher reliability is preferable. As such, the reliability of the bolts is chosen to be 99.9999%, which sets k_e to 0.620 [-].

Finally, k_f is the miscellaneous factor and is meant to consider any irregularities, conditioning, or other modifications made to the inspected machine element. Since this factor is entirely empirical and the manufacturer gave no indication of any abnormalities in the screws, this factor is ignored.

Multiplying the rotating element endurance limit by the determined Marin Factors yields a true machine element endurance limit of 24.20 [kpsi]. Rewriting the Modified-Goodman equation to calculate for factor of safety yields:

$$n = \frac{1}{\frac{\sigma_a}{\sigma_{e,true}} + \frac{\sigma_m}{\sigma_{ut}}} \tag{36}$$

Plugging in for the known values yields a factor of safety of 110. This is well beyond the minimum desired value of 3 and as such, well within acceptable bounds for this design.

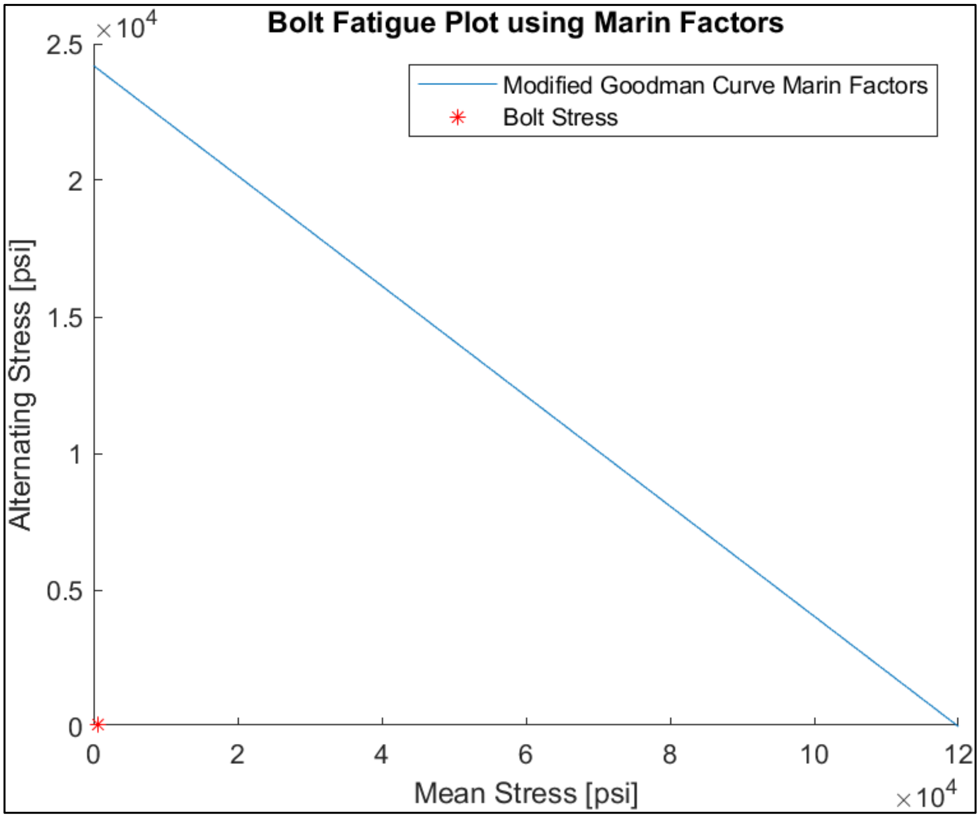

Figure 22: Bolt Fatigue Plot using Calculated True Endurance Limit

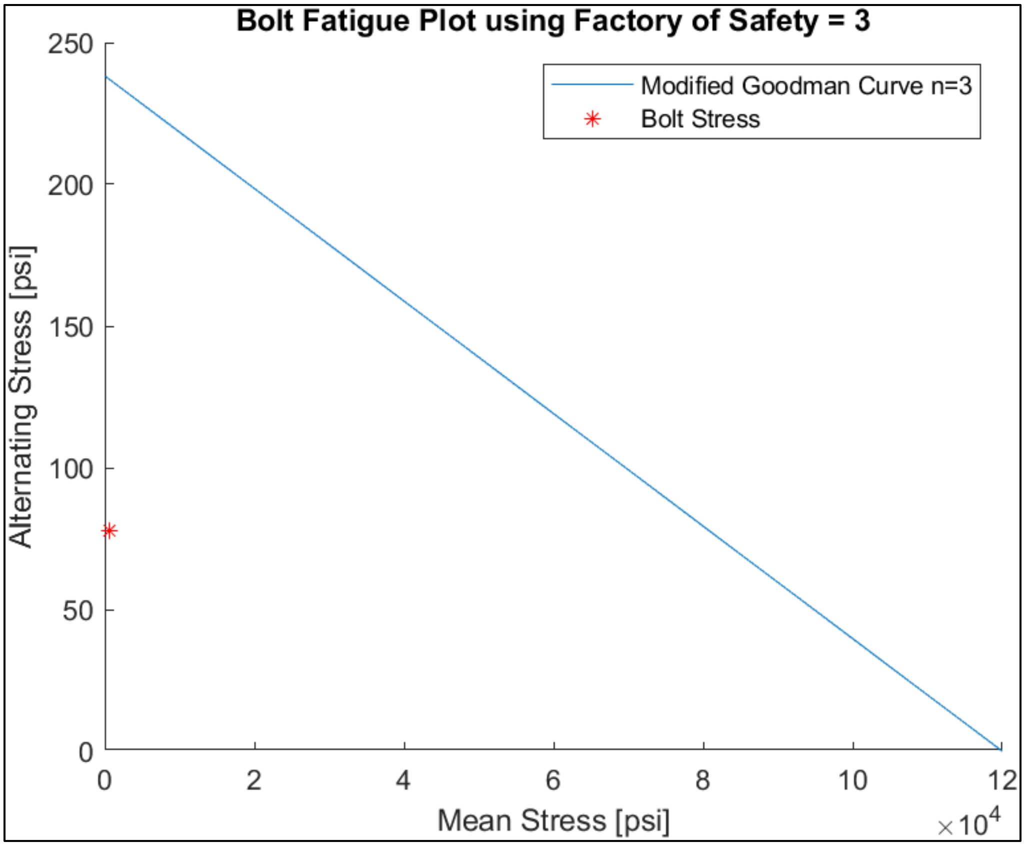

Figure 23: Bolt Fatigue Plot using Assumed n=3 Factor of Safety

As is clearly shown in Fig. 22 and Fig. 23, the Bolt Stresses lie well below the Modified-Goodman curve and as such, indicate an infinite lifetime for the bolts holding the flanges to the faceplates.

4.6 THERMAL EXPANSION CALCULATIONS

When designing systems that undergo substantial changes in temperature between idling and operation, one concern that needs to be addressed is the potential for components in the system to undergo thermal expansion. Currently, the system is designed to be run using room-temperature compressed air at 100[psig] of pressure. However, due to the rate at which the system will be cycling this air to achieve accelerated valve actuation, friction will likely cause the steady state operating temperature to be higher than ambient. This, coupled with a designed

10[thou] distance between the rotating disc and the manifold faceplate (Fig. 24), means that with enough of an increase in temperature, there may be interference between moving components which could lead to damage or possibly destruction of the system.

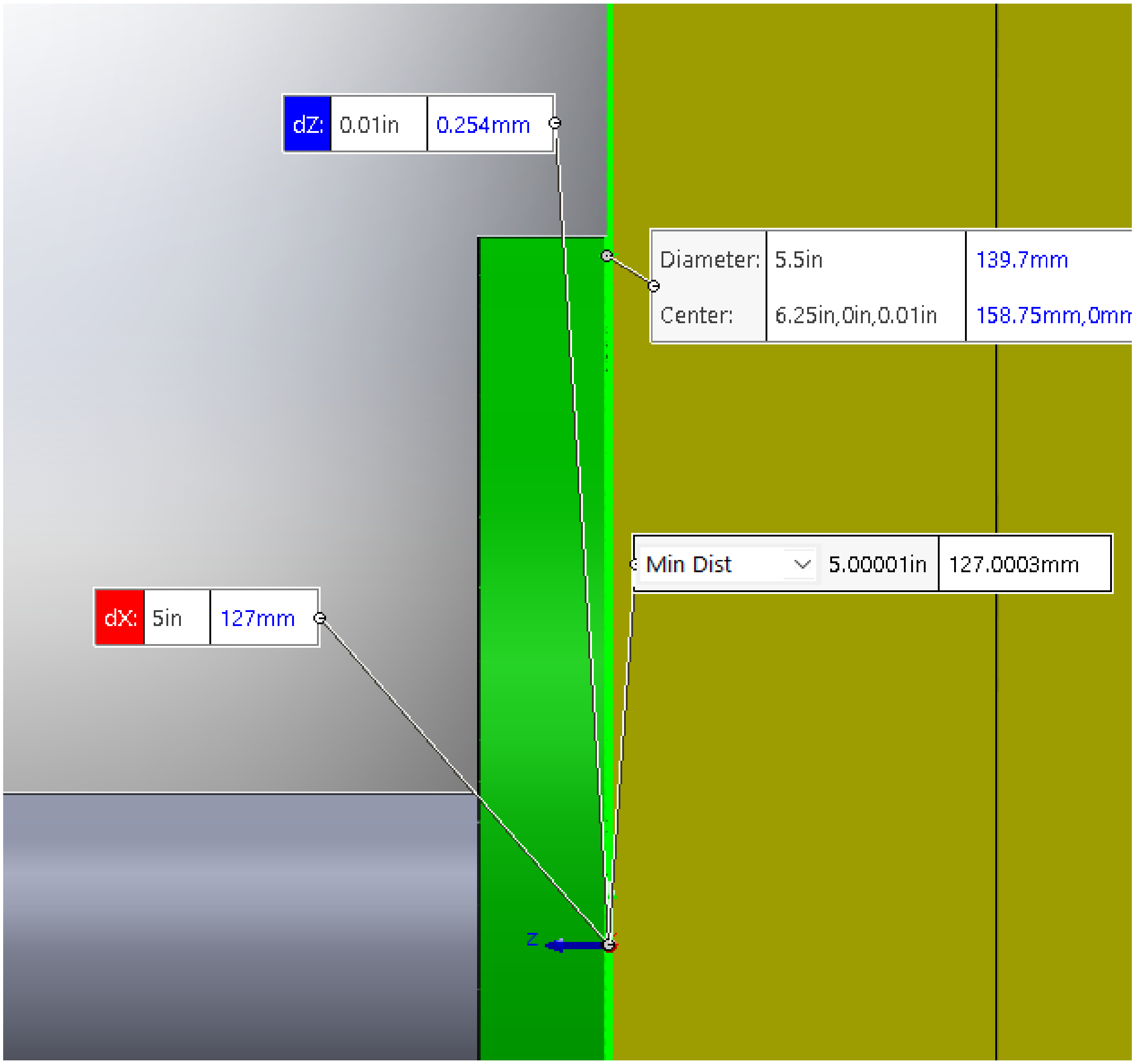

Figure 24: 10[thou] Gap Between Manifold Faceplate and Rotating Disc

In bodies where the temperature is increased at a uniform rate, the normal strain a component undergoes is defined by the equation[16]:

$$\epsilon_x = \epsilon_y = \epsilon_z = \alpha \Delta T \tag{37}$$

This equation implies that component normal strain in all directions due to thermal expansion is equal, meaning that bodies that are unconstrained by other components will expand at equal rates. As such, by rewriting strain in terms of the rate of the change of length along a given axis, eqn. 37 becomes:

$$\frac{\Delta L_x}{L_{x,0}} = \frac{\Delta L_y}{L_{y,0}} = \frac{\Delta L_z}{L_{z,0}} = \alpha \Delta T \qquad (38)$$

Which can further be rearranged into the equation:

$$\Delta L = L - L_0 = \alpha \Delta T L_0 \qquad (39)$$

Using a thermal expansion coefficient of $9.89 \frac{\mu\text{in}}{in°F}$ for 304 stainless steel and assuming the system starts at 68°F and linearly increases to 212°F (boiling point of water), we determine that the originally 0.5[in] thick rotating disc has a change in length of 7.071e-04 [in] or 0.7071 [thou]. This expansion is well below the 10 [thou] limit set by the designed gap seen in Fig. 24, which indicates that expansion is not an issue between these two components. Assuming the 1.5[in] thick manifold faceplate is free to expand inward towards the rotating disc (which it is not due to the pressure vessel bolted between the faceplates), it still only expands by 2.1e-03 [in] or 2 [thou], which added to the expansion from the rotating disc is still below the 10[thou] limit. We can determine the maximum allowable temperature for the system by rearranging eqn. 39 as:

$$T_f = \frac{\Delta L}{\alpha L_0} + T_0 \qquad (40)$$

Where $\Delta T = T_f - T_0$. By setting the initial length to 2[in] (a combination of the thickness of the manifold faceplate and the disc thickness) we find that the temperature at which these components will interfere with one another is 573.5612[°F], which is well above any temperature that the system will reasonably see without the installation of a heating element or the introduction of heated gas.

Another area of concern in the system is the difference in expansion rates between the rotating disc and the hardened steel shaft. The thermal expansion coefficient α is a material property, which means that systems with components comprised of different materials will have different expansion rates. This can lead to issues such as press-fit components with internal dimensions loosening if the expansion rate of the retaining component is higher than that of the pressed component. While all mating components within the lifetime accelerator are made of stainless steel, the rotating shaft is made of 440C case-hardened martensitic stainless steel which has an expansion coefficient of $5.67\,\frac{\mu\text{in}}{in°F}$ [20] compared to the coefficient of $9.89\,\frac{\mu\text{in}}{in°F}$ [17] for the 304 stainless steel disc. This means that the expansion rate for the rotating disc is roughly double that of the shaft. The thermal expansion equation in two dimensions is represented by the equation:

$$\Delta A = A - A_0 = 2\alpha\Delta T A_0 \tag{41}$$

Since the cross-section of the hole is circular, eqn. 41 can be rewritten as:

$$\pi r^2 - \pi r_0^2 = 2\pi r_0^2 \alpha\Delta T \tag{42}$$

Solving for the expanded radius r yields the equation:

$$r = r_0\sqrt{2\alpha\Delta T + 1} \tag{43}$$

Which written to find Δr yields:

$$\Delta r = r - r_0 = r_0\sqrt{2\alpha\Delta T + 1} - r_0 \ = r_0(\sqrt{2\alpha\Delta T + 1} - 1) \tag{44}$$

Assuming the same temperatures as above and an initial radius of 1.11[in], the expansion of the 304 stainless steel is 1.569e-03[in] or 1.6[thou] and the expansion for the 440C stainless steel is 8.996e-04 [in] or 0.8996[thou]. This is a difference of 0.7004 [thou], which is below the tolerance of roughly 1 to 2.5 [thou] typical in machined tolerance fits.

4.7 SEALING

In this system, there are three main methods of sealing the pressurized volumes from each other and atmospheric pressure. The first method used is simple rubber gaskets placed between interfaces that do not rely on high tolerance length dimensions such as the interface between the valve assembly retaining plates, the interface between the manifold volume and valve assembly retaining plates, the interface between the valve assembly retaining plates and the mid-pressure vessel, and the interface between the mid-pressure vessel and the endcap. These gasket seals are made from sheets of rubber with cutouts for bolt holes and internal radii, and all are 1/8 [in] thick.

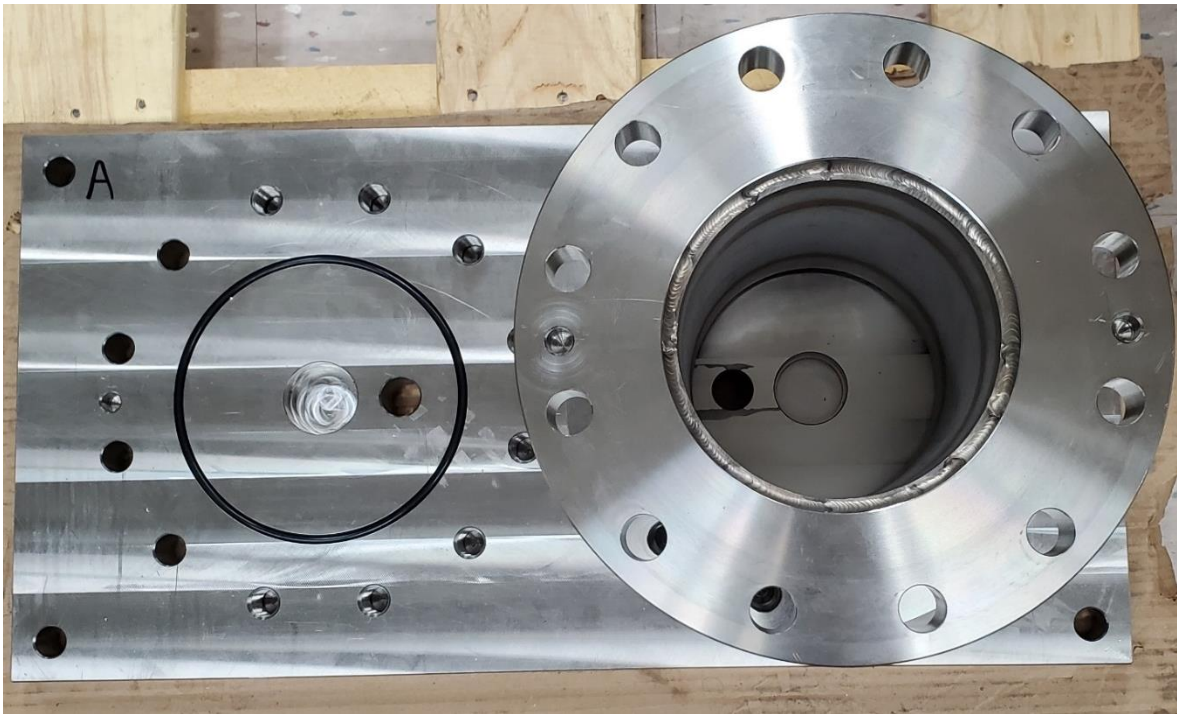

Figure 25: O-Ring and Flanged Pipe Side-By-Side

O-rings are placed between the interface of the high- and low-pressure pipe flanges and the manifold and front faceplates respectively. O-rings were selected for these interfaces mainly due to the dimensional sensitivity of the shafts and the bearings inside these volumes. When gaskets are tightened, they do not allow for surfaces on either side to contact each other. While this is acceptable when simply maintaining pressure is the only concern for the vessel, when there are high tolerance lateral dimensions such as the length of the shaft and how the bearings and shaft seals interface with the faceplates, it becomes necessary to be able to bolt components together reliably and repeatedly without any spacing between interfaces. O-rings can deform during tightening, allowing for the end of the pressure vessel pipe flanges to lie flush against the faceplates.

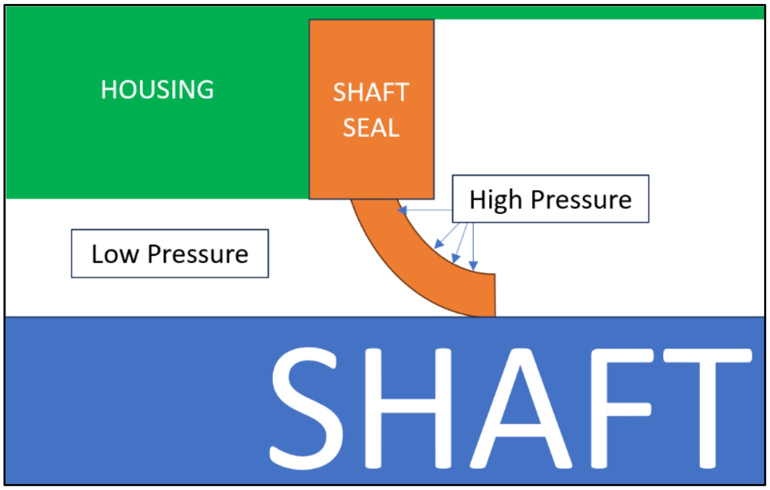

Figure 26: Diagram of Shaft Seal Function

The third type of seal that needed to be accounted for in the system was a rotary shaft seal. This seal is made of PTFE and designed for high-speed rotary systems. These seals were selected due to their durability, which coupled with the long runtimes this system is expected to undergo make them an ideal candidate for use. These seals function by holding a plastic lip along the rotating shaft that is folded inward in the direction of higher pressure. As the volume pressurizes, this lip is forced further against the shaft, sealing the volume while still allowing the rotating shaft to be accessible externally. A diagram of this is shown in Fig. 26.

5.0 ORIFICE FLOW SYSTEM MODEL

To determine whether the test rig would feasibly be able to attain a valve actuation rate of 100[Hz], we created a differential equation-based orifice flow system model. In this type of model, all holes through which gas is transferred are assumed to be square-edged thin-walled orifices.

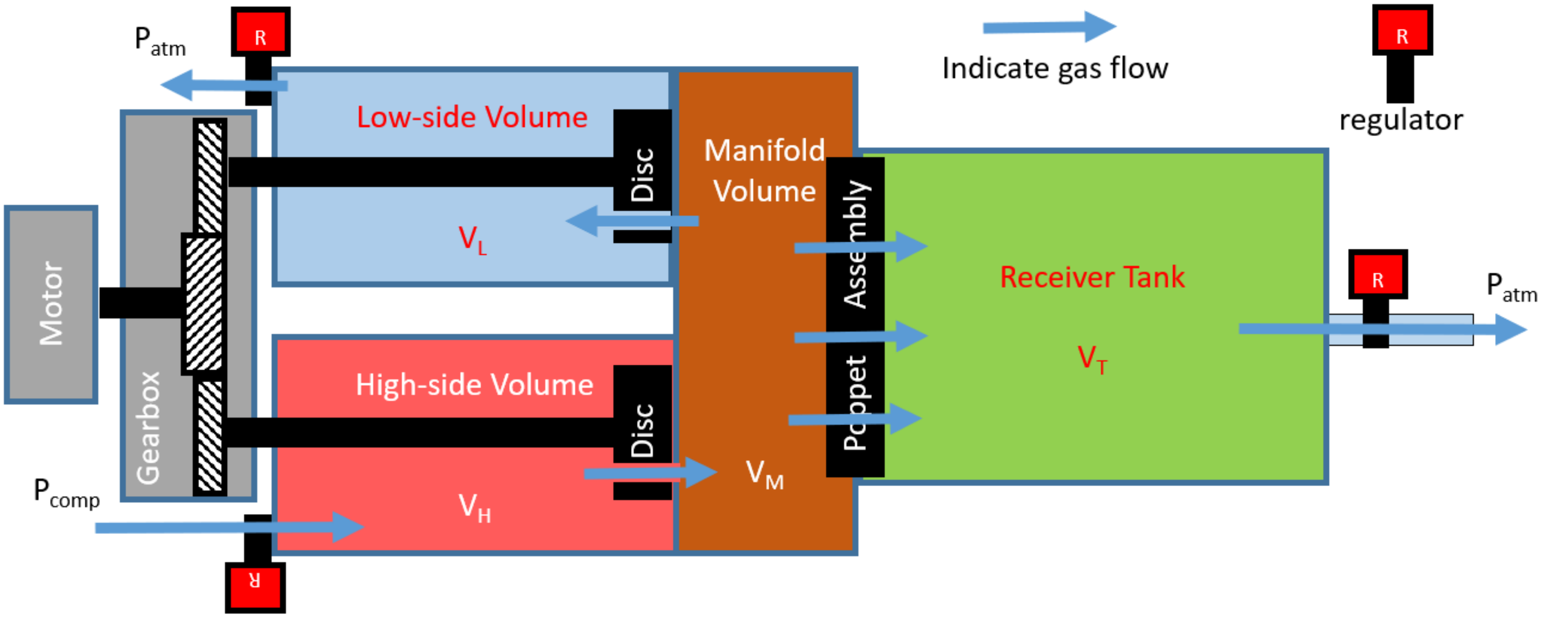

Figure 27: Orifice Flow Model Diagram

First, the model checks the percentage of a full disc rotation an opening will take up via the equation:

$$\%Open = \frac{\left(\frac{d}{r_{hole}}\right)}{2\pi} \tag{45}$$

This equation is calculated twice for the low-pressure vessel and high-pressure vessel discs respectively, and then used to determine the opening time each valve experiences via:

$$\boldsymbol{t}_{open} = \frac{\%Open}{f_{act}} \tag{46}$$

The opening time determines the length of time to run the opening displacement calculation for the poppet valves. After this, a profile of the orifice area relative to the rotational position is generated via a set of geometric equations.

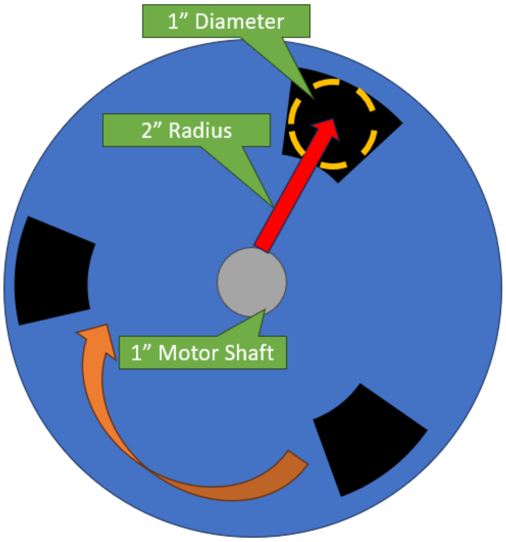

Figure 28: Rotating Disc Model

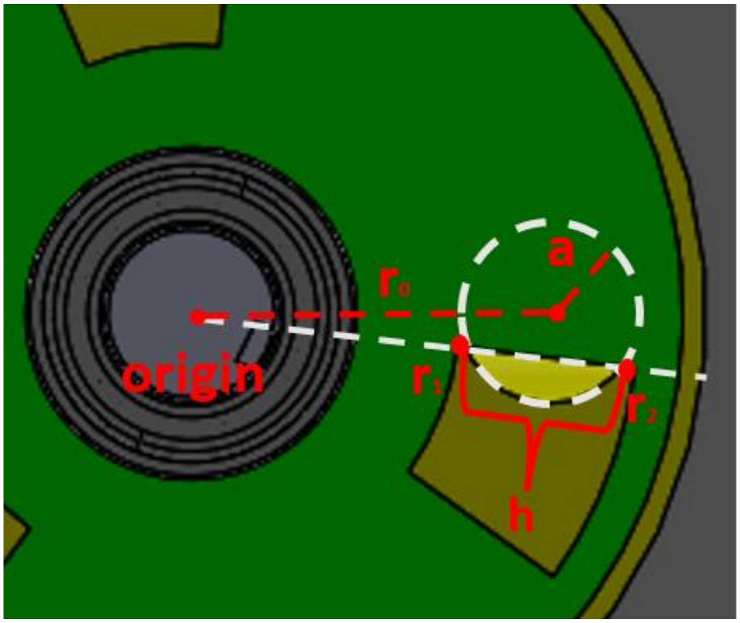

Figure 29: Hole Location Diagram

First, the location of the pass-through hole allowing gas to transfer between the high- or low-pressure volumes and the manifold volume is defined by the equation:

$$a^2 = r^2 + r_0^2 - 2rr_0\cos(\theta - \theta_0) \tag{47}$$

Which defines the position of a circle in polar coordinates, with a being the radius of the hole, r_0 being the radial distance from the origin, and Θ_0 being the rotational location of the hole.

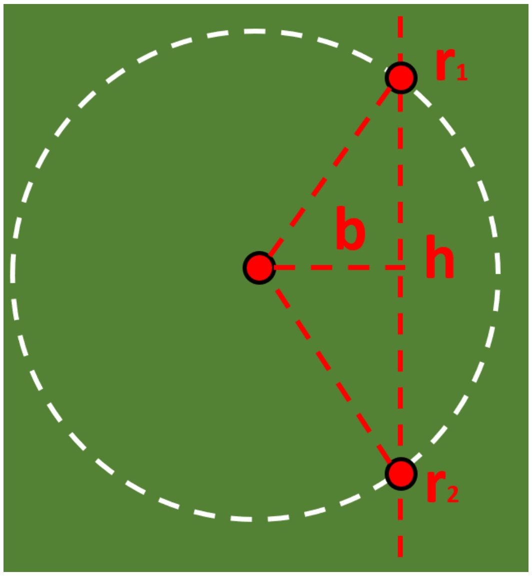

Figure 30: A_{tri} Diagram

Next, to determine the area of the opening orifice, the area of a circle segment is calculated using the equation:

$$A_{seg1} = A_{sect} - A_{tri} = \frac{\Theta_{sect}}{360°}\pi a^2 - \frac{1}{2}bh \tag{48}$$

Where the area segment is calculated as the difference between the area of a circle sector and the area of an internal triangle. The height of the internal triangle h is defined by the intersection of two radii as a line passes over the circle as seen in Figure 30. This value changes as the disc rotates, getting larger until it intersects with the center of the hole at a maximum value of 1[in]. To calculate this value, taking eqn. 47 and rearranging it into the general form of a quadratic function yields:

$$0 = r^2 - (2r_0\cos(\Theta - \Theta_0))\,r + ({r_0}^2 - a^2) \tag{49}$$

In this equation, the angular displacement is a known quantity that changers as the disc rotates, and the placement and geometry of the pass-through hole define all other constants, leaving just the radius r as the sole variable.

By finding the roots of this polynomial for a given angular displacement, the height of the triangle h is calculated as:

$$h = r_2 - r_1 \tag{50}$$

The base of the triangle b is derived from the deconstruction of the isosceles internal triangle into two right triangles as seen below in Figure 31.

From here, simply using the Pythagorean theorem allows for the base of the triangle to be calculated as:

$$b = \sqrt{a^2 - 0.25h^2} \tag{51}$$

Next, the angular width of the sector Θ_{sect} is determined by taking this same triangle and recognizing that:

$$\Theta_{sect} = 2\,\mathrm{asin}\left(\frac{0.5h}{a}\right) \tag{52}$$

Where the arcsine is doubled to account for the initial isosceles triangle being split into two identical and mirrored right triangles. Combining eqns. 48, 51, and 52 together yields:

$$A_{seg1} = \frac{\mathrm{asin}\left(\frac{0.5h}{a}\right)}{180°}\pi a^2 - \frac{1}{2}h\sqrt{a^2 - 0.25h^2} \tag{53}$$

Where h, which was derived in eqn. 50, iterates as the angular displacement iterates. After the value of h reaches its maximum value when the hole is exactly halfway exposed, the opening area equation is swapped, now being calculated as:

$$A_{seg2} = A_{hol} - (A_{sect} - A_{tri}) = \pi a^2 - \left(\frac{\mathrm{asin}\left(\frac{0.5h}{a}\right)}{180°}\pi a^2 - \frac{1}{2}h\sqrt{a^2 - 0.25h^2}\right) \tag{54}$$

This accounts for the fact that for the first half of the opening rotation, the area of the segment is the area that is exposed to the high-pressure volume and allowing gas to transfer through. Once this rotation passes the halfway point, the area of the segment now represents the remaining passthrough hole area that is still covered. Combined, the area calculations from eqns. 53 and 54 represent the orifice going from a fully closed to a fully open state. The table of the opening area for each angular position is then mirrored to simulate the passthrough hole going from a fully open to a fully closed state. Due to the design of the rotating disc, the passthrough hole is only fully exposed for an instant before closing begins. While this approach works for the current disc geometry, if the holes are lengthened to allow for longer opening times, some adjustments will need to be made. As currently configured, the easiest way to account for this would be generating a third data vector with the fully open hole area. Relating the length of this vector to the angular displacement and inserting it between the calculated opening and mirrored closing curves covers any such changes in the system.

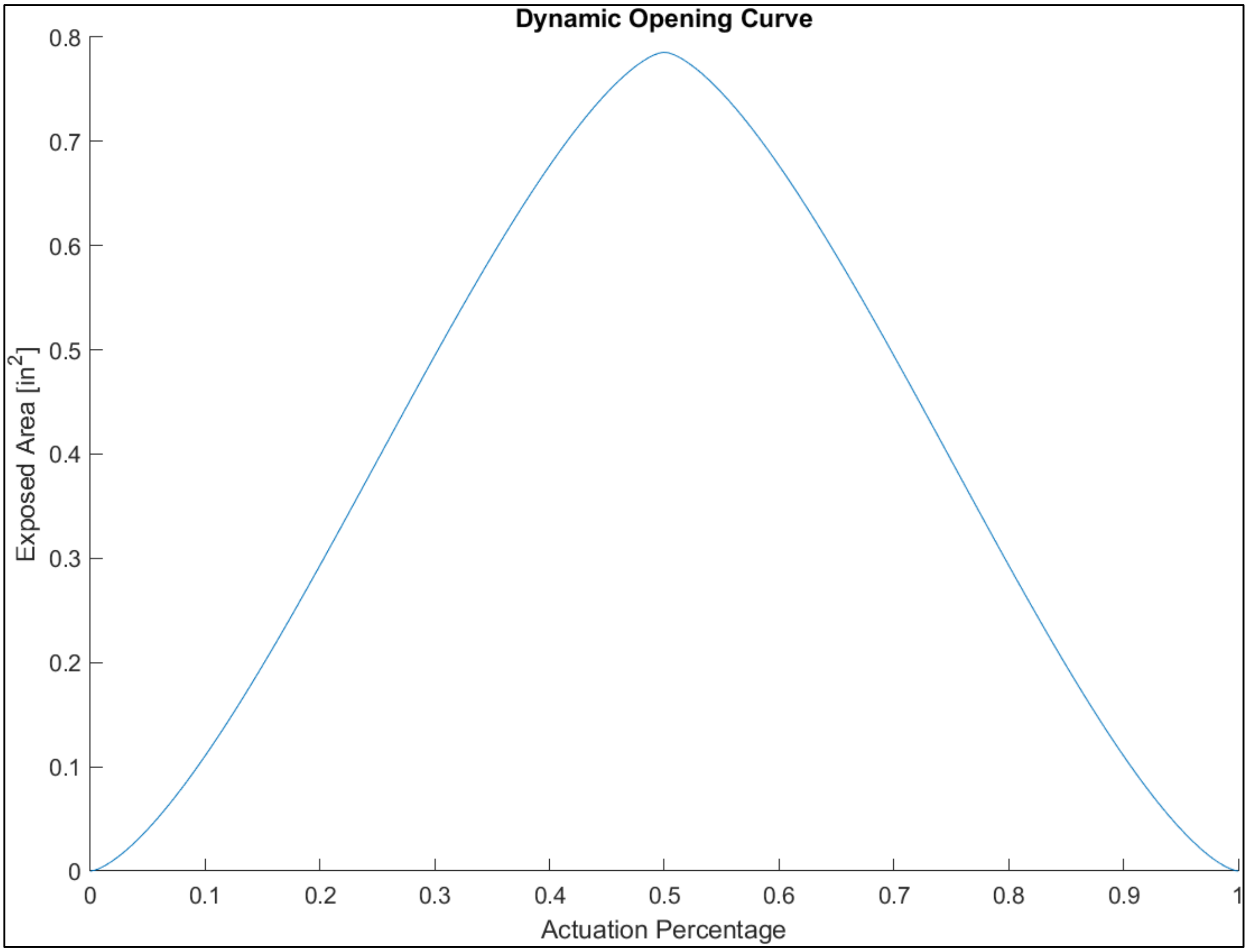

Figure 31: Opening Orifice Area Profile for Rotating Disc

From here, the opening profile is imported into the main model code, where it is then interpolated to fit within the length of the vector allocated towards the rotation opening event created using eqns. 53 and 54.

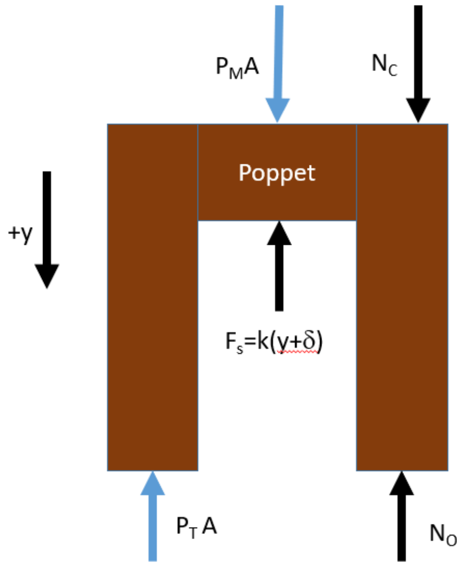

Figure 32: FBD of Poppet Valve

From Fig. 32, the displacement of the poppet is derived from the equations of motion based on the free-body diagram. In the y direction:

$$P_M A_p + N_C - F_s - P_T A_p + N_o = m\ddot{y} \tag{55}$$

Where the poppet spring force is:

$$F_s = k(y - \delta) \tag{56}$$

Since the poppet mass is small relative to the force due to pressure and the spring force, it can be assumed to be effectively zero. Further, when the poppet valve is in motion it loses contact with the valve seat. This in turn causes the normal forces on the poppet valve to cancel out. As such, the equation of motion for the poppet valve becomes:

$$-(P_T - P_M)A_p - k(y - \delta) = -\Delta P A_p - k(y - \delta) = 0 \tag{57}$$

Rearranging this to solve for displacement yields:

$$y = \frac{\Delta P A_p - k\delta}{k} \tag{58}$$

After the poppet displacement is calculated, the model then calculates mass transfer assuming orifice flows. With this assumption, unchoked orifice mass flow can be calculated from the equation:

$$\dot{\mathrm{m}} = C_d A \sqrt{\frac{2}{RT_u}} \sqrt{P_d(P_u - P_d)} \tag{59}$$

Where R is a constant based on the gas being transferred (air) and T_t is assumed to be constant at room temperature. However, the fluid will enter choked flow if the gas flow becomes supersonic, where:

$$P_{cr} = \frac{P_d}{P_u} = \left(\frac{2}{k+1}\right)^{\frac{k}{k-1}} \tag{60}$$

When this occurs, the mass flow is calculated using the equation:

$$\dot{\mathrm{m}} = C_d A \sqrt{\frac{2}{RT_u}} P_u \sqrt{P_{cr} - P_{cr}^2} \tag{61}$$

Opening events are simulated by taking these mass flow equations and changing the orifice area A based on the displacement of the poppet valve. A_{poppet} starts at zero when the valve displacement is zero which blocks any mass flow. As displacement increases, A_{poppet} is recalculated to reflect the increasing orifice size, resulting in an increasing mass flow through the orifice.

$$A_{poppet} = \pi d_{poppet} y \tag{62}$$

This represents the curved cylindrical surface area exposed by the motion of the poppet valve from its fully closed position.

Valve displacement then decreases once the differential pressure across the poppet valve is determined to be lower than the spring force acting on the poppet, causing $A_{poppet}$to decrease back down to zero. However, to account for the lack of a proper sealing mechanism between the rotating discs in the high- and low-pressure tanks, a leakage path with a gap of 10 [thou] was added to the model as an additional orifice.

In this model, the high-pressure and the manifold volume pressure are variable. The inlet pressure for the high-pressure vessel and the pressure inside mid-pressure vessel are assumed to be constant. This is due to the inlet pressure being provided by a constantly operating compressor, and the mid-pressure vessel's pressure being regulated by a backpressure regulator. Pressure is recalculated constantly in the high-pressure vessel, low-pressure vessel, and manifold volumes to model the proper gas dynamics in the system. By using the pneumatic capacitance approach, the change in pressure over time can be calculated using the equations:

$$\dot{\mathrm{P}}_{hi} = \frac{\left(\dot{\mathrm{m}}_{comp} - \dot{\mathrm{m}}_{hileak}\right)}{C_{hi}} \tag{63}$$

$$\dot{\mathrm{P}}_{man} = \frac{(\dot{\mathrm{m}}_{hi} + \dot{\mathrm{m}}_{hileak} - \dot{\mathrm{m}}_{lo})}{C_{man}} \tag{64}$$

$$\dot{P}_{lo} = \frac{(\dot{m}_{lo} + \dot{m}_{loleak} - \dot{m}_{outlet})}{C_{lo}} \tag{65}$$

Solving this series of coupled nonlinear differential equations yields pressures for each vessel of the model. Starting the inlet and high-pressure vessel pressures at 100[psig], the mid-pressure vessel pressure at 50[psig], and the low and manifold pressure vessels at atmospheric pressure, the results of the model for 30 rotations at a shaft speed of 100[Hz] are as follows:

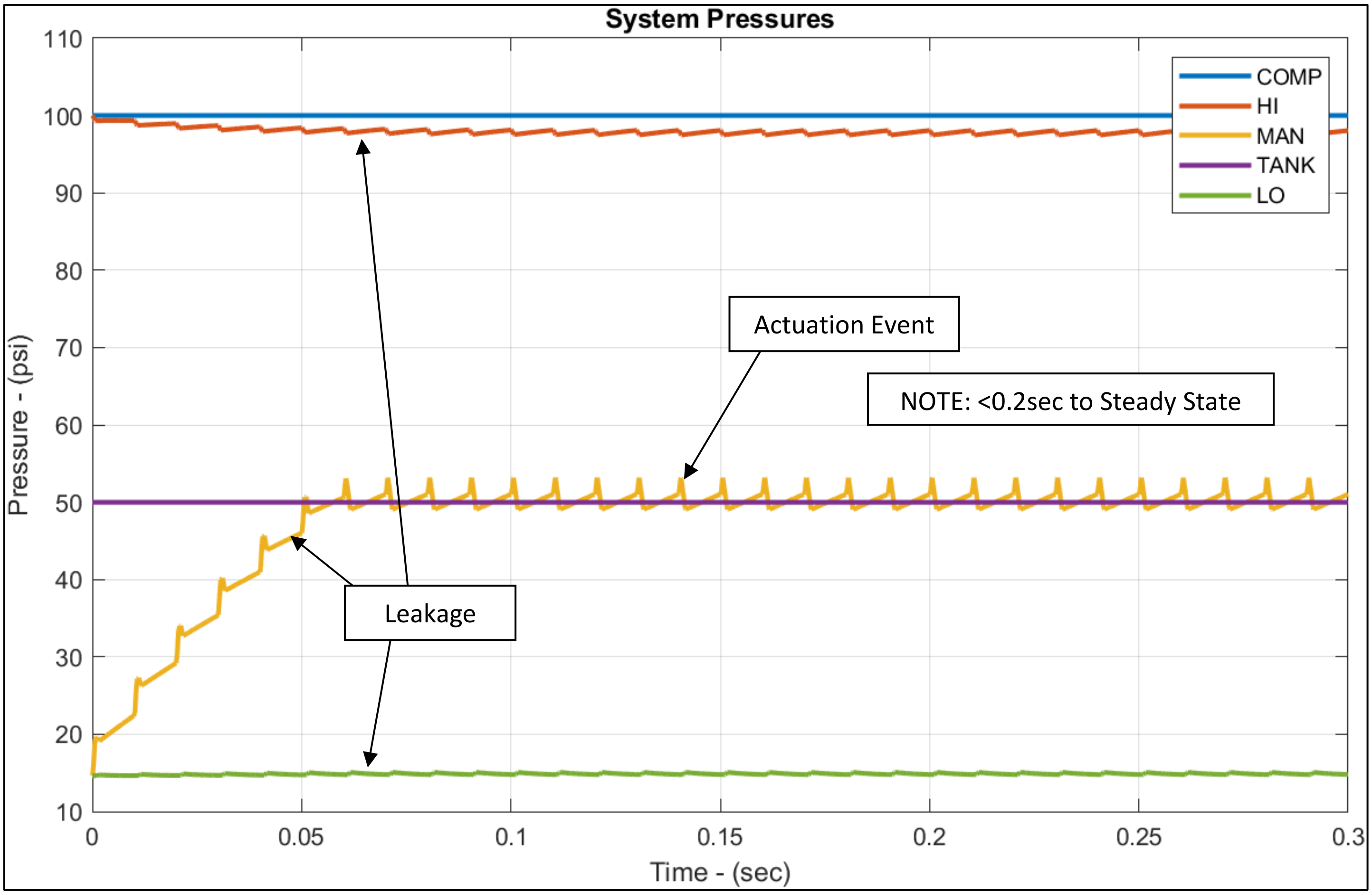

Figure 33 – Orifice Flow Model System Pressures

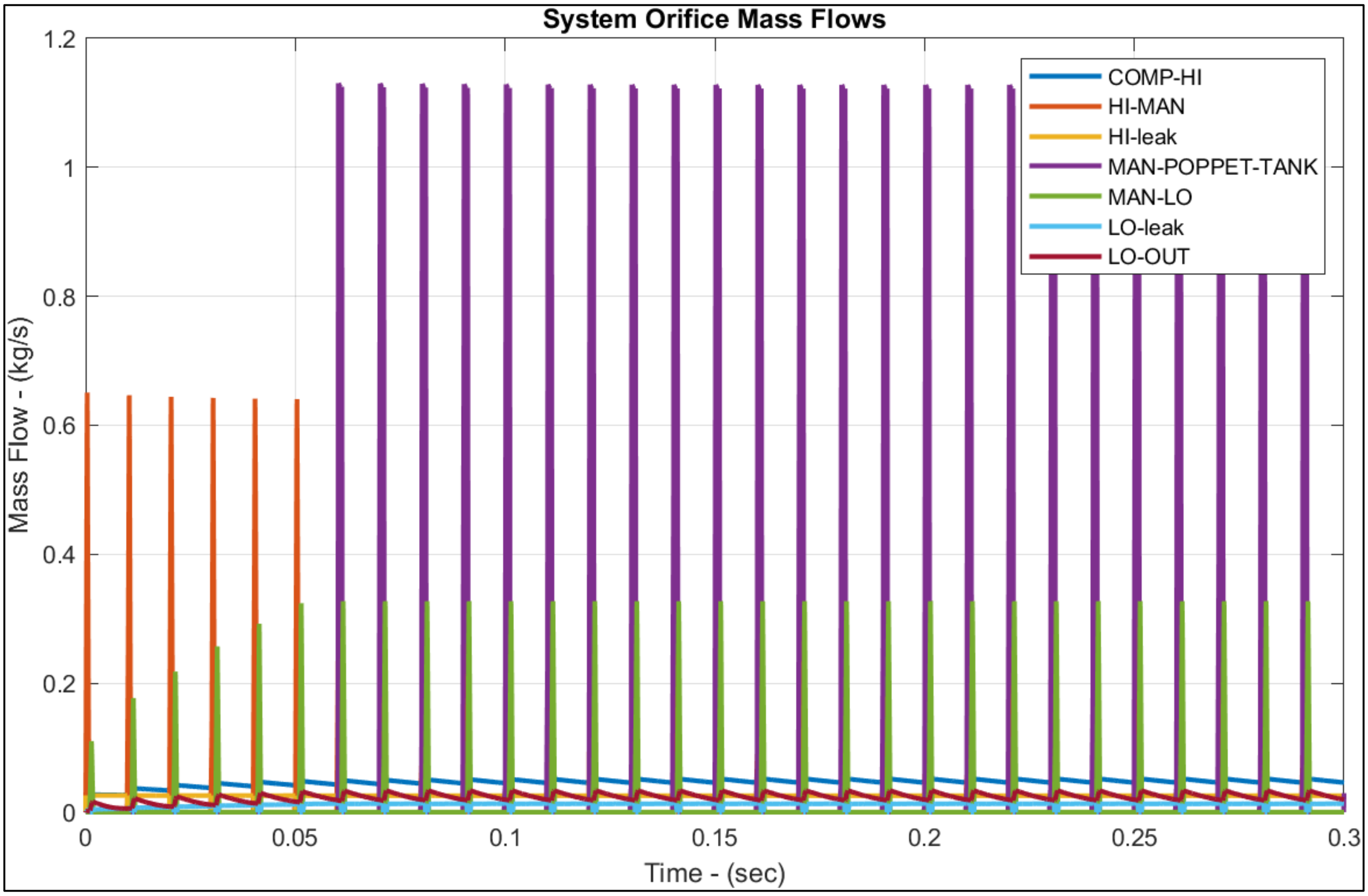

Figure 34 – Orifice Flow Model for Mass Flow of Air

The model predicts that the design will function as intended by showing how the system can quickly achieve and maintain pressure in individual vessels at their desired points. However, since the model assumes a constant supply pressure of 100[psig], the test bed needs to be attached to a constant source of pressurized air.

6.0 RESULTS

6.1 BILL OF MATERIALS

Table 4: Bill of Materials for Full System

Component/Process	**Description**	**Cost**
Front/Manifold Faceplate and Manifold	Plates holding up pressure vessels & allowing gas transfer between volumes. 304 Stainless Steel	**$3017.00**
Pipe Flanges (x6), Size 6 Pipe 1[m]	Flanges and piping used to create low-, mid-, and high-pressure vessels. 304 Stainless Steel	**$2383.90**
Stainless Steel Machining	Machining process for above components.	**$4950.00**
Rotary Shaft Steel 1[m]	Shaft steel for use in disc/shaft subsystem. 440 Stainless Steel	**$357.84**
Grinding/Tolerancing for Shaft	Machining process for rotary shaft to specified diameters and balancing. For 2 shafts	**$568.94**
Tight-Tolerance Low-Carbon Steel Bar	Flat stock steel for rotating discs. +/-0.003[in] ASTM A36 Carbon Steel	**$130.66**
2 ½” Length ¾”-10 Thread Steel Bolts (x20)	Used in interfaces where components are secured directly to plates. Low Strength Steel	**$29.94**
4” Length ¾”-10 Thread Steel Bolts (x50)	Used in interfaces where components are secured using nut/bolt. Low Strength Steel	**$141.00**
5 ¼” Length ¾”-10 Thread Steel Bolts (x12)	Used only at location of valve assembly retaining plates/manifold/mid-pressure vessel interface. ASTM A325 Steel	**$49.80**
Extra Wide ¾”-10 Thread Hex Nuts (x50)	Used for all locations 4” length bolts are needed. Medium Strength Steel	**$69.15**
Quick Disconnect Bushing for 5/8” Diameter Shaft	Used to secure sprocket to motor.	**$42.30**
Timing Belt Sprocket 6.61” Outer Diameter	For 1” width pulleys. Driven directly by motor.	**$156.27**
Quick Disconnect Bushing for 15/16” Diameter Shaft (x2)	Used to secure sprockets to shafts	**$34.36**

Timing Belt Sprocket 2.47" Outer Diameter (x2)	For 1" width pulleys. Drive rotating shafts	**$101.68**
Machine Key 3/16"x3/16"x1-1/2" (x10)	Machine key used with shaft sprockets	**$4.03**
Machine Key 1/4"x1/4"x1-1/2" (x10)	Machine key used with motor sprocket	**$5.43**
Angle Iron [6ft]	Used to create brackets to hold faceplates to optical table. Low Carbon Steel	**$105.00**
Shaft Bearings (x7)	Bearings to allow shaft to rotate freely. Extras purchased.	**$283.01**
PTFE Shaft Seals (x3)	Shaft seals rated for up to 6000 [RPM] continual use. Specified for future testing	**$437.19**
Blind Flange Endcaps (x2)	Used to create valve assembly retaining plates. Low Carbon Steel	**$356.96**
O-Rings (x5)	#365 Size. Nitrile	**$7.55**
Butyl Sheet 23"x12"x0.125" (x2)	Used to create gasket seals. Butyl	**$107.02**
½"x1-1/4" Dowel Pins (x10)	Used to align low- and high-pressure vessels to faceplates	**$9.11**
	TOTAL PRICE:	**$13,348.14**

Items unlisted due to being recycled from previous projects: Pressure Transducers (x4), 1650[RPM] ½[HP] Electric Motor, DART Motor Speed Controller, National Instruments USB-6212 DAQ, Poppet Valve Assembly (x2)

Notably, the bulk of the cost for this project came from the purchasing and machining processes for the front faceplate, manifold faceplate, and manifold. These were selected to be made of 304 stainless steel to cover future potential tests using corrosive gases or testing environments. However, if these were to have been made of aluminum instead and designed properly for the lower yield stresses of that metal, large portions of the cost can be reduced.

6.2 INSTRUMENTATION

There are numerous tests that this bench will be used for that will require the installation of displacement probes, accelerometers, thermocouples, and other such devices. However, to verify the actuation rate of the test bench, we have elected to use a system of four pressure transducers attached at the high-pressure air inlet, low-pressure air outlet, manifold volume, and mid-pressure vessels. The layout of the sensors and their location on the full system can be seen in Figure 35.

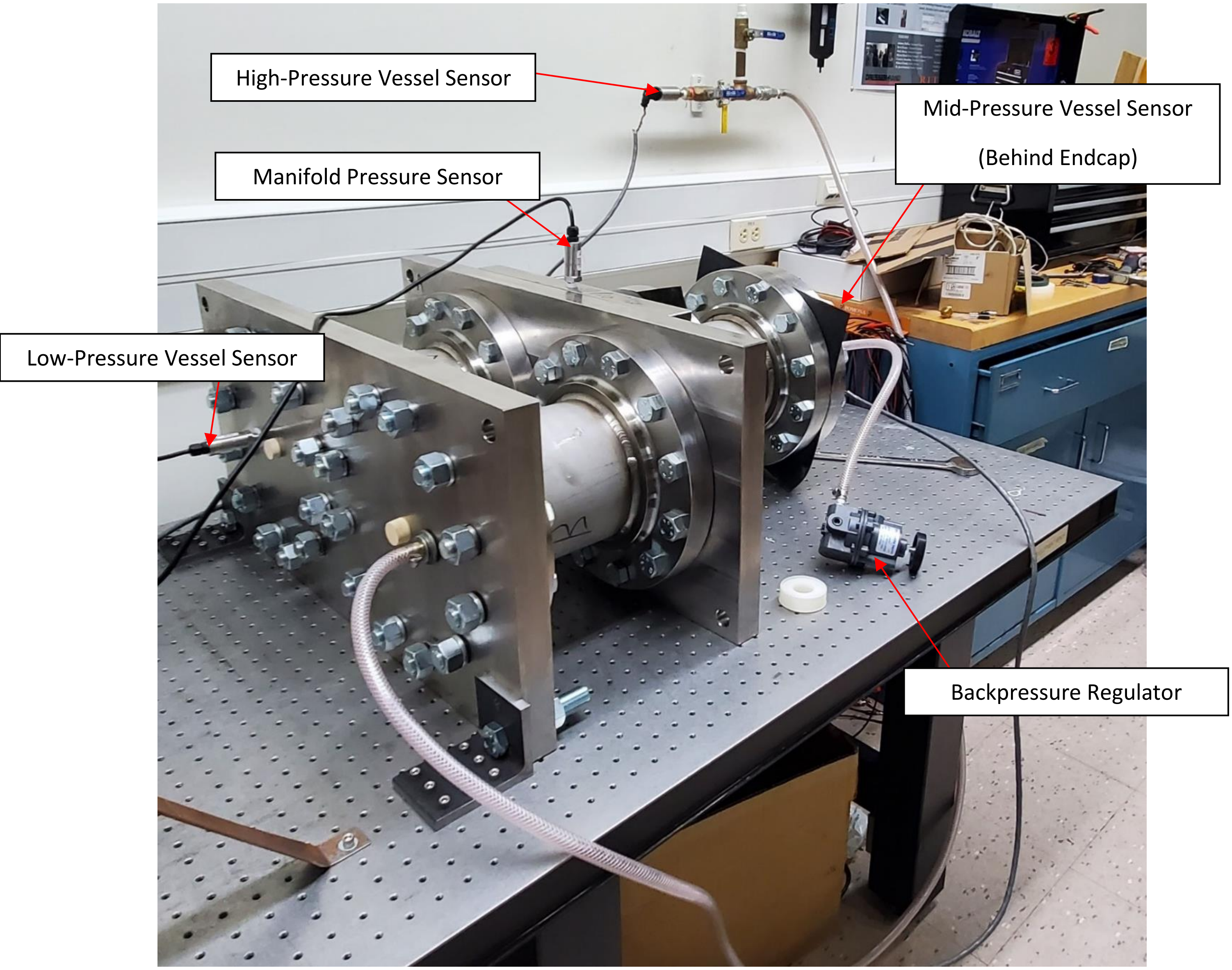

Figure 35: Full Assembly for Pneumatic Pressure Validation Test

The high-pressure inlet and mid-pressure outlet are being monitored using two PCB 1501B02EZ100PSIG pressure transducers. These sensors can detect pressures from 0-100[psig] with a response time of <1 millisecond and a resolution of <0.01% of the full measurement scale[21]. The manifold volume and low-pressure vessel are being monitored using two Omega PX309-100G10V pressure transducers. These sensors are also rated for a range of 0-100[psig] with a response time of <1 millisecond and an accuracy of +/- 0.25%[22]. Both transducers function through the use of a thin film system, wherein a film is deformed due to pressure in the sensor. This causes a change in the voltage running through the sensor, which in turn is scaled to an associated pressure.

6.3 HYDROSTATIC PRESSURE TESTING

To validate the maximum allowable pressure for our pressure vessels, as well as verify the integrity of our O-ring and gasket sealing methods, we subjected our pressure vessels to hydrostatic pressure tests. Hydrostatic pressure testing is the procedure through which a pressure vessel is filled with water and pressurized; generally using a pump. This pump brings the internal pressure of the vessel being tested up to a given hydrostatic pressure, after which a valve is closed to prevent any water from leaking back through the pump system. The internal pressure is then monitored using a pressure gauge on the pump, as well as visually checking the vessel for any leaks. Due to the internal pressure, any leaks which do occur tend to cause a spray of mist, which is both visible to the naked eye, and generally accompanied by an auditory response. After testing has been conducted for a sufficiently long period, the vessel is depressurized and drained of water.

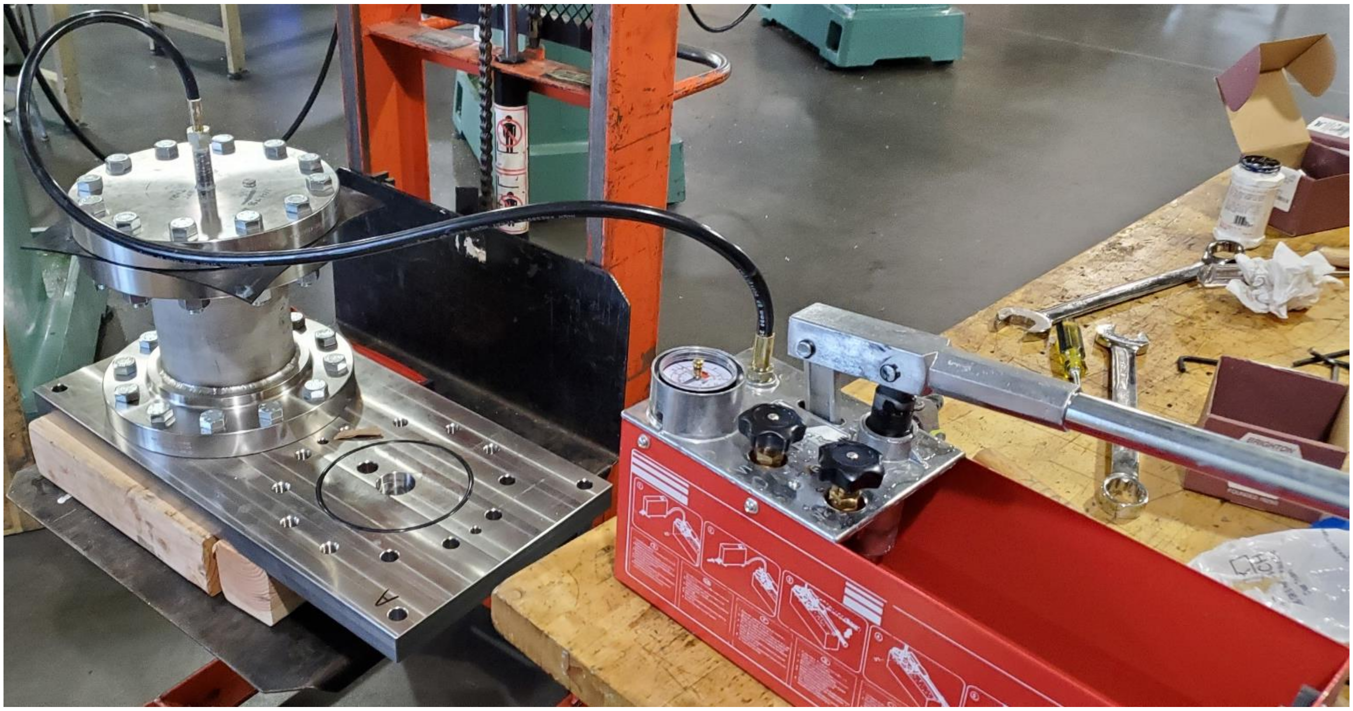

Figure 36: Assembly for Hydrostatic Pressure Test

ASME Section VIII-1 UG-99 outlines the procedure for verifying the integrity of pressure vessels[23]. For components that can contain water without impacting the core functionality of the tested system, the recommended hydrostatic pressure level is defined as:

$$P_h = 1.3MAWP\left(\frac{\sigma_{test}}{\sigma_{design}}\right) \tag{66}$$

Since the hydrostatic pressure testing was completed in the same environment as the system was designed to run in, the stress effects cancel out of the equation. This makes the hydrostatic pressure level for the test defined as simply:

$$P_h = 1.3MAWP \tag{67}$$

Where MAWP is the maximum allowable working pressure for the system.

While initial pneumatic testing was completed using the KGCOE building provided air pressure of 65[psig], our intention for future use testing outlines experiments being run using a high-pressure value of 100[psig]. As such, for the hydrostatic pressure test, we targeted a minimum pressure of 130[psig] to verify the integrity of our pressure vessels. Further, each pressure vessel was maintained at pressure for ten minutes to verify that there was no leakage in the system.

We conducted hydrostatic pressure testing in three sets, one for each pressure vessel in the system. These tests were conducted using a 2[gal] IRONWALLS hand-pumped hydrostatic pressure tester rated for tests up to 726[psig]. Each test was completed by first securing the manifold faceplate to a fixed surface. Next, the passthrough hole that would normally allow air to travel into the manifold volume was plugged using a stopper to prevent water from leaking out of the system during testing. This plug also allowed us easy access to drain the pressure vessel after testing was concluded. After this, we would secure one of the pipe segments acting as pressure vessels to the manifold faceplate before securing the endcap to the top of the vessel. The vessel was pressurized through the passthrough hole in the endcap intended for use on the backpressure regulator during normal operation. An O-ring was used to seal the interface between the manifold faceplate and the vessel, while a gasket was used to seal the interface between the vessel and the endcap. The fully assembled hydrostatic test apparatus can be seen in Figure 36.

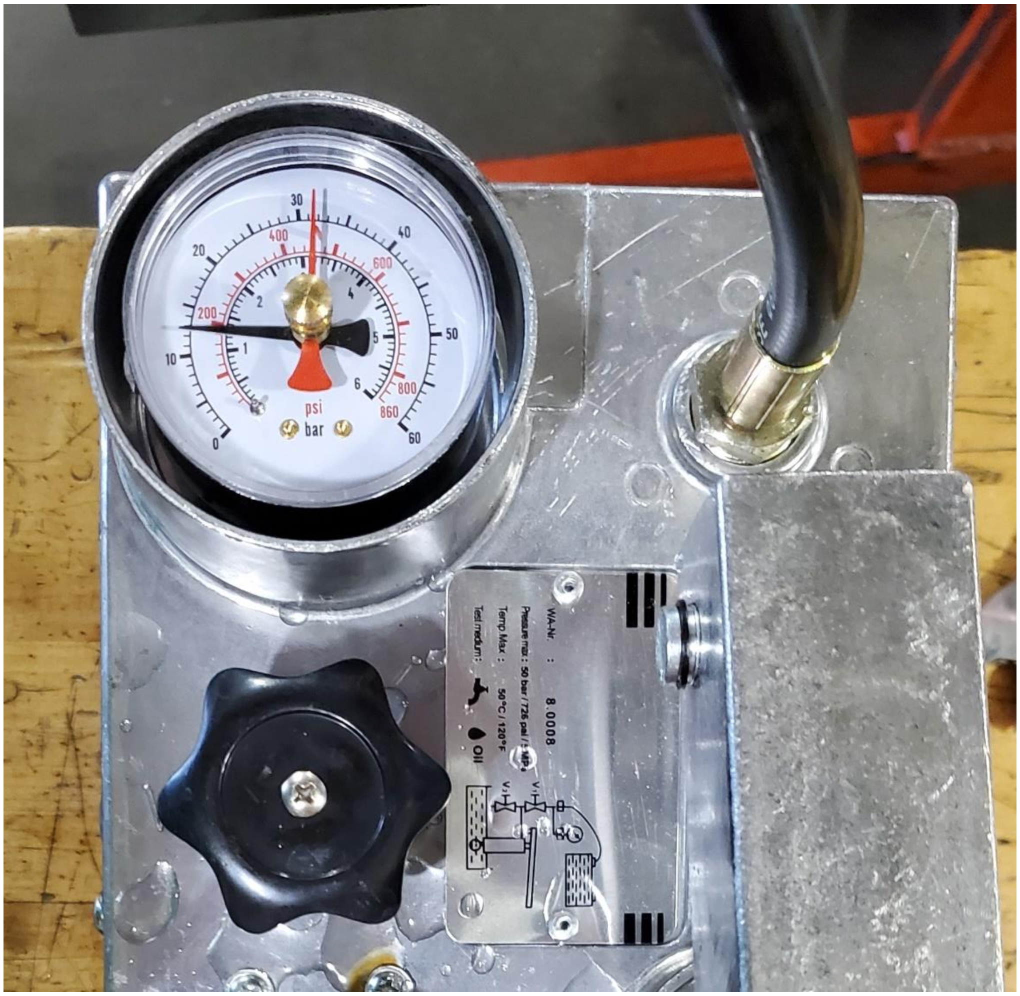

Figure 37: Hydrostatic Pressure Test Gauge Reading

As can be seen in Figure 37, we elected to test our pressure vessels at 200[psig] rather than the minimum of 130[psig] necessary to validate our system. This was done primarily to add an additional factor of safety to the test by allowing us to verify the integrity of the system at pressures beyond what we expect to see during prolonged testing. At these pressures, we can safely validate our system to run at pressures up to 150[psig]. We found that all vessels were able to maintain an internal pressure of 200[psig] for ten minutes, validating the safety of these components.

6.4 PNEUMATIC PRESSURE VALIDATION TESTS

To validate the accuracy of our pressure transducers, determine the location of leaks in the system, and determine whether our system would be able to maintain specified pressures, we conducted a set of two pneumatic static pressure tests. To this end, we constructed the full system without the rotating shaft/disc subsystem and installed pressure transducers throughout the system to monitor the pneumatic pressure of each vessel. We also installed a backpressure regulator at the mid-pressure vessel to modulate the pressure of the system to our specifications. Once the system was assembled, we conducted two separate validation tests. For the first test, we pressurized the system using the KGCOE building air and set the backpressure regulator to open at 56[psig]. The full assembly can be seen in Figure 35.

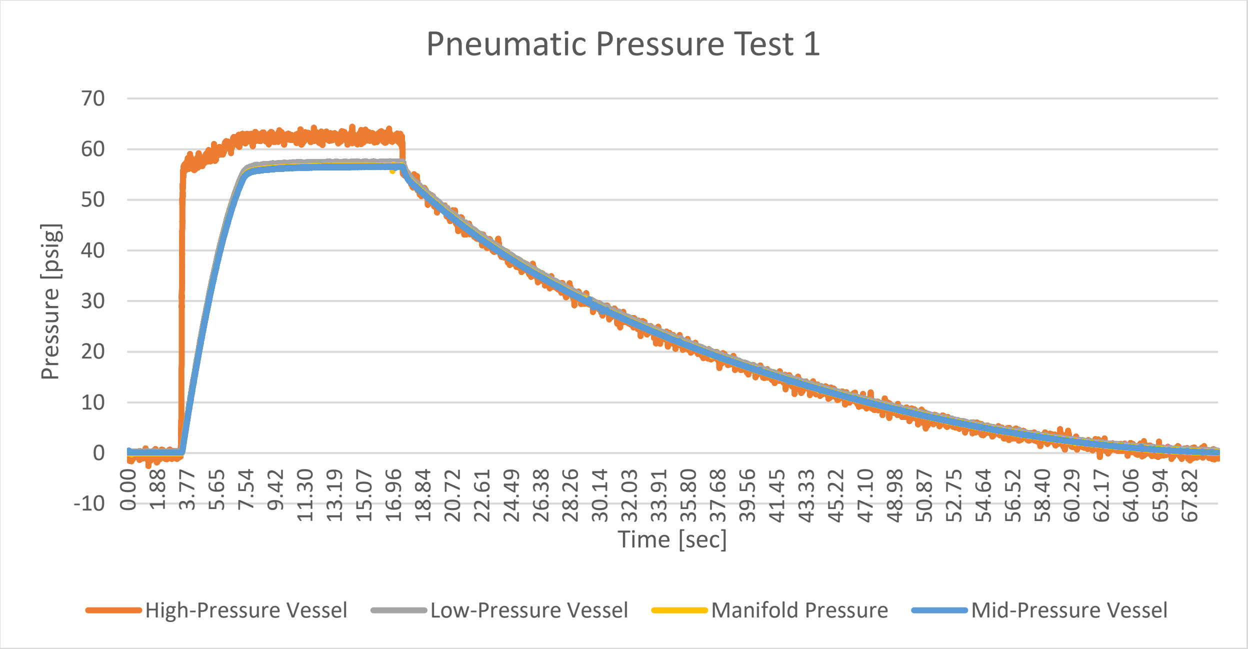

Figure 38: Pneumatic Pressure Test, 56[psig] Maintained Pressure

In this experiment, air was supplied to the system as a step function beginning three seconds on the plot above. The air supply was maintained for fourteen seconds, after which it was shut off. As can be seen from Figure 38, we were successfully able to build pressure in the system and maintain it at 56[psig] without loss of integrity due to leakage. That said, there was still leakage in the system, mainly at the temporary passthrough port installed at the low-pressure vessel. This leakage can be seen in the results above after the shutoff of the air supply. Should the system have been entirely airtight, system pressure would have remained at 56[psig] in the system until manually released using the backpressure regulator. Instead, the air slowly bled out of the system until the system reached atmospheric pressure. Another important observation of note is the deviation of the high-pressure vessel reading from the other transducer outputs. This sensor reads at the supplied pressure rather than at the system pressure due to its placement in line with the building air supply (Fig. 35). Due to the temporary placement of this sensor pressure drop in the supply line between the manual ball valve and the high-pressure vessel. This test was still successful as it showed that the amount of leakage in the system is negligible compared to the mass flow of air into the system. We were able to maintain the desired system pressure while also demonstrating that our sensors are all working as intended.

For the second validation test, we pressurized the system with the same source at 65[psig] and set the backpressure regulator to release air at 50[psig].

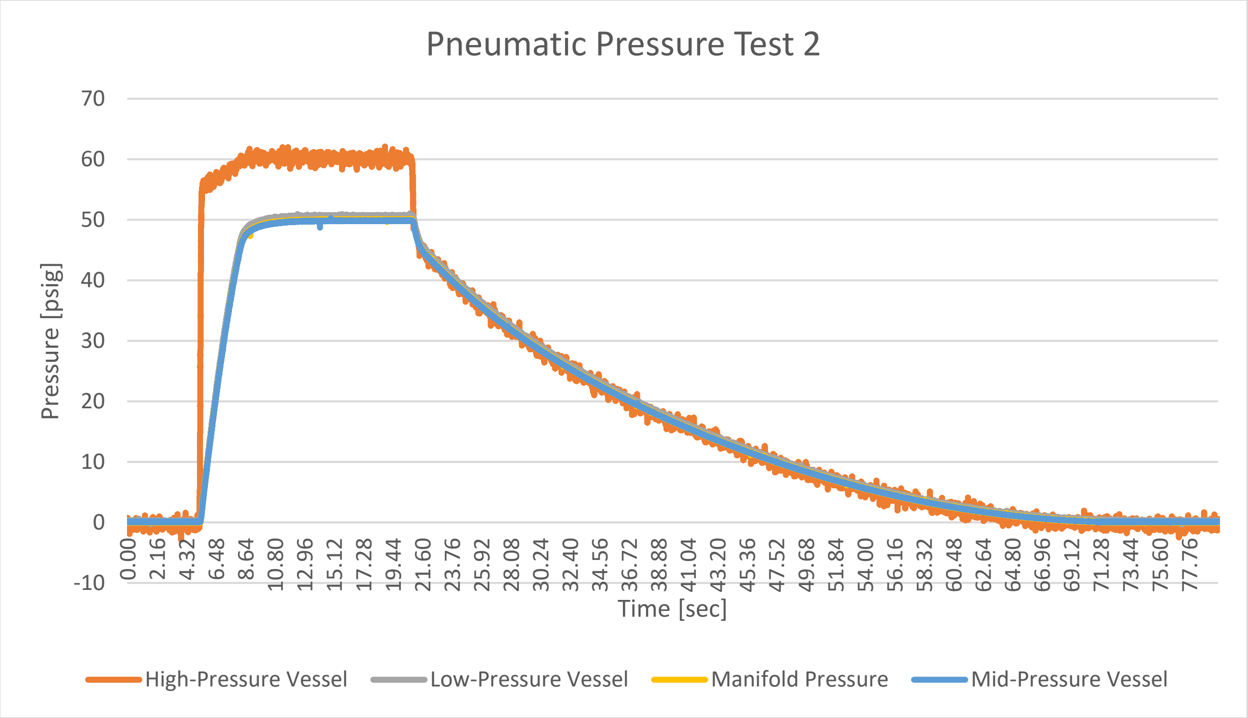

Figure 39: Pneumatic Pressure Test, 50[psig] Maintained Pressure

As with the first validation test, we found that we were able to maintain the system at the desired pressure with minimal leakage. One point of concern in both validation tests is the amount of noise that the high-pressure vessel sensor is recording in its reading. This may be due to the positioning of the sensor at the junction of the building supply air and the hose bringing compressed air into the rest of the system. However, more testing is needed to determine whether this sensor will be acceptable for use in long-term pressure cycling tests to accelerate valve lifetime, or if it needs to be replaced. Further, the limitations of the building air providing a maximum pressure of 65[psig] means that we were unable to validate our pressure transducer and our system at the desired operating pressure of 100[psig].

7.0 CONCLUSIONS

While we were unable to conduct pressure cycle testing in our system due to supply chain constraints with machining the rotating shafts, validation for this system for long-term use has been completed. Our dynamic simulation demonstrates that our system will be able to actuate poppet valves at 100[Hz] with an input pressure of 100[psig] and the backpressure regulator set to 50[psig] (see Figure 33). Calculations for the internal hoop stress of the system indicate our system is safely able to hold pressures up to 100[psig], with hydrostatic pressure testing supporting these calculations. Further calculations demonstrate that our test apparatus should have no issues with resonant frequency in any of the rotary components, nor should the thermal expansion of any components become an issue to the functionality of the system when operating at 100[Hz]. Fatigue analysis of the bolts in our system also shows these components remain well under the Modified-Goodman Curve and maintain an infinite lifetime. As such, alongside our pneumatic validation tests, the design for our poppet valve lifetime accelerator has demonstrated itself to be theoretically sound and possible to construct practically.

8.0 RECOMMENDATIONS FOR FUTURE WORK

While logistical constraints prevented us from doing so, the very first test that needs to be conducted before any lifetime acceleration testing occurs is a pressure cycling test of the system. Due to the missing disc/shaft system, we were unable to determine the efficacy of our model in predicting the air mass flow and pressure dynamics of our system while operating at normal speed. Additionally, a modal analysis of the system should be conducted to ensure that the fully constructed system will not see any issues with resonant frequencies causing damage. While a theoretical frequency analysis was completed for the shaft/disc subsystem, how the dynamics of these components will interact with factors such as the movement of gas through the system, movement of the poppet valves, and vibrations coming from the motor are not yet known. Upon successful conclusion of these tests, the system will be fully prepared to conduct lifetime acceleration tests for poppet valves.

To conduct initial lifetime accelerator testing, it may be necessary to install additional sensors to track areas of interest in the performance of the system. For instance, in the Dresser-Rand ESH-1 compressor in our lab, we have thermocouples installed throughout the system to monitor the temperature of various components and volumes during operation. As such, should future testing be conducted using this apparatus, thermocouples will need to be installed to monitor the temperature in each volume. The addition of thermocouples would also be key in monitoring the effects of heated gas on the lifetime of compressor valves should that be an avenue of interest for future research. Additionally, the compressor in our lab contains fiber-optic displacement probes that monitor the displacement of poppet valves inside of the valve assembly during operation. Having displacement information for valves in the test apparatus would be useful in developing a methodology to determine whether those valves have reached the end of their accelerated lifetime without needing to dismantle the system to check. For instance, should one of the displacement probes read that a valve is not moving despite the system remaining pressurized, it could indicate that the valve has either jammed (and thus failed) or that the valve has potentially broken apart entirely.

There are many potential avenues for future research on this system. On top of being designed to withstand elevated operational temperatures, this system was also designed to be able to operate in suboptimal conditions. For instance, due to the system being mainly composed of stainless steel, it is resistant to damage from corrosive gases and rust. Furthermore, while the system is mainly designed around a maximum pressure of 100[psig], hydrostatic pressure testing and material strength calculations of the pressure vessels suggest that the system may be safely operated at pressures of up to 150[psig]. Should this be a desired avenue of research, a more thorough investigation of the sealing solutions used in this system needs to be conducted. Sealing components such as the butyl gasket seals used were selected based on their ability to maintain lower pressures. Should higher differential pressures be desired within the system, these seals may need to be exchanged for more robust sealing solutions such as custom metal gaskets or O-rings (which require additional machining for components). Investigations into more robust sealing mechanisms would also open potential research avenues into using gases with different molar weights in the system such as helium, hydrogen, and carbon dioxide.

It will also be necessary to purchase an external compressor with the capability to constantly supply the system with highly pressurized air for the extended periods of time we expect our valve durability tests to run. Currently, our system is equipped to operate using the KGCOE building air. While this is sufficient for initial validation, using the building air as a source of pressure will tax our building sir supply and cause problems for other laboratories and machine shops that need access to pressurized air. If a high-pressure vessel pressure of 100[psig] is desired to test the effects of increased stress on components to their lifetimes, alternative methods for providing the system with gas will be necessary.

9.0 SOCIETAL CONTEXT

Despite the ongoing push in the energy sector to convert the power grid to renewable energy resources, there is still a need for traditional petrochemical energy sources such as oil and natural gas. In fact, over the past 20 years, natural gas as a share of the total energy generated in the US has grown from 24.2% to 32.2%[24]. With this growing demand for natural gas-produced energy, any increase in efficiency along the natural gas transport and production supply chain leads to savings for companies, consumers, and the environment. This interest in saving time, money, and resources is why the petrochemical industry is particularly interested in developing predictive maintenance procedures for their gas and oil pipelines.

Through the information gathered using this test apparatus, predictive maintenance algorithms will be developed to directly help in reducing downtime in the petrochemical industry. By decreasing this downtime, consumers will have a more secure energy supply. Companies will save money on labor and the lost productivity of downed pipelines, as well as reduce the number of times components are replaced before they need to be. Lastly, these predictive maintenance algorithms will help decrease the amount of waste going into landfills due to maintenance conducted on healthy components. Reducing the number of maintenance cycles on parts that are not close to failure helps to both reduce the waste these components generate, as well as decrease the demand (and therefore production) of replacement parts.

10.0 REFERENCES

[1] Phillippi, G., Manthey, T., Sutter, J., Williams, B., and Mccain, B., 2016, “Your Gas Compression Application - Reciprocating, Centrifugal or Screw?,” *45th Turbomachinery & 32nd Pump Symposia*, Turbomachinery and Pump Symposia, Houston.

[2] Jandjel, D. G., 2000, “Select the Right Compressor,” Chem Eng Prog, **96**(7), p. 15.

[3] Dsilva, P. C., Shetty, P., Sondar, P. R., Ganesh Kumar, B., and Hegde, S. R., 2021, “Failure Analysis of Reciprocating CO2 Compressor,” Journal of Failure Analysis and Prevention, **21**(2), pp. 595–603.

[4] Guilherme, A., Schirmer, F., Nelmo, R., Fernandes, F., de Caux, J. E., and Nelmo,), 2004, “On-Line Monitoring of Reciprocating Compressors,” *NPRA Maintenance Conference*, San Antonio.

[5] Metcalf, J. R., and Woollatt, D., 1995, “Reciprocating Compressor Valve Reliability Improvements,” *Twenty-Fourth Turbomachinery Symposium*, pp. 167–174.

[6] 2016, “CPI Compressor Valves,” RJ Mann & Associates Inc. [Online]. Available: https://www.rjmann.com/cpi/cpi_compressor_valves.html. [Accessed: 01-Dec-2022].

[7] Chaykosky, S., 2010, “Resolution of a Compressor Valve Failure: A Case Study,” *Compressor Handbook*, River Publishers, Painted Post, NY.

[8] Motriuk, R. W., 1996, “Reciprocating Compressor Valve Failure - Digital Modelling and Analysis,” International Pipeline Conference, **2**, pp. 993–1002.

[9] 2022, “Engineering Statistics Handbook,” National Institute of Standards and Technology [Online]. Available: https://doi.org/10.18434/M32189. [Accessed: 28-Nov-2022].

[10] Pu, S., Yang, F., Vankayalapati, B. T., and Akin, B., 2022, “Aging Mechanisms and Accelerated Lifetime Tests for SiC MOSFETs: An Overview,” IEEE J Emerg Sel Top Power Electron, **10**(1), pp. 1232–1254.

[11] Monroe, E. M., Pan, R., Anderson-Cook, C. M., Montgomery, D. C., and Borror, C. M., 2011, “A Generalized Linear Model Approach to Designing Accelerated Life Test Experiments,” Qual Reliab Eng Int, **27**(4), pp. 595–607.

[12] Chernoff, H., 1962, “Optimal Accelerated Life Designs for Estimation,” Technometrics, **4**(3), pp. 381–408.

[13] Martins, J. A., Ferreira, I., Leite, D., and Romão, E. C., 2013, “Failure Analysis of a Set of Flapper Valves under ALT with Alternative Test Device,” J Test Eval, **41**(2).

[14] Choi, J., Lee, J., Jun, N., Seok, C. S., Park, S., and Kim, G., 2019, “Development of Laboratory Fatigue Testing Apparatus for Automotive Vehicle Engine Valve Simulating Actual Operating Conditions,” International Journal of Precision Engineering and Manufacturing, **20**(7), pp. 1241–1253.

[15] Hartshorn, K., 1986, “An Experimental Test Device for Accelerated Endurance Evaluation of Compressor Valve Assemblies,” *International Compressor Engineering Conference*, pp. 364–381.

[16] Shigley, J., and Mischke, C., 1989, *Mechanical Engineering Design*, McGraw-Hill, New York.

[17] 2022, “304 Stainless Steel ,” matweb.com [Online]. Available: https://www.matweb.com/search/DataSheet.aspx?MatGUID=abc4415b0f8b490387e3c922237098da&ckck=1. [Accessed: 28-Nov-2022].

[18] Juvinall, R., and Marshek, K., 2000, *Fundamentals of Machine Component Design*, John Wiley & Sons.

[19] 2022, “SkyCiv Beam Calculator,” SkyCiv Engineering [Online]. Available: https://skyciv.com/free-beam-calculator/. [Accessed: 01-Dec-2022].

[20] 2023, “AISI 440 Stainless Steel,” matweb.com.

[21] PCB Piezotronics, 2004, “Model 1501B02EZ100PSIG Pressure Transducer Installation and Operating Manual.”

[22] Omega, “1 All Stainless Steel Transducer/Transmitter Multimedia Compatibility High-Performance Silicon Technology Imperial Model.”

[23] 2023, “Hydrostatic Pressure Tests ASME Pressure Vessels,” Engineers Edge.

[24] 2022, “U.S. Energy Facts Explained,” US Energy Information Administration [Online]. Available: https://www.eia.gov/energyexplained/us-energy-facts/. [Accessed: 28-Nov-2022].

Appendices

A pipestresscalcv2.m

```
%% Michael Anderson - Thick-Walled Pipe Stress Calcs
%This is based on a series of equations from Shigley's Mechanical
%Engineering Design 8th Edition (page 107) for thick walled pressurized
%cylinders
clear
close all
clc
patm = 14.7; %[psi]
FS = 3; %Factor of Safety, Bump this up to increase multiplier on internal pressure
p_o = patm; %[psi], this should be atmospheric pressure
p_i = (FS*814) + patm; %[psi] this should be the gauge pressure + atmospheric
r_i =(6+1/8)/2; %[in] This is inner pipe radius
dr = 0.280; %[in], this is pipe thickness
r_o = (6+5/8)/2; %[in] This is outer pipe radius
r = [r_i:0.0001:r_o]; %[in], creates range of radii to provide stress profile
FSstr = sprintf('Internal Pressure = %.1f psi',p_i/FS);

%% Thick Walled Stresses
%Calculate Stresses
%1 modifier indicates special condition where outer pressure "0". Unclear if
%this implies vacuum or atmospheric... Both variations are calculated [psi]
stress_hoop_thic = ((p_i * r_i * r_i) - (p_o * r_o * r_o) - (r_i * r_i * r_o *
r_o*(p_o-p_i)./(r.*r)))./(r_o*r_o - r_i*r_i);
stress_radi_thic = ((p_i * r_i * r_i) - (p_o * r_o * r_o) + (r_i * r_i * r_o *
r_o*(p_o-p_i)./(r.*r)))./(r_o*r_o - r_i*r_i);

figure(1)
hold on
grid on
plot(r, stress_hoop_thic);
plot(r,stress_radi_thic);
plot(r(1,1),stress_radi_thic(1,1)); %DUMMY POINT TO ALLOW FS/vars IN LEGEND
ylim([[min(stress_radi_thic)-1000], [max(stress_hoop_thic)+1000]]); %Set axes to
prevent legend covering curve
xlabel('Radius [in]');
ylabel('Stress [psi]');
title('Stress Profile of Thick-Walled Pipe')
legend('Hoop Stress', 'Radial Stress', FSstr)
hold off



%% Thin Walled Stresses
%stress_hoop_thin = (p_i*(r_i*2 + dr))/(2*dr);
%stress_long_thin = (p_i*2*r_i)/(4*dr);
```

B fatigueplots.m

```
%Michael Anderson
%Fatigue Plots using Shigley Equations (8th Edition w/ Mischke)
clear
close all
clc
utstress = 60000;
stress80 = ((80*9*pi)/12)/0.302;
stress100 = ((100*9*pi)/12)/0.302;
astress = 0.5*(stress100-stress80);
mstress = 0.5*(stress100+stress80);
estress = astress/((1/3)-(mstress/utstress));
n = 1/((astress/estress)+(mstress/utstress));
eprime = 0.504*utstress;
ka = 2.7*(utstress/1000)^(-0.265);
kb = 1;
kc = 0.85;
kd = 1;
ke = 0.620;
emarin = ka*kb*kc*kd*ke*eprime;
n = 1/((astress/emarin)+(mstress/utstress));
x = [0 utstress];
y = [emarin 0];
xtru = mstress;
ytru = astress;
figure(1)
hold on
xlabel('Mean Stress [psi]')
ylabel('Alternating Stress [psi]')
title('Bolt Fatigue Plot using Marin Factors')
plot(x,y)
scatter(xtru, ytru, '*', 'r')
legend('Modified Goodman Curve Marin Factors', 'Bolt Stress')
xm = [0 utstress];
ym = [estress 0];
figure(2)
hold on
xlabel('Mean Stress [psi]')
ylabel('Alternating Stress [psi]')
title('Bolt Fatigue Plot using Factory of Safety = 3')
plot(xm,ym)
scatter(xtru, ytru, '*', 'r')
legend('Modified Goodman Curve n=3', 'Bolt Stress')
```

C HoleOpeningCalc_v2.m

```
%% Hole Opening Calculation v2
%Based on derived geometry. Not using any particular source
clc
clear
close all
a = 0.5;
r0 = 2;
angdisp0 = 0.252680255; %3*pi/2;
angdispend = 0.252680255*2;
angdisp = 0;
index = 1;
%% Determine h for a given angular displacement
while angdisp<angdispend

    hbounds = roots([1 -2*r0*cos(angdisp-angdisp0) r0*r0-a*a]); %RADIANS Self
consistent so shouldn't need to convert to degrees for later
    h(index) = max(hbounds)-min(hbounds);
    index = index+1;
    angdisp = angdisp+0.001;
    if angdisp>angdispend
        angdisp = angdispend;
        hbounds = roots([1 -2*r0*cos(angdisp-angdisp0) r0*r0-a*a]); %RADIANS Self
consistent so shouldn't need to convert to degrees for later
        h(index) = max(hbounds)-min(hbounds);
    end
end

theta = 180-2*acosd((0.5.*h)/a); %DEGREES
Atri = 0.5.*h.*sqrt(a*a-0.25*h.*h);
Asector = (theta/360)*pi*a*a;
Aseg = Asector-Atri;
%hrev = flip(h);
Aseg(1, round(0.5*length(h)):end) = (pi*(a^2)) - Aseg(1,round(0.5*length(h)):end);
%Aseg = [Aseg Asegrev];
%h = [h hrev];
Asegpercent = Aseg/(pi*(a^2));
Aopen = [Aseg flip(Aseg)];
t = linspace(0,1,1014);
figure(3)
hold on
plot(t, Aopen);
hold off

figure(1)
hold on
plot(h, Aseg)
hold off

figure(2)
hold on
plot(h, Asegpercent);
hold off
```

D BeamDeflection_Calc.m

```
%% Beam Deflection Curve
% Michael Anderson
% Using Fundamentals from Strengths 2. I think a lot also came from
% Shigley???
clear
close all
clc
%% Initialize Variables
Lshaft = 15*.0254; %[m] Length of Shaft
rshaft = .025/2; %[m] Radius of Shaft
g = 9.81; %[m/s^2] gravity
dsteel = 8000; %[kg/m^3] Density of 304 Stainless Steel
rdisc = (5.5/2)*.0254; %[m] radius of rotating disc
tdisc = 0.5*.0254; %[m] thickness of rotating disc
wdisc = g*dsteel*pi*rdisc*rdisc*tdisc; %[N] Weight of rotating Disc in N (Maybe
rewrite w/ Volume from Solidworks)
wpulley = g * 0.473; %[N] Weight of pulley (bushing + sprocket)
tpulley = 1.75*0.0254; %[m] Thickness of bushing + sprocket. Name is legacy from
earlu assumptions
a = 0.925*0.0254; %[m] Length to disc
b = 0.262461+.012; %[m] Length between bearings
c = Lshaft-0.5*tpulley; %[m] Length to pulley
U = g*dsteel*pi*rshaft*rshaft; %[kg/m] Distributed weight of shaft over its length. =
F/L = m*g/L = V*rho*g/L = pi*r^2*L*rho*g/L = pi*r^2*rho*g
Esteel = 193e+09; %[Pascals] Young's Modulus for 304 Stainless Steel
Ishaft = pi*rshaft*rshaft*rshaft*rshaft*0.25; %[m^4] Area moment of inertia for
circular cross section
wshaft = U*Lshaft; %[N] Shaft weight from distributed load
RReac = (wdisc*a+wshaft*(0.5*Lshaft)+wpulley*c)/b; % [N] Right hand Reaction Force
LReac = wshaft+wdisc-RReac+wpulley; %[N] Left hand Reaction Force
xset = 0:0.00001:Lshaft; %[m] Length of shaft for deflection calc
C2 = (-(LReac/6)*b^2)+((wdisc/(6*b))*(b-a)^3)+((1/24)*U*b^3);
beamindex = 1;
shear = nan(1, length(xset));
moment = nan(1, length(xset));
deflection = nan(1, length(xset));
for x = xset
    if x<a
        %C2 = (-LReac*b^2)+(0.25*U*b^3);
        shear(beamindex) = (LReac*x^0) - (U*x^1);
        moment(beamindex) = (LReac*x^1) - ((U/2)*x^2);
        deflection(beamindex) =1/(Esteel*Ishaft)*(((LReac/6)*x^3)-((U/24)*x^4)+C2*x);
    elseif x<b
        %C2 = (-LReac*b^2)+((wdisc/b)*(b-a)^3)+(0.25*U*b^3);
        shear(beamindex) = (LReac*x^0) - (wdisc*(x-a)^0) - (U*x^1);
        moment(beamindex) = (LReac*x^1) - (wdisc*(x-a)^1) - ((U/2)*x^2);
        deflection(beamindex) =1/(Esteel*Ishaft)*(((LReac/6)*x^3)-((wdisc/6)*(x-
a)^3)-((U/24)*x^4)+C2*x);
    elseif x<c
        shear(beamindex) = (LReac*x^0) - (wdisc*(x-a)^0) + (RReac*(x-b)^0) - (U*x^1);
        moment(beamindex) = (LReac*x^1) - (wdisc*(x-a)^1) + (RReac*(x-b)^1) -
((U/2)*x^2);
        deflection(beamindex) =1/(Esteel*Ishaft)*(((LReac/6)*x^3)-((wdisc/6)*(x-
a)^3)+ ((RReac/6)*(x-b)^3)-((U/24)*x^4)+C2*x);
```

```
    else
        shear(beamindex) = (LReac*x^0) - (wdisc*(x-a)^0) + (RReac*(x-b)^0) -
wpulley*(x-c)^0 - (U*x^1);
        moment(beamindex) = (LReac*x^1) - (wdisc*(x-a)^1) + (RReac*(x-b)^1) -
wpulley*(x-c)^1 - ((U/2)*x^2);
        deflection(beamindex) =1/(Esteel*Ishaft)*(((LReac/6)*x^3)-((wdisc/6)*(x-
a)^3)+ ((RReac/6)*(x-b)^3)-((wpulley/6)*(x-c)^3)-((U/24)*x^4)+C2*x);
    end
    beamindex = beamindex+1;
end
figure(1)
hold on
grid on
xlabel('x [m]')
ylabel('V [N]')
title('Shear Force Diagram')
plot(xset, shear)
hold off

figure (2)
hold on
grid on
xlabel('x [m]')
ylabel('M [N*m]')
title('Moment Diagram')
plot(xset, moment)
hold off

figure (3)
hold on
grid on
xlabel('x [m]')
ylabel('Deflection [m]')
title('Beam Deflection Diagram')
plot(xset, deflection)
hold off
```

E ConceptValveTestRigParams_Poppets_v2.m

```
% Parameters for Valve Test Rig
%
% J. Kolodziej & Michael Anderson

%Call Opening Mechanics
HoleOpeningCalc_v2;

%clear all

Patm=101000;
n=1.0;                      % Polytropic Exponent
Rgas= 287.05;               % J/kg/degK
T=298;                      % degK

% Compressor Volume to High Pressure volume
%       This assumes compressor volume is infinity large (can expand model
%       to include compressor tank volume.
Pcomp = 65*6894.76; % [Pa]   % 175 psi of maximum pressure and 7.6 SCFM at 90 psi (2-
Stage 60 Gal. Stationary Electric Air Compressor)
%d_comp_in = 1; % [in] - diameter of high-side plate orifice (old value
%that met goals
d_comp_in = 0.5; % [in] - diameter of high-side plate orifice
Ao_comp_in2 = pi/4*(d_comp_in)^2;  % There is a brass fitting/nozzle on the valve for
tube connection - measured
Ao_comp_m2 = Ao_comp_in2 * (0.0254/1)^2;
Cd_comp = 0.8;%0.95;%0.6;%0.8;

% High Pressure Orifice to Manifold
d_hi_in = 1.0;
Ao_hi_in2 = pi/4*(d_hi_in)^2;  %
Ao_hi_m2 = Ao_hi_in2  * (0.0254/1)^2;
%* Aopenpercent

Cd_hi = 0.8;%0.95;%0.6;%0.8;

% High Pressure Orifice to Manifold leakage path
d_disk_in = 5.0;            % [in] - diameter of rotating disc
%t_disk_in = 0.0313;         % [in] - gap between rotating disc and from (1/32")
t_disk_in = 0.01;         % [in] - gap between rotating disc and from (10 mil)
Ao_disc_in2 = pi*d_hi_in*t_disk_in;  % [in] - surface area of gap
Ao_hileakdisc_m2 = Ao_disc_in2 * (0.0254/1)^2;
Cd_hileak = 0.8;

% Manifold to Low-side Pressure Volume
d_lo_in = 1.0; % [in] - diameter of low-side plate orifice
Ao_lo_in2 = pi/4*(d_lo_in)^2;  % There is a brass fitting/nozzle on the valve for
tube connection - measured
Ao_lo_m2 = Ao_lo_in2 * (0.0254/1)^2;
Cd_lo = 0.8;%0.95;%0.6;%0.8;

% Manifold to Low-Pressure leakage path  -  ASSUMES Lo-side leakage has the
% same area as the high side.
```

```
Ao_loleakdisc_m2 = Ao_hileakdisc_m2;
Cd_loleak = 0.8;

% Poppet orifice from manifold to tank
% PoppetArea_in2 = pi*0.5*0.055;  % [in2] - gap in manifold ...poppet travel may be
larger.
% %PoppetArea_in2 = pi/4*0.188^2;  % hole diameter after poppet opens.
% Ao_poppet_in2 = NumPoppets*PoppetArea_in2;
% Ao_poppet_m2 = Ao_poppet_in2 * (0.0254/1)^2;

% with 16 poppets and actual dimensions this is equivalent to a single
% 1.32" diameter orifice. That is HUGE!
NumPoppets = 16;     %
PoppetDiam_in = 0.5;                    % [in] - Poppet Diameter
PoppetDiam_m = 0.5 * (0.0254/1);        % [m] - Poppet Diameter
PoppetPreDisp_x0 = 0.875 - 0.716;                           % [in] - Preload
displacement (0.159") 0.875" poppet and spring alone, 0.716"  is the height in the
maniforld
PoppetPreDisp_x0_m = PoppetPreDisp_x0 * (0.0254/1);         % [m] - Preload
displacement (0.159") 0.875" poppet and spring alone, 0.716"  is the height in the
maniforld
PoppetMass_kg = 0.00221;                 % [kg] - Poppet Mass (2.21 grams) measured
PoppetSpringConst_k = 1.25;             % [lb/in] - poppet spring stiffness
PoppetSpringConst_k_kg_m = PoppetSpringConst_k * (175.12/1);           % [kg/m] -
poppet spring stiffness
MaxPoppetDisp = 0.055;                                      % [in]
MaxPoppetDisp_m = MaxPoppetDisp * (0.0254/1);               % [m]
Cd_poppet = 0.8;%0.95;%0.6;%0.8;
areaPoppet_in2 = pi/4*PoppetDiam_in^2;
areaPoppet_m2 = pi/4*PoppetDiam_m^2;

% Discharge orifice from tank
d_dist_in = 0.5; % [in]
Ao_dist_in2 = pi/4*(d_dist_in)^2;  % There is a brass fitting/nozzle on the valve for
tube connection - measured
Ao_dist_m2 = Ao_dist_in2 * (0.0254/1)^2;
Cd_dist = 0.8;%0.95;%0.6;%0.8;

% Low-side Pressure Volume to Atmosphere
d_outlet_in = 1.0; % [in] - diameter of low-side plate orifice
Ao_outlet_in2 = pi/4*(d_outlet_in)^2;  % There is a brass fitting/nozzle on the valve
for tube connection - measured
Ao_outlet_m2 = Ao_outlet_in2 * (0.0254/1)^2;
Cd_outlet = 0.8;%0.95;%0.6;%0.8;

% ------------------------------------------------------------------------
% ------------------------------------------------------------------------
% System Volumes
% ------------------------------------------------------------------------
% ------------------------------------------------------------------------
% High-side Pressure Volume
%V_hi_in3 = pi/4*6^2*6;                             % [in3] - hi-side pressure volume
(old value that met goals)
V_hi_in3 = pi/4*6^2*10 - pi/4*1^2*10;               % [in3] - hi-side pressure volume
(10" length volume minus the shaft volume..more accurate than before)
```

```
V_hi_m3 = V_hi_in3 * 1.63871e-5;                    % [m3] - hi-side pressure volume
C_hi=V_hi_m3/(n*Rgas*T);                            % Pneumatic Capacitance

% Manifold Pressure Volume
%V_man_in3 = pi/4*6^2*1;                            % [in3] - manifold pressure
volume (old value that met goals)
V_man_in3 = (pi*2^2+3.5*4)*1.5;%+2 hole channel volumes and + volume in front of
valve assembly                  % [in3] - manifold pressure volume (close to
accurate from CAD)
V_man_m3 = V_man_in3 * 1.63871e-5;                  % [m3] - manifold pressure volume
C_man=V_man_m3/(n*Rgas*T);

% Tank Pressure Volume (not used as it is assumed perfectly controlled by
% BP regulator at Ptank pressure)
%V_tank_in3 = pi/4*12^2*12;                         % [in3] - tank volume (old value
that met goals)
V_tank_in3 = pi/4*6^2*10;                           % [in3] - tank volume (current
design..could be longer for more volume)
V_tank_m3 = V_tank_in3 * 1.63871e-5;                % [m3] - tank volume
C_tank=V_tank_m3/(n*Rgas*T);

% Low-side Pressure Volume
%V_lo_in3 = pi/4*6^2*6;                             % [in3] - lo-side pressure volume
(old value that met goals)
V_lo_in3 = pi/4*6^2*10 - pi/4*1^2*10;               % [in3] - lo-side pressure volume
V_lo_m3 = V_lo_in3 * 1.63871e-5;                    % [m3] - lo-side pressure volume
C_lo=V_lo_m3/(n*Rgas*T);

% Simscape Specific Constants
% TankMass_kg = 3.878215;  %lb = 8.55;
 TankSpecHeat_J_g_degC = 0.466*1000; %J/kg/degC - steel
```

F f_ConceptValveTestRig_PtankConstLeakage_metric_v2.m

```
% Program written to simulate the compressor valve test rig


% Compressor - fixed pressure
% Fixed orifice - to high-side pressure volume
% Hi-side pressure Volume
% Fixed orifice - opening on a profile (rotating valve plate) to high-side
% Fixed orifice - opening on a profile (rotating valve plate) to low-side
% Manifold volume
% Poppet Valves - with displacments based on pressure. (NO Dynamics)
% Tank volume
% Fixed orifice - to atmosphere
% Patm

% J. Kolodziej & Michael Anderson

function
Pdot=f_ConceptValveTestRig_PtankConst_metric_v2(t,P,flag,T,Pcomp,Ptank,tm,CdA_comp,Cd
A_hileakdisc,CdA_loleakdisc,CdA_hi_profileN,Cd_poppet,NumPoppets,PoppetDiam_m,PoppetP
reDisp_x0_m,PoppetSpringConst_k_kg_m,MaxPoppetDisp_m,CdA_lo_profileN,CdA_outlet,C_hi,
C_man,C_lo);

t
Patm=101000;

Phi=P(1);
Pman=P(2);
Plo=P(3);

% calculating when the rotating disc orifices align
CdA_hi=interp1(tm,CdA_hi_profileN,t);
CdA_lo=interp1(tm,CdA_lo_profileN,t);

% Air flow from compressor tank to high-side pressure volume
md_comp=orif_pneu(Pcomp,Phi,CdA_comp,T);

% Air flow from high-side pressure volume through rotating valve plate
md_hi=orif_pneu(Phi,Pman,CdA_hi,T);
if CdA_hi > 0 % orifices are aligned. (no leakage)
    md_hileak = 0;
else
    md_hileak = orif_pneu(Phi,Pman,CdA_hileakdisc,T);
end

%---------------------------------------------------------------
%---  POPPET VALVE ORIFICE FLOW --------
%---------------------------------------------------------------

areaPoppet = pi/4*PoppetDiam_m^2;
dP=(Pman-Ptank);
Nc=PoppetSpringConst_k_kg_m*PoppetPreDisp_x0_m-areaPoppet*dP;  % Normal Force When
Closed
if Nc > 0
    x = 0;
```

```
else
    x = (areaPoppet*dP)/PoppetSpringConst_k_kg_m - PoppetPreDisp_x0_m;
end
if x >= MaxPoppetDisp_m  % if poppets bottom out set to maximum possible
displacement.
    x = MaxPoppetDisp_m;
end
x;
PoppetArea_m2 = pi*PoppetDiam_m*x;  % [m2] - orifice area opening from one poppet.
PoppetOrifice_m2 = NumPoppets*PoppetArea_m2;   % [m2] - total orifice are for all
poppets.
CdA_poppet = Cd_poppet*PoppetOrifice_m2;
%--------------------------------------------------------------
md_poppet=orif_pneu(Pman,Ptank,CdA_poppet,T);

% Air flow from manifold to low-side pressure volume through rotating valve plate
md_lo=orif_pneu(Pman,Plo,CdA_lo,T);  %
if CdA_lo > 0 % orifices are aligned. (no leakage)
    md_loleak = 0;
else
    md_loleak = orif_pneu(Pman,Plo,CdA_loleakdisc,T);
end

% Air flow from low-side pressure volume to ambient
md_outlet=orif_pneu(Plo,Patm,CdA_outlet,T);  %

% pneumatic capacitance version
Pdot(1,1)=(md_comp-md_hi-md_hileak)/C_hi;                       % hi-side volume
Pdot(2,1)=(md_hi+md_hileak-md_poppet-md_lo-md_loleak)/C_man;  % maniforl volume
Pdot(3,1)=(md_lo+md_loleak-md_outlet)/C_lo;                   % lo-side volume


end
```

G orif_pneu.m

```
% Orifice Flow model for pneumatic systems assuming air is the working
% fluid.
%
% J. Kolodziej
%
% Equations come from Systems Modeling book by Woods and Lawrence 1997.

function mdot=orif_pneu(P_hi,P_lo,CdA,T)

% preventing imaginary number is the simulation (near zero it could go
% sqrt(minus number)
if P_hi<P_lo
    %disp('alert')
    P_hi=P_lo;
end

Pcrit=P_lo/P_hi;     % Calculating the critical pressure
if(Pcrit>0.528)    % subsonic
    mdot = 0.0822*CdA*sqrt(P_lo*(P_hi-P_lo))/sqrt(T);
else    % sonic (choked)
    %disp('Choked inlet')
    mdot = 0.0404*CdA*P_hi/sqrt(T);
end
```

H runme_ConceptValveTestRig_PtankConstLeakage_metric_v5.m

```
% Program written to simulate the compressor valve test rig

% ADDED Leakage around rotating plate.

% TODO Add in opening mechanics.

% Compressor - fixed pressure
% Fixed orifice - to high-side pressure volume
% Hi-side pressure Volume
% Fixed orifice - opening on a profile (rotating valve plate) to high-side
% Fixed orifice - opening on a profile (rotating valve plate) to low-side
% Manifold volume
% Poppet Valves - with displacments based on pressure. (NO Dynamics)
% Tank volume
% Fixed orifice - to atmosphere
% Patm

% J. Kolodziej & Michael Anderson

clear all
close all
tic
ConceptValveTestRigParams_Poppets_v2          %loading testbed parameters to the
workspace

CdA_comp =  Ao_comp_m2 * Cd_comp;
%CdA_hi =  Ao_hi_m2 * Cd_hi; %Comment out with opening dynamics at some point? Would
do in params but really should be tied to angular displacement
%^^^^ REPLACED WITH HOLE OPENING CURVE
CdA_hileakdisc =  Ao_hileakdisc_m2 * Cd_hileak;
% CdA_poppet = Ao_poppet_m2 * Cd_poppet;
CdA_dist =  Ao_dist_m2 * Cd_dist;
%CdA_lo = Ao_lo_m2 * Cd_lo; %Comment out with opening dynamics at some point? Would
do in params but really should be tied to angular displacement
CdA_loleakdisc =  Ao_loleakdisc_m2 * Cd_loleak;
CdA_outlet = Ao_outlet_m2 * Cd_outlet;

% Move to Params file eventually
% This needs to be integrated into a single plate but ok for initial model
r_hi = 2;   % [in] - location of high-side plate orifice
r_lo = 2;   % [in] - location of lo-side plate orifice
d_hi_in = 1.0; % [in] - diameter of high-side plate orifice (also in Params.m)
d_lo_in = 1.0; % [in] - diameter of lo-side plate orifice (also in Params.m)
%theta_hi = d_hi_in / r_hi; % [rad] - angle covering the plate orifice REPLACED BY
OPENING MECHANIC CODE
theta_hi = 0.252680255*2;
%theta_lo = d_lo_in / r_lo; % [rad] - angle covering the plate orifice REPLACED BY
OPENING MECHANIC CODE
theta_lo = 0.252680255*2;
PctOpen_hi = theta_hi / (2*pi);
PctOpen_lo = theta_lo / (2*pi);
RotFreq = 100;               % [Hz] - rotational frequency
RotPer = 1 / RotFreq;        % [sec] - rotational period
TimeOpen_hi = PctOpen_hi * RotPer;
```

```
TimeOpen_lo = PctOpen_lo * RotPer;
%TimeOpen_hi = 0.0031; %the code above is for the rotating disc final design.

N_rot=30;  % number of rotations
%disp_rot = [0:0.01:N_rot*2*pi]';
tm_profile=[0:0.00001:RotPer-0.00001]';
tStart = 0.00;   % [sec] when the high side pressure opens. should be tied to RPM and
angle
CdA_hi_profile1=zeros(length(tm_profile),1);
%CdA_hi_profile1(tm_profile<TimeOpen_hi)=CdA_hi;

%Interpolate HI SIDE to fit opening mechanics
index_CdA_hi_length = linspace(0,1,length(CdA_hi_profile1(tm_profile >tStart &
tm_profile<(tStart+TimeOpen_hi))));
A_hi_interp = interp1(linspace(0,1,length(Aopen)), Aopen,
linspace(0,1,length(CdA_hi_profile1(tm_profile >tStart &
tm_profile<(tStart+TimeOpen_hi)))));
CdA_hi = A_hi_interp * Cd_hi;
CdA_hi_profile1(tm_profile >tStart & tm_profile<(tStart+TimeOpen_hi))=CdA_hi;
CdA_hi_profileN=repmat(CdA_hi_profile1,N_rot,1);
CdA_lo_profile1=zeros(length(tm_profile),1);
tStart = RotPer/10;   % [sec] when the low side pressure opens after high side.
should be tied to RPM and angle

%Interpolate LO SIDE to fit opening mechanics
index_CdA_lo_length = linspace(0,1,length(CdA_lo_profile1(tm_profile >tStart &
tm_profile<(tStart+TimeOpen_lo))));
A_lo_interp = interp1(linspace(0,1,length(Aopen)), Aopen,
linspace(0,1,length(CdA_lo_profile1(tm_profile >tStart &
tm_profile<(tStart+TimeOpen_lo)))));
CdA_lo = A_lo_interp * Cd_lo;
CdA_lo_profile1(tm_profile >tStart & tm_profile<(tStart+TimeOpen_lo))=CdA_lo;
CdA_lo_profileN=repmat(CdA_lo_profile1,N_rot,1);

figure(100), clf
plot(tm_profile,[CdA_hi_profile1 CdA_lo_profile1])

tm=[0:0.00001:RotPer*N_rot-0.00001]';
figure(101), clf
plot(tm, [CdA_hi_profileN CdA_lo_profileN]), legend('Hi - valve open','Lo - valve
open')
%tm=[0:0.00001:0.05]';

Ptank = 50*6894.76; % [Pa]   % Fixed Discharge Tank Pressure (rather than dynamics)
P0=[Pcomp ; Patm*ones(2,1)];
opts = odeset('MaxStep',0.0001); % used to not have issues with going negative in the
square root term
%opts=[];
[t,P]=ode23s('f_ConceptValveTestRig_PtankConstLeakage_metric_v2',tm,P0,opts,T,Pcomp,P
tank,tm,CdA_comp,CdA_hileakdisc,CdA_loleakdisc,CdA_hi_profileN(1:length(tm)),Cd_poppe
t,NumPoppets,PoppetDiam_m,PoppetPreDisp_x0_m,PoppetSpringConst_k_kg_m,MaxPoppetDisp_m
,CdA_lo_profileN(1:length(tm)),CdA_outlet,C_hi,C_man,C_lo);

Phi=P(:,1);
Pman=P(:,2);
```

```
Plo=P(:,3);

%------------------------------------------------------------
% Poppet Displacement Calculation (just for plotting purposes)
areaPoppet = pi/4*PoppetDiam_m^2;
for i = 1:length(Phi)
dP=(Pman(i)-Ptank);
Nc(i)=PoppetSpringConst_k_kg_m*PoppetPreDisp_x0_m-areaPoppet*dP;
if Nc(i) > 0
    x(i)= 0;
else
    x(i)= (areaPoppet*dP)/PoppetSpringConst_k_kg_m - PoppetPreDisp_x0_m;
end
if x(i) > MaxPoppetDisp_m
    x(i) = MaxPoppetDisp_m;
end
PoppetArea_m2 = pi*PoppetDiam_m*x(i);  % [m2] - gap in manifold ...poppet travel may
be larger.
PoppetOrifice_m2(i,1) = NumPoppets*PoppetArea_m2;
CdA_poppet(i,1) = Cd_poppet*PoppetOrifice_m2(i,1);
end
%------------------------------------------------------------
figure(2), clf
plot(tm,x,[tm(1) tm(end)],[MaxPoppetDisp_m MaxPoppetDisp_m]), title('Poppet
Displacement')
legend('Poppet Disp','Max Poppet Disp.')

Pcomp_psi=ones(length(tm),1)*Pcomp*0.000145038;
Phi_psi=Phi*0.000145038;
Pman_psi=Pman*0.000145038;
Ptank_psi=Ptank*ones(length(tm),1)*0.000145038;
Plo_psi=Plo*0.000145038;

% figure(1), clf
% plot(tm,[Pcomp_psi Phi_psi Pman_psi Ptank_psi Plo_psi]), grid on, xlabel('Time -
(sec)'), ylabel('Pressure - (psi)'),
% legend('COMP','HI','MAN','TANK','LO'), title('System Pressures')

% Calculating Mass Flows Through Orifices
for i=1:length(tm)
    % Air flow from compressor tank to high-side pressure volume
    md_comp(i,1)=orif_pneu(Pcomp,Phi(i,1),CdA_comp,T);
    % Air flow from high-side pressure volume through rotating valve plate
    md_hi(i,1)=orif_pneu(Phi(i,1),Pman(i,1),CdA_hi_profileN(i,1),T);
    % Air flow leakage around rotating disc into the gap to the manifold
    if CdA_hi_profileN(i,1) > 0 % orifices align
        md_hileak(i,1) = 0;
    else
        md_hileak(i,1)=orif_pneu(Phi(i,1),Pman(i,1),CdA_hileakdisc,T);
    end
    % Air flow from manifold through poppets to tank
    md_poppet(i,1)=orif_pneu(Phi(i,1),Ptank,CdA_poppet(i,1),T);
    % Air flow from tank to ambient
    md_lo(i,1)=orif_pneu(Pman(i,1),Plo(i,1),CdA_lo_profileN(i,1),T);  %
    if CdA_lo_profileN(i,1) > 0 % orifices align
```

```
        md_loleak(i,1) = 0;
    else
        md_loleak(i,1)=orif_pneu(Pman(i,1),Plo(i,1),CdA_loleakdisc,T);
    end
    % Air flow from low-side pressure volume to ambient
    md_outlet(i,1)=orif_pneu(Plo(i,1),Patm,CdA_outlet,T);  %
end

% figure(3), clf
% plot(tm,[md_comp md_disc md_hi md_poppet md_lo md_outlet]), grid on, xlabel('Time -
(sec)'), ylabel('Mass Flow - (kg/s)'),
% legend('COMP-HI','HI-DISC','HI-MAN','MAN-POPPET-TANK','MAN-LO','LO-OUT'),
title('System Orifice Mass Flows')
%
figure(110), clf
subplot(411), plot(tm, [CdA_hi_profileN(1:length(tm))
CdA_lo_profileN(1:length(tm))]),
legend('Hi - valve open','Lo - valve open'), grid on, ylabel('Port Area')
subplot(412), plot(tm,[Pcomp_psi Phi_psi Pman_psi Ptank_psi Plo_psi]), grid on,
xlabel('Time - (sec)'), ylabel('Pressure - (psi)'),
legend('COMP','HI','MAN','TANK','LO'), title('System Pressures')
subplot(413), plot(tm,x,[tm(1) tm(end)],[MaxPoppetDisp_m MaxPoppetDisp_m]),
title('Poppet Displacement'), grid on,
legend('Poppet Disp','Max Poppet Disp.'), ylabel('Poppet Displacement - (m)')
% subplot(414), plot(tm,[md_comp md_disc md_hi md_poppet md_lo md_outlet]), grid on,
xlabel('Time - (sec)'), ylabel('Mass Flow - (kg/s)'),
% legend('COMP-HI','HI-DISC','HI-MAN','MAN-POPPET-TANK','MAN-LO','LO-OUT'),
title('System Orifice Mass Flows')
subplot(414), plot(tm,[md_comp md_hi md_hileak md_poppet md_lo md_loleak md_outlet]),
grid on, xlabel('Time - (sec)'), ylabel('Mass Flow - (kg/s)'),
legend('COMP-HI','HI-MAN','HI-leak','MAN-POPPET-TANK','MAN-LO','LO-leak','LO-OUT'),
title('System Orifice Mass Flows')

figure(111), clf
subplot(211), plot(tm, [CdA_hi_profileN(1:length(tm))
CdA_lo_profileN(1:length(tm))]), legend('Hi - valve open','Lo - valve open'), grid
on,
subplot(212), plot(tm,[Pcomp_psi Phi_psi Pman_psi Ptank_psi Plo_psi]), grid on,
xlabel('Time - (sec)'), ylabel('Pressure - (psi)'),
legend('COMP','HI','MAN','TANK','LO'), title('System Pressures')

figure(112), clf
H=plot(tm,[Pcomp_psi Phi_psi Pman_psi Ptank_psi Plo_psi]); grid on, xlabel('Time -
(sec)'), ylabel('Pressure - (psi)'),
legend('COMP','HI','MAN','TANK','LO'), title('System Pressures'), H(1).LineWidth=2,
H(2).LineWidth=2,H(3).LineWidth=2, H(4).LineWidth=2,H(5).LineWidth=2,
figure(13), clf
H=plot(tm,[md_comp md_hi md_hileak md_poppet md_lo md_loleak md_outlet]), grid on,
xlabel('Time - (sec)'), ylabel('Mass Flow - (kg/s)'),
legend('COMP-HI','HI-MAN','HI-leak','MAN-POPPET-TANK','MAN-LO','LO-leak','LO-OUT'),
title('System Orifice Mass Flows')
H(1).LineWidth=2, H(2).LineWidth=2,H(3).LineWidth=2,
H(4).LineWidth=2,H(5).LineWidth=2, H(6).LineWidth=2,H(7).LineWidth=2,
```

```
figure(114), clf
subplot(211), H=plot(tm,[Pcomp_psi Phi_psi Pman_psi Ptank_psi Plo_psi]); grid on,
xlabel('Time - (sec)'), ylabel('Pressure - (psi)'),
legend('COMP','HI','MAN','TANK','LO'), title('System Pressures')
H(1).LineWidth=2, H(2).LineWidth=2,H(3).LineWidth=2,
H(4).LineWidth=2,H(5).LineWidth=2,
subplot(212), H = plot(tm,x,[tm(1) tm(end)],[MaxPoppetDisp_m MaxPoppetDisp_m]),
title('Poppet Displacement'), grid on,
legend('Poppet Disp','Max Poppet Disp.'), ylabel('Poppet Displacement - (m)')
H(1).LineWidth=2,H(2).LineWidth=2,


figure(4), clf
H=plot(tm,[md_hileak  md_loleak]), grid on, xlabel('Time - (sec)'), ylabel('Mass Flow
- (kg/s)'),
legend('HI-leak','LO-leak'), title('System Orifice Mass Flows')
H(1).LineWidth=2, H(2).LineWidth=2,


% Compare to Simulink
Z0=P0;
sim('ValveTestRig_WithPoppetsWithLeakage_v3.slx')
Z0=P0;
tsim=SimResults(:,1);
PortAreaHi=SimResults(:,2);
PortAreaLo=SimResults(:,3);
HiPress=SimResults(:,4);
ManPress=SimResults(:,5);
LoPress=SimResults(:,6);
PoppetDisp=SimResults(:,7);
mdot_comp=SimResults(:,8);
mdot_hi=SimResults(:,9);
mdot_poppet=SimResults(:,10);
mdot_lo=SimResults(:,11);
mdot_outlet=SimResults(:,12);

figure(1001), clf
plot(tm,[Pcomp_psi Phi_psi Pman_psi Ptank_psi Plo_psi]), hold on
plot(tsim,[HiPress ManPress LoPress]),grid on, xlabel('Time - (sec)'),
ylabel('Pressure - (psi)'),
legend('COMP','HI','MAN','TANK','LO','Sim-HI','Sim-MAN','Sim-Lo'), title('System
Pressures')
figure(1002), clf
plot(tm,[md_comp md_hi md_hileak md_poppet md_lo md_loleak md_outlet]), hold on,
plot(tsim,[mdot_comp mdot_hi mdot_poppet mdot_lo  mdot_outlet]), grid on,
xlabel('Time - (sec)'), ylabel('Mass Flow - (kg/s)'),
legend('COMP-HI','HI-MAN','HI-leak','MAN-POPPET-TANK','MAN-LO','LO-leak','LO-
OUT','Sim-COMP-HI','Sim-HI-MAN','Sim-MAN-POPPET-TANK','Sim-MAN-LO','Sim-LO-OUT'),
title('System Orifice Mass Flows')
figure(1003), clf
plot(tm,x,[tm(1) tm(end)],[MaxPoppetDisp_m MaxPoppetDisp_m]), hold on,
plot(tsim,PoppetDisp), title('Poppet Displacement'), grid on,
legend('Poppet Disp','Max Poppet Disp.','Sim-PoppetDisp'), ylabel('Poppet
Displacement - (m)')
toc
```